Aérojoules project: Vertical Axis Wind Turbine

Cristian José Bottero

Master's Thesis

presented in partial fulfillment of the requirements for the double degree:
"Advanced Master in Naval Architecture" conferred by University of Liège
"Master of Sciences in Applied Mechanics, specialization in Hydrodynamics, Energetics and Propulsion" conferred by École Centrale de Nantes

developed at West Pomeranian University of Technology, Szczecin
in the framework of the

"EMSHIP"
Erasmus Mundus Master Course
in "Integrated Advanced Ship Design"

Ref. 159652-1-2009-1-BE-ERA MUNDUS-EMMC

Supervisors:	Prof. Maciej Taczała, West Pomeranian University of Technology
	Prof. Hervé Le Sourne, ICAM Nantes
Reviewer:	Prof. Philippe Rigo, University of Liège

Nantes, February 2011

Contents

List of Figures

List of Tables

Nomenclature

Greek Symbols

α	Angle of attack $[rad]$
$\Delta\theta$	Increment in the azimuthal angle $[deg]$
Δt	Time step $[s]$
Δx_i	Increment in the position along the the airfoil's surface $[m]$
Δz	Increment in the position along the blade in a direction perpendicular to the plane containing the airfoil $[m]$
ν	Air kinematic viscosity $[m^2/s]$
ω	Rotational velocity of the turbine $[rad/s]$
ρ	Air density $[Kg/m^3]$
σ_U	Standard deviation of the wind velocity $[m/s]$
θ	Turbine azimuth angle $[rad]$

Roman Symbols

A	Area perpendicular to the wind direction $[m^2]$
c	Airfoil chord $[m]$
C_d	Drag force coefficient [–]
C_l	Lift force coefficient [–]
C_P	Power coefficient or efficiency of the turbine [–]
e_{rel}	Relative error between solutions [%]
f_C	Correction function for the pressure distribution [–]
F_d	Drag force over the airfoil $[N]$
F_l	Lift force over the airfoil $[N]$
F_r	Radial force over the airfoil $[N]$
F_t	Tangential force over the airfoil $[N]$
l	Airfoil length $[m]$
M_T	Torque generated by the turbine $[Nm]$
M_t	Torque generated by an airfoil $[Nm]$
M_{Ta}	Mean torque generated by the turbine $[Nm]$

M_{ta}	Mean torque generated by an airfoil $[Nm]$
N_B	Number of blades [–]
$\hat{\mathbf{n}}$	Normal vector to the blade surface [–]
n_c	Number of points along the discretized airfoil contour of the blades [–]
n_Z	Number of points along the discretized height of the blades [–]
N_T	Number of turns for the simulation [–]
P_{2D}	Pressure in the two-dimensional models of the turbine $[deg]$
$P''_{\text{3D}i}$	Estimated pressure in the three-dimensional models of the turbine with shape correction $[deg]$
$P'_{\text{3D}i}$	Estimated pressure in the three-dimensional models of the turbine $[deg]$
P_{3D}	Pressure in the three-dimensional models of the turbine $[deg]$
P_w	Power available in the wind for in a particular area $[W]$
$\mathbf{r}$	Distance vector between the point considered and the turbine center in a plane containing the analyzed point and normal to the turbine axis $[m]$
R	Turbine radius $[m]$
Re	Reynolds number [–]
S	Surface of the blade $[m^2]$
t_{sim}	Time for the simulation [s]
$\overline{U}$	Mean wind velocity $[m/s]$
V_∞	Freestream wind velocity $[m/s]$
V_a	Induced velocity $[m/s]$
V_c	Velocity in the chord direction of the airfoil $[m/s]$
V_n	Velocity in the normal direction of the airfoil $[m/s]$
V_r	Relative velocity of the flow in the airfoil $[m/s]$
x_c	Position along the airfoil's surface $[m]$
z	Position along the blade in a direction perpendicular to the plane containing the airfoil $[m]$

Subscripts

0	Initial or first value
i	Related to the position discretization of the solution along the airfoil
j	Related to the time discretization of the solution
k	Related to the position discretization of the solution along the blade

Glossary

CLT	Classic Laminate Theory
DNS	Direct Numerical Simulation
DMS	Double Multiple Streamtube
EMI	Electromagnetic Interference
GSE	Ground Support Equipment
HAWT	Horizontal Axis Wind Turbine
ICAM	Institut Catholique d'Arts et Métiers – École d'ingénieurs généralistes
LES	Large Eddy Simulation
PIV	Particle Image Velocimetry
RANS	Reynolds Averaged Navier–Stokes
VAWT	Vertical Axis Wind Turbine

Declaration of Authorship

I declare that this thesis and the work presented in it are my own and have been generated by me as the result of my own original research.

Where I have consulted the published work of others, this is always clearly attributed.

Where I have quoted from the work of others, the source is always given. With the exception of such quotations, this thesis is entirely my own work.

I have acknowledged all main sources of help.

Where the thesis is based on work done by myself jointly with others, I have made clear exactly what was done by others and what I have contributed myself.

This thesis contains no material that has been submitted previously, in whole or in part, for the award of any other academic degree or diploma.

I cede copyright of the thesis in favor of the West Pomeranian University of Technology.

Date: February 2012 *Signature:*

Abstract

Recent years have seen more focus on the development of small and medium sized wind turbines aimed to urban or remote areas. For this reason, the vertical axis wind turbines (VAWTs) present an attractive alternative to the traditional horizontal axis wind turbines (HAWTs) in the environment of fluctuating wind.

Particularly in France, the intention is to increase the proportion of energy produced by means of both on-shore and off-shore wind farms, including the development of small generators that can be used as power supply for remote residences, ships, or any residence in urban areas in order to reduce the consumption from the general power grid. This served the basis for the development of a series of VAWTs in the framework of the Aérojoules Project for the Nantes region.

This work is oriented to the study and development of a small VAWT, with a specific focus on its aerodynamic and structural optimization, in order to maximize the power extracted from the wind. A design loop is presented, detailing the procedure for a decoupled fluid-structure analysis. Two main pillars of the design process are, therefore, the aerodynamic and the structural analysis. In relation to the aerodynamic design, a preselection of design alternatives for the turbine is carried out and a series of simplified CFD simulations are performed in order to define candidate solutions for detailed CFD models. With respect to the structural analysis, a simplified method to estimate the pressure loads on the blades for preliminary verifications is presented and its results are compared to those of available three-dimensional CFD simulations. A general discussion on the structural design of the blades is introduced, setting the basis for further work in this aspect.

Finally, conclusions and recommendations are presented, as well as suggestions about future work related to the project.

Introduction

Nowadays, a large percentage of the electric power demand of the modern societies is satisfied by generators based on fossil fuels. The collateral effect of using these power sources is generation of greenhouse gases, such as carbon dioxide, which play a main role in the global climate change.

Due to the serious and sometimes irreversible consequences associated to this phenomenon and taking into account the non–renewable characteristic of fossil fuels, it is imperative to encourage the development of alternative renewable power sources with a lower impact on the environment.

Based on the previously mentioned concepts, the wind generators present an attractive option to replace conventional power sources, with no direct emissions or fuel consumption during their operation. Particularly in France, the intention is to increase the proportion of the energy produced by means of both on–shore and off–shore wind farms.

However, in addition to the current development focused on high power turbines, it is also of great interest to develop small generators that can be used as power supply for remote residences, ships, or any residence in urban areas in order to reduce their consumption from the general power grid.

This served the basis for the development of a series of vertical axis wind turbines (VAWTs) that is currently being done at ICAM, sponsored by the Ocean Vital Foundation, among others. The present thesis research is conducted within the framework of this project, and aimed at the study and development of vertical axis wind turbines for electricity generation involving participation in different stages of the project.

Objectives

The main objective of this study is to design and optimize a vertical axis wind turbine. The focus is put on its geometrical optimization, in order to maximize the aerodynamic performance during the operation.

Regarding the structural design, several aspects of the geometry and material selection are also presented. Related to this last topic, a simplified method to assess the time–dependent aerodynamic pressure loads from a simplified two-dimensional CFD model is proposed.

Thesis Outline

Chapter 1 presents the current state of the art in small and medium–sized VAWT and introduces the project Aérojoules.

Chapter 2 focuses on the theoretical concepts and flow phenomena associated with the VAWT operation and presents the common methods for their analysis.

Chapter 3 introduces the characteristics of the design inherited from previous works and presents new tasks performed in search of an optimum turbine.

Chapter 4 presents the preliminary CFD analysis with two-dimensional simulations of the turbine.

Chapter 5 extends the CFD analysis to three-dimensional models of the turbine.

Chapter 6 focuses on the main aspects and considerations related to the turbine structural design.

Chapter 7 presents a simplified method to estimate the three-dimensional pressure loads on the blades based on results from two-dimensional CFD simulations.

Chapter 8 contains the conclusions, recommendations and future work related to the turbine design.

Chapter 1

State of the Art in VAWT Design

In this chapter, the state of the art of the vertical axis wind turbines is presented. Section 1.2 focuses on a general classification of the different designs. In Section 1.3 a description of the project motivating this work is presented.

1.1 Why Vertical Axis Wind Turbines?

As it has been previously mentioned, the focus of this study is the design of a small VAWT. The advantages of this type of turbines are presented by Manwell *et al.* (2009) and Paraschivoiu (2002) and are summarized as follows. The main advantage of this configuration is the fact of not requiring any special mechanism for yawing into the wind. This is particularly advantageous in urban or low altitude applications where the wind is highly turbulent and experiences frequent changes in direction that may induce perturbations and affect the performance of an horizontal axis wind turbine.

Another advantage of this type of turbines is that the power generator is located closer to the ground, allowing a simpler maintenance. Concerning the environmental impact of the installation of the turbine and due to the fact that the operational speed is lower than that of the HAWTs, the noise generated is less severe making it suitable for urban installation.

1.2 Classification of VAWTs

There are several types of VAWTs, each with its own distinctive features and characteristics (Paraschivoiu, 2002). They can be classified into three groups depending on the main aerodynamic principle on which they operate: Drag Turbines, Lift Turbines or a combination of both. In the first type, the difference of drag forces acting on the rotor blades produces the required torque, whereas in the later, the lift of an aerodynamic profile is used to produce a net positive torque on the shaft. In Figure 1.1, several types of wind turbines are shown according to their classification. In the following paragraphs, some of the main types are briefly described.

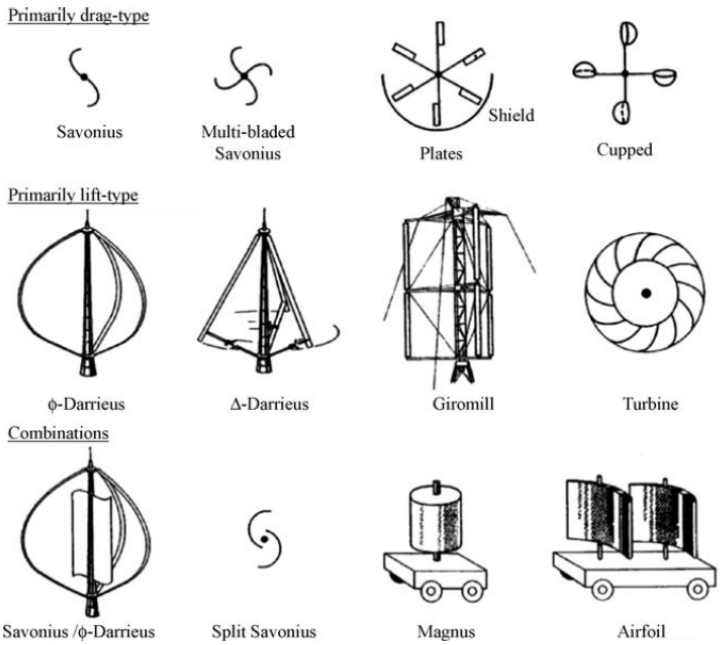

Figure 1.1: VAWT General classification and types. (Manwell *et al.*, 2009)

1.2.1 Savonius Type Wind Turbine

This is one of the most common drag–driven vertical axis turbines. It is characterized by an S–shaped cross–section when viewed from above. Its operation is based on the difference of pressure between the blade retreating from the wind and the one advancing into the wind. One of its main advantages is a relatively low initial cost but, on the other hand, they have low efficiencies. In Figure 1.2, different configurations of this turbine are presented.

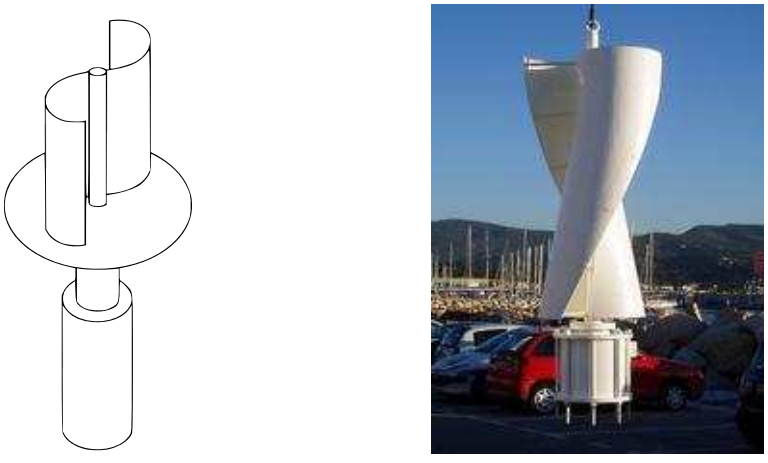

(a) General view (IE, 2009–2010) (b) Modern application (IE, 2009–2010)

Figure 1.2: Savonius type rotors

1.2.2 Darrieus Type Wind Turbine

This turbine consists of a number of airfoils mounted on a rotating shaft or framework. Lift forces are induced when the rotating rotor is exposed to a stream, resulting in a net produced torque. There are several possible configurations that can be adopted, depending on the airfoil set up. In general, this type of turbine requires initial rotation of the rotor to start working autonomously.

The most common configuration, sometimes referred to as Giromill or H-Bar, is obtained when the blades are vertically mounted. Such a configuration with no twist or curvature of the blades allows for manufacturing by extrusion, which reduces the cost and production time.

A variation of this last design consists of placing the blades with an inward angle at the top, leading to a conical configuration known as Δ–Darrieus.

One of the particularities of these designs is the characteristic pulsating power cycle caused by the uneven force distribution on the blades as the generator spins. Another main drawback is related to the high bending moments exerted on the blades which, combined with the cyclic loading, caused many problems during the early developments of this type of turbines, some of them deriving in catastrophic failures (Mcgowan and Connors, 2000). To mitigate this problem, a particular design in which the blades' tips are joined together to form an "egg-beater" or "troposkein" shape was introduced. In this way, the loads are transmitted as tension in the blades, allowing more efficient designs from the structural point of view.

Finally, one of the most recent variations of the design is characterized by the use of helicoidal blades. The purpose of this blade shape is mainly the homogenization of the generated torque along each turn, reducing the fatigue loads on the blades and the rest of the structure. The present Master's thesis is focused primarily on this last particular configuration of the Darrieus turbine.

Figure 1.3 presents several working models corresponding to the mentioned designs.

1.2.3 Combined Darrieus–Savonius Wind Turbine

As has been previously mentioned, the traditional Darrieus wind turbines are not self–starting. In general, they require a motor to initiate the rotation so that the airfoils start generating torque and the rotor is driven around by the wind. Alternatively it is possible to add small Savonius rotors on the shaft to start the rotation. The disadvantage of this system is that the turbine is slowed down while turning but, on the other hand, the whole device is simpler and easier to maintain. In Figure 1.4 a schematic view of this

configuration can be seen.

(a) Egg-beater rotor (TPE, 2008)

(b) H-Type rotor (ES, 2008)

(c) Helicoidal rotor (ES, 2008)

Figure 1.3: Darrieus type rotors

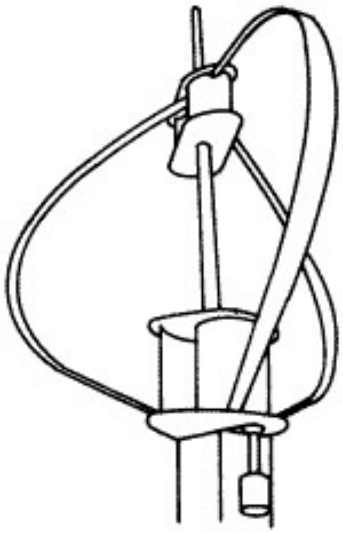

Figure 1.4: Combined Darrieus-Savonius turbine.(REUK, 2006–2012)

1.3 Description of the Aérojoules Project

The Aérojoules project focuses on the development of three vertical axis wind turbines of 300W, 1500W and 3000W, including the optimization in geometry and material of an existing Darrieus type wind turbine and the related electronic system (generator, regulator and battery). Most of the information presented in this section derives from official presentations of the project in early stages of its development.

Due to the multidisciplinary nature of the project, various partners are involved in work on its different aspects, as it can be seen below:

ICAM: Blade modeling and optimization, the development of an electronic regulator and for the turbine mechanical design (balance, test preparation, among others).

Ocean Vital Foundation: Wind turbine prototypes manufacturing.

CSTB: Wind field study and for wind tunnel testing.

Jallais: 300W turbine industrialized manufacturing.

Garos: Electronic regulator design and manufacturing.

AIC: 300W wind turbine marketing.

The first model of the turbine was tested in a wind tunnel and in the field during a global maritime race in 2008, as can be seen in Figure 1.5. The success of this initiative triggered the development of the project, that has been active for over a year. The main conclusions from the test result combined with an analysis of the general problem can be summarized as follows:

- The design proved to be mechanically robust.
- The turbine has good starting characteristics at very low wind speed.
- The performance in terms of energy production is non–satisfactory, related to the obtained torque and the electronic controller.
- It is not possible to find in the market turbines that are efficient for the prevailing winds in the region.
- Application in diverse environments is possible.

(a) Model built (b) Model installed for the Vendée Globe 2008

Figure 1.5: First Darrieus Turbine motivating the Aérojoules project.

Concerning the context in which the project was born, there are several positive aspects and considerations that encouraged its development, not only from the economical point of view but also from the social and political ones, as described below:

- The project is in line with the regional strategy for sustainable development.
- Emergence of a local industry in the small and medium–sized wind turbines.
- Potential creation of workplaces.
- Technology transfer from the research area to the industry.
- Synergy between involved partners.
- Assertion of the academic and industrial technological competence.

Finally, from the commercial and marketing point of view, the project was promoted based on four current design trends:

Ecology Use of natural renewable resources to produce electrical energy.

Nomadism Being able to transport the energy where it is required, for diverse purposes.

Scalable Evolution of the solution in power output, energy storage and application in order to meet the customers' changing needs.

Freedom No longer be dependent on the regular power grid, either by conviction or necessity.

Chapter 2

Basic Concepts and Turbine Aerodynamics

In this chapter, the predominant physical phenomena and the flow conditions associated with the VAWT operation are introduced, setting the bases to present several analysis methods. The nature of the wind and the power available in the freestream are briefly described in Section 2.1. The basic aerodynamic concepts related to VAWTs are presented in Section 2.2, along with the diverse phenomena associated with the flow in two and three dimensions. Finally, in Section 2.3 the main methods currently used for turbine analysis are described.

2.1 Wind Energy

The origin of the wind is directly related to uneven heating of the planet's surface by the sun. The radiated energy from the star is absorbed by land and water to be then transferred to the atmosphere. When combined with other factors, this generates a complex patter of atmospheric air circulation.

Deep analysis of the mechanics of wind motion exceeds the scope of this work and, therefore, only the essential information pertinent to the analyses performed here is presented. For further reference, detailed descriptions specifically related to wind turbine design can be found in the works of Manwell *et al.* (2009) or Jain (2011), among others.

As wind is an stochastic quantity with temporal and spatial variations, statistical analysis is required to evaluate the mean energy available at a certain location. One of the most common probability distributions used in wind data analysis is the Weibull distribution that is dependent of two parameters: the mean wind speed ($\overline{U}$) and its standard deviation (σ_U). In this way, based on the different wind speeds and their probability of occurrence, it is possible to compute the mean power available in a particular location. For the case of analysis in this work and based on the information measured for the Nantes region, the design wind speed was set as $5m/s$ in the conceptual stage of the project. Further details on the wind characteristics of the region can be found in Appendix A.

Knowing the amount of energy that can be extracted from the wind is fundamental to evaluate the turbine design. If a homogeneous freestream is considered, the power that is

theoretically available from the wind can be expressed as in equation (2.1). It can be seen that the power depends on the mass of air flowing through a determined area. Logically, the actual power that can be extracted by a wind turbine will be inferior to this amount and directly proportional to its efficiency. Further discussion on this topic can be found in Section 2.3.

$$P_w = \frac{1}{2}\rho\, A\, V_\infty^3 \tag{2.1}$$

2.2 Basic Relations and Flow Characteristics

In order to introduce the study of the basic aerodynamic models for VAWTs, a two–dimensional section containing the airfoils will be analyzed to derive the different parameters detailed in the following subsections. Later on, some specific details associated with the flow during the VAWT operation are described.

2.2.1 Velocity and Angle of Incidence of the Flow

This analysis is based on an airfoil of chord c rotating at a speed ω and exposed to a freestream of speed V_∞, as shown in Figure 2.1. At the rotor, the velocity has reduced its magnitude to V_a due to the induction factor, as described by South *et al.* (1983). Another thing that can be noted is the variation in the speed of the air before (V_∞) and after (V_W) passing through turbine. Logically, the difference in the kinetic energy of the flow was transformed or dissipated in the process.

As it can be seen from the previous figure, the total incident velocity is obtained combining the freestream component and the rotational one, that can be expressed as in equation (2.2). The ratio between the blade tip speed and the speed of the incident flow is known as tip speed ratio (λ) and its expression can be found in equation (2.3).

$$V_t = R\,\omega \tag{2.2}$$

$$\lambda = \frac{V_t}{V_a} = \frac{R\,\omega}{V_a} \tag{2.3}$$

At the same time, the velocity over the airfoil can be divided in a component parallel to its chord (V_c) and one normal to it (V_n). Their expressions can be found in equations (2.4) and (2.5) respectively, and the total incident velocity can be expressed as in equation (2.6).

$$V_c = V_t + V_a\, \cos\theta \tag{2.4}$$

$$V_n = V_a\, \sin\theta \tag{2.5}$$

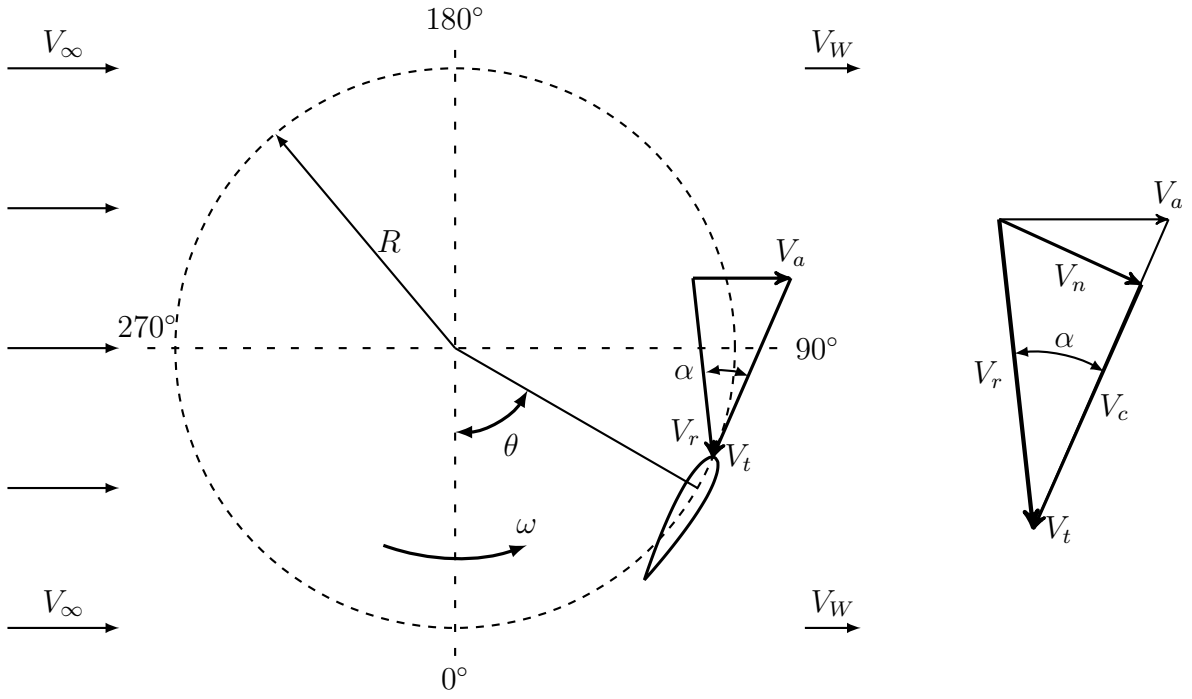

(a) Schematic view (b) Force diagram

Figure 2.1: Scheme of the flow velocities in a VAWT.

$$V_r = \sqrt{V_c^2 + V_n^2} \tag{2.6}$$

Equations (2.2), (2.4) and (2.5) can be replaced in equation (2.6) to shield equation (2.7).

$$V_r = \sqrt{V_a\big(\frac{R\,\omega}{V_a} + \cos\theta\big)^2 + V_a\,\sin^2\theta} \tag{2.7a}$$

$$= V_a\,\sqrt{\big(\lambda + \cos\theta\big)^2 + \sin^2\theta} \tag{2.7b}$$

It should be noted here that the incident speed over the airfoil varies along the turn, associated with the dependence with the azimuthal angle θ. Recalling the definition of the Reynolds number for a body immersed in a flow (equation (2.8)), it can be seen that the variation of the flow velocity leads to a variation in the local Reynolds number. This will have associated a variation in the flow conditions over the airfoil, as well as in the flow patterns that will be present. This will be further discussed in Section 2.2.6.

$$Re = \frac{c\,V_r}{\nu} \tag{2.8}$$

Another parameter that is of fundamental importance to understand the phenomena associated to the turbine operation is the angle of incidence of the flow over the airfoil. This is defined as the angle between the direction of the incident flow and the chord of the airfoil. Looking at Figure 2.1, the angle can be expressed as a function of different

velocity components, as seen in equation (2.9).

$$\alpha = \tan^{-1}\left(\frac{V_n}{V_c}\right) \tag{2.9}$$

Replacing the definitions of V_n and V_c from equations (2.4) and (2.5) into the last expression and simplifying, the incident angle can be written as in equation (2.10).

$$\alpha = \tan^{-1}\left(\frac{\sin\theta}{\left(\lambda + \cos\theta\right)}\right) \tag{2.10}$$

In Chapter 4, a graphical representation of this expression is analyzed for a particular turbine configuration.

2.2.2 Forces Over the Airfoil

Finally, the forces generated on the airfoil must be analyzed. Their importance lays in the fact that they are responsible for the output torque of the turbine.

Analyzing Figure 2.2, it can be seen that from the aerodynamic point of view, the forces on the airfoil can be divided in a drag force (F_d) parallel to the incident flow and a lift force (F_l), perpendicular to the flow direction. However, even when that division is useful from the point of view of the quantification of the forces, a more practical division will be done to have a better understanding of the driving forces of the turbine. Therefore, a division in a tangential force (F_t), contributing to the torque generation of the turbine, and a radial force (F_r), absorbed by the structure and not being useful for the operation of the turbine, will be implemented.

These forces can be expressed as a function of nondimensionalized force coefficients and the blade dimensions, as seen in equations (2.11) and (2.12) for the lift and drag force

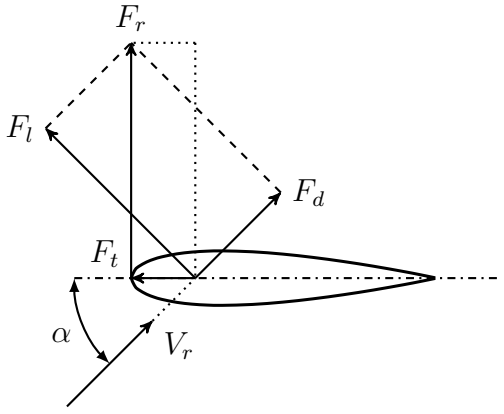

Figure 2.2: Force diagram on an airfoil.

respectively.

$$F_l = \frac{1}{2}\,\rho\, c\, l\, C_l\, V_r^2 \tag{2.11}$$

$$F_d = \frac{1}{2}\,\rho\, c\, l\, C_d\, V_r^2 \tag{2.12}$$

Logically, in order to obtain the tangential and radial forces, the lift and the drag must be decomposed in the tangential and radial direction and then subsequently added to find the expression of the tangential force and the radial force, as seen in equations (2.13) and (2.14), respectively.

$$\begin{aligned} F_t &= F_l \sin\alpha - F_d \cos\alpha \\ F_t &= \frac{1}{2}\,\rho\, c\, l\, V_r^2\,(C_l \sin\alpha - C_d \cos\alpha) \end{aligned} \tag{2.13}$$

$$\begin{aligned} F_r &= F_l \cos\alpha + F_d \sin\alpha \\ F_r &= \frac{1}{2}\,\rho\, c\, l\, V_r^2\,(C_l \cos\alpha + C_d \sin\alpha) \end{aligned} \tag{2.14}$$

Later on, in Section 4.1, particular cases will be analyzed to show the relation between these two forces and how the lift and drag contribute to them.

Even though it was not explicitly specified, it is understood that the lift and drag coefficients (C_l and C_d) depend on the selected airfoil and the flow incident angle, making the understanding of the underlaying behavior of the force variation more complex. More details concerning this topic can be found in Chapter 3.

2.2.3 Torque and Power Output

As it has been mentioned in the previous subsection, there is a dependence of the incident flow characteristics and of the forces with the azimuthal angle. In the same way, the torque generated by the airfoil will vary along a turn, as seen in equation (2.15).

$$M_t = F_t\, R \tag{2.15}$$

It is important, however, to have an averaged or mean value of the generated torque and therefore, of the gross power output. As the motion of the airfoil is periodic, the mean torque over a turn (M_{ta}) can be computed as follows:

$$M_{ta} = \frac{1}{2\pi}\int_0^{2\pi} F_t(\theta)\, R\, \mathrm{d}\theta. \tag{2.16}$$

The average torque for the turbine (M_{Ta}) will be the contribution of the N_B blades, as shown in equation (2.17).

$$M_{Ta} = N_B M_{ta} \tag{2.17}$$

Finally, the mean power output of the turbine can be computed considering its rotational speed, as shown in equation (2.18).

$$P_a = M_{Ta}\,\omega \tag{2.18}$$

This last expression will be used to assess the efficiency of the different designs, comparing it to the maximum theoretical available power in the freestream. The ratio between the extracted power from the wind and the total power available in the free stream is known as the power coefficient or efficiency of the turbine and can be expressed as in equation (2.19).

$$C_P = \frac{P_a}{P_w} \tag{2.19a}$$

$$= \frac{P_a}{\frac{1}{2}\,\rho\,S\,V_\infty^3} \tag{2.19b}$$

2.2.4 Cycling Loading

It was shown with the expressions developed in Sections 2.2.2 and 2.2.3 that the forces and the torque have a dependence with the azimuthal position of the airfoil. This clearly implies the existence of cyclic efforts applied over the blades and the whole structure. For a three-blades turbine, the frequency of the effort is, logically, three times the rotational speed. The cyclic loading has a negative impact in the fatigue life of the different components of the structure, but mainly the blades themselves. They are also directly related to the characteristics of the power generator and to the overall performance and behavior of the turbine.

This is an inherent problem of VAWTs of the Darrieus type and is one of the main aspects for which there was a lost of interest in this type of turbines in the early years of its development due to the abundance of catastrophic fatigue failures (Mcgowan and Connors, 2000).

2.2.5 Dynamic Stall

When an airfoil experiences a time–dependent change of its angle of incidence, an unsteady flow separation might occur, causing what is known as dynamic stall. In general, this phenomenon has associated the shedding of a turbulent flow structure that then moves

over the low pressure side of the airfoil. Logically, this disturbance induces a variation in the aerodynamic forces exerted over the body. Even though the main research in the topic is related to rotorcrafts and fighter aircrafts, the number of studies specifically focused on wind turbine analysis is increasing. Early in the investigation of wind turbines, it was shown by Noll and Ham (1982) that the dynamic stall could act positively in the power generation and that, at the same time, the loads and moments are increased, raising a warning about disregarding this phenomenon. It should be also noted that the presence of dynamic stall will also have other disadvantages, related mainly to increased noise generation and the effect of aeroelastic induced vibrations affecting the blades fatigue life.

As the dynamic stall is associated with great changes in the angle of incidence of the airfoil, the lift–based wind turbines are susceptible to it, principally at low tip speed ratios (λ) where the angles of incidence are bigger.

Experiments conducted by Fujisawa and Shibuya (2001) using particle image velocimetry (see Figure 2.3), showed that as a consequence of the dynamic stall, two sets of counter–rotating vortices are detached from the airfoil at different intervals and then travel downstream, growing in size. It can be observed that the size of the turbulent structures increases as the tip speed ratio (λ) decreases.

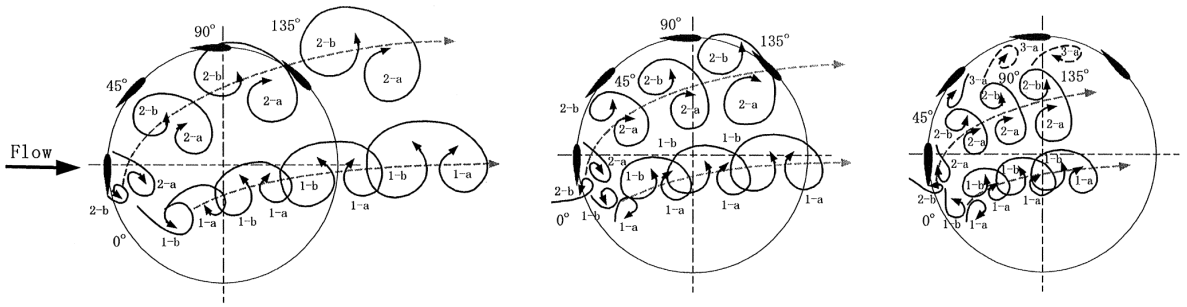

(a) $\lambda = 1$ (b) $\lambda = 2$ (c) $\lambda = 3$

Figure 2.3: Schematic illustration of dynamic stall. (Fujisawa and Shibuya, 2001)

2.2.6 Effect of Reynolds Number

Most of the small wind turbines operate in a range of Reynolds number below 1×10^6. On the other hand, most of the information concerning airfoil performance comes from the aircraft industry, obtained for much higher Reynolds numbers. When using information derived from tests at higher Reynolds numbers, it is important to consider the possible effect on the airfoil performance. In general, the maximum stall angle and the maximum lift coefficient decrease as the Reynolds number decreases. Studies concerning this effect were conducted by Jacobs and Sherman (1937) but in general, each case should be analyzed independently.

2.2.7 Laminar Separation Bubbles

This is a particular phenomenon that can be found in airfoils operating at low Reynolds numbers. Its origin is related to the fact that as the Reynolds number decreases, the laminar boundary layer cannot withstand the effect of a prolonged adverse pressure gradient, leading to its detachment from the airfoil's surface. In the detached area, the flow can become turbulent due to the increase in the instability and, under certain conditions, it can reattach to the surface, enclosing a laminar separation bubble over the airfoil. In general, as the angle of attack increases, the bubble moves towards the leading edge. The presence of this phenomenon results in an increase of the airfoil drag and a loss of efficiency.

As explained by Saeed *et al.* (2008), two different techniques are the most commonly used to mitigate this problem. One consist in the use of turbulators or boundary layer trips to force the flow transition from laminar to turbulent before the bubble appears. The disadvantage of this method arises if the airfoil operates in a wide range of Reynolds numbers, as the use of trips could not be beneficial for certain conditions. Another solution is related to the design of the airfoil incorporating a transition ramp in the pressure distribution over the airfoil, gradually promoting the flow transition without the appearance of laminar bubbles. Logically, in this way the airfoil is designed to operate in a determinate range of Reynolds numbers.

2.2.8 Self–Starting Characteristics

The self–starting characteristic of a VAWT is related to its behavior at low or non–rotational speed. It is known that in general the Darrieus-type VAWTs with fixed blades are unable to start by themselves as they have a negative power coefficient (see equation (2.19)) for low tip speed ratios. This problem can be solved by either using a combined turbine as explained in Subsection 1.2.3 or implementing a starting system that, based on a measurement of the current wind speed, proceeds to spin up the turbine until the external support is no longer required. Due to the loss of efficiency during the operation in the first case and the complexity of the control system in the second one, studies like the ones of Kirke and Lazauskas (1991) or Habtamu and Yingxue (2011) related to the turbine geometry were done to analyze how to passively improve the self–starting characteristics.

In general, it was observed that an increased airfoil curvature improves the self–starting characteristics, reducing and even eliminating the negative power coefficients at low tip speed ratios. However, the main drawback associated with this is reduction of the maximum achievable efficiency of the turbine.

With respect to the blade thickness, its increment has a positive effect on the performance of the turbine at low tip speed ratio but it is not possible to ensure that the ultimate

consequence will be a turbine with self–starting characteristics.

2.3 Methods for Wind Turbine Analysis

All the wind turbines base their working principle on the aerodynamic forces exerted on specially designed blades. A general analysis of a blade section (the airfoil) has already been done in the previous section. The shape and dimension of these profiles have a great impact on the performance and cost of the machine and, therefore, on their economical viability. It is then fundamental to assess the characteristics of a particular design in order to properly adapt it to achieve the maximum efficiency.

There are several methods to evaluate the forces exerted on the rotors as well as the consequent delivered power and efficiency. Here a briefly description of them will be provided since detailed developments can be found in the literature.

2.3.1 Actuator Disk Method

In this method, an ideal rotor is assumed. It is postulated that there is a pressure difference across the rotor, leading to the production of a thrust which performs work on the turbine. In exchange, the actuator disk induces a reduction of the free–stream wind speed as energy is transferred to it (South *et al.*, 1983; Manwell *et al.*, 2009). This model is used to describe the Lanchester-Betz or Lanchester-Betz-Joukowsky Limit, which is a theoretical limit on the amount of energy that can be extracted by a rotor-based wind turbine. The maximum efficiency for an actuator disk is found to be 59.3% (Bergey, 1979; Kuik, 2007).

2.3.2 Double Actuator Disk Method

It was shown by Paraschivoiu (1982) that the theoretical limit found for the single actuator disk was pessimistic when applied for a VAWT. This is mainly due to the fact that the fluid intercepts the rotor twice per rotation: in the upstream and in the downstream parts of the turn. Therefore, if the methodology used in the previous case is applied for two actuator disks in series, the maximum efficiency is found to be 64%, as described by South *et al.* (1983, Appendix B) and Newman (1983).

2.3.3 Rotor Disk Method

In this case, instead of proposing a thrust as in the previous cases, a torque is used (Jain, 2011; Manwell *et al.*, 2009). It therefore moves away from an abstract turbine to a more

realistic one, that delivers energy to a generator using torque. The airflow through the turbine rotor is also modeled more realistically, incorporating the rotation of the wake. This implies that, as part of the energy is transferred to the wake, the overall extracted energy will be reduced. However, it should be taken into account that this theory assumes an infinite number of blades and, more importantly, was developed considering the wake pattern induced by an HAWT.

2.3.4 Blade-Element/Momentum Theory (BEM)

Also known as strip theory, it is a combination of two theories. The momentum theory is applied to a control volume in the blade to analyze the forces on it based on the conservation of linear and angular momentum in a streamtube. In the blade element theory, the forces are analyzed at a section of the blade and depend on the blade geometry.

BEM Theory is more rigorous and can be used to obtain the theoretical performance curves, the axial forces and the torque of wind turbines. The blades are divided in sections that are studied separately in a stream that moves in the opposite sense of the rotation of the rotor. The forces in each section are obtained from the tests performed in wind tunnel for the different airfoils and, therefore, the viscosity is indirectly taken into account. As the interaction between each blade with the wake of the other is not considered, this method is not suitable for the design and analysis of VAWTs and has been primarily applied on HAWTs.

2.3.5 Double Multiple Streamtube Method (DMS)

This model is a combination of a derivation of the Momentum Theory using multiple streamtubes and the Double Actuator Disk method (Loth and McCoy, 1983; Paraschivoiu and Delclaux, 1983). It has the disadvantage that effect of the two disks is the same for all the streamtubes and cannot be adjusted for each of them. Its application is limited to low values of tip speed ratios and with certain limitations to the blades dimensions in order to stay in the range of validity of the momentum theory. Modifications to the method include the incorporation of dynamic stall models that can be either theoretical or semi–empirical, as introduced by Gormont (1973) for helicopter rotor studies and later modified for use in VAWTs as presented by Strickland (1975), Paraschivoiu and Delclaux (1983) and Brahimp *et al.* (1995).

2.3.6 Vortex Method

In this method, the blades and the vorticity upstream and downstream are modeled with lifting lines, as explained by Milne-Thomson (1966). The vortex strength is determined taking into account the circulation on the blades and the lift generated by the flow over them. There is also a trailing wake generated by a spanwise variation of the circulation and a shed wake generated by the temporal variation of the circulation. It is then possible to obtain the induced velocity at any point from the strength and position of the vortices.

This method has been later replaced with the introduction of the concept of free vortices being shed from the rotating blades. These vortices define a slipstream and generate induced velocities. However, it is possible to use a discrete implementation of the vortex method in order to compute the aerodynamic sound of a VAWT as it was shown that the complicated wake structure can be captured (Iida *et al.*, 2004).

2.3.7 Computational Fluid Dynamics

This method involves the numerical solution of the governing laws of the fluid dynamics. The continua is divided or discretized in small volumes, leading to what is known as mesh or grid, where the complex partial differential equations are solved. Nowadays and due to the increase in computational power, it is more common to use Computational Fluid Dynamics (CFD) to perform the study and analysis of wind turbines. In this way, if the adequate models and hypotheses are implemented, it is possible to use the CFD simulations as a tool to test and qualitatively compare a wide range of configurations and working conditions before defining a group of promising designs to proceed with the construction of prototypes and experimental testing.

The tasks developed as a part of this thesis will be based mainly in CFD calculations, with the appropriate theoretical and analytical verifications whenever possible. In more advanced stages of the project, a set of experimental tests will be performed, providing valuable results to validate the calculations performed here.

Chapter 3

Turbine Design

In this chapter, the general aspects of the wind turbine design are presented. In Section 3.1, an overview of the initial status of the project can be found. A general view of the tasks concerning the turbine design is introduced in Section 3.2. In Section 3.3, the main aspects considered for the airfoil selection are introduced, laying the basis for the analysis performed in the subsequent chapters. Finally, Section 3.4 provides an overview of several design aspects regarding the interface between the blades and the support structure.

3.1 Design Constraints and Previous Works

As it has been mentioned in Section 1.3, the project has been running for some time. Several studies on the design of the turbine itself have been conducted at ICAM by Moutaki (2010) and Brunellière and Bibard (2011), among others, in order to define its dimensional and geometrical characteristics. The main constraints imposed on the current design deriving from those previous studies are presented in the following sections.

3.1.1 Power Availability: Swept Area

This refers to the area swept by the blades, measured in a plane perpendicular to the freestream direction. As explained in Section 2.1, this is directly related to the maximum theoretical power that can be extracted from the wind. In this case, this parameter was set to 2 m^2 in the stage of conceptual design of the project.

3.1.2 Turbine Main Dimensions

The diameter and height of the turbine are logically connected to its swept area and, therefore, are not independent of each other. Considering the relations developed in Section 2.2.3, a turbine with a small diameter and a big height will result in low torque values. This also implies that the rotational speed will be high in order to keep the balance in the output power. On the other hand, a turbine with a diameter that is greater than its height will produce a bigger torque at a lower rotational speed.

Due to the multidisciplinary nature of the project, the effect of operational parameters such as the torque or the rotational speed will have an impact on the design of the generator. From the point of view of the power generation, a high rotational speed is preferred. However, as it has been explained in Section 2.2, the interaction between the blades and the aerodynamic performance at high rotational speed will be negatively affected.

A compromise solution that also took into account a balance in the global dimensions of the turbine was found with the selection of a squared swept area, meaning a height and a diameter equal to $1.4m$.

3.1.3 Blade Shape and Selected Airfoil

As it has been presented in Chapter 1.2.2, there are several geometrical shapes that can be adopted when designing a Darrieus–type wind turbine. In this case, when the project of a three–bladed turbine was started, it was decided to have helicoidal blades. Moreover, each blade spans over one third or $120\,^{\circ}$ of the circumference of the turbine. There are several reasons for choosing this option. First of all, taking into account the effects of the cyclic loads discussed in Section 2.2.4 both on the structure and on the power generation, the helicoidal blades distribute the torque more evenly over a turn and, therefore, there is a significant reduction of many negative aspects of the operation, like fatigue of the structure and noise generation. It was also considered that from the aesthetic point of view and the perception of the client, the helicoidal shape was a more attractive and suitable option.

With respect to the airfoil, a NACA 6412 profile was selected based on a study of the lift polar data of several airfoils, with the objective of maximizing the lift forces of the blades and, therefore, the produced torque (Brunellière and Bibard, 2011). Given that this approach is based only on the analysis of the lift forces obtained from static airfoil tests and, as it will be further explained in Subsection 3.3.2, it was decided to implement the approach described in Section 3.2 in order to determine an optimized airfoil for the turbine.

3.1.4 Support Structure

Concerning this topic, it was decided that the blades were to be linked by two tripods close to their extremities, as it is shown in the model of Figure 1.5. These elements are logically contained in two planes transversal to the axis of rotation and absorb the radial loads produced by the blades. A central shaft connects both tripods and has the interface with the power generator.

The turbine and the generator are then linked to the mounting interface that, depending on the final destination for the turbine, can be a simple base or a mast.

In Section 3.4 of this chapter, a more extensive discussion regarding the design of the interface will be carried out.

3.1.5 Material Selection

In early stages of the project, it was decided in agreement with the future manufacturer of the turbine that the blades and the support structure are to be built in composite materials, specifically, fiber glass cloth and epoxy resin.

In Chapter 6, more details about the diverse design considerations regarding the material layup will be presented.

3.2 Analysis and Optimization

One of the main objectives of the Aérojoules project is related to the development of optimized wind turbines. In order to achieve that objective, it is important to have a clear view of the global design cycle that will be implemented, that is summarized in the diagram of Figure 3.1.

Concerning the tasks presented in this report, the initial work plan included the design, simulation, testing and validation stages. However, due to a general delay in the project, the prototype construction was not finalized on time to perform the tests. As a consequence, the tasks are focused on the optimization of the turbine geometry and material in order to maximize the power extracted from the wind.

For better understanding, the tasks related to the design and simulation of the turbine are detailed in Figure 3.2a considering the original plan. It can be seen that the key to determine the performance and behavior of the turbine is given by a set of aeroelastic simulations, implying that a coupled analysis is performed taking into account the interaction between the fluid and the structure. Unfortunately, due to technical problems with the implementation of the aeroelastic models experienced in previous stages of the project, it was decided that an alternative analysis scheme should be followed. The result is the work flow presented in Figure 3.2b. One of the main differences is related, as expected, to the decoupling of the aerodynamic and structural analysis. With the new methodology, the results of the aerodynamic simulations are used as input in the structural verification and analysis. Another addition to the original plan is the incorporation of a simplified preliminary analysis of the possible solutions before proceeding with a more detailed simulation of their performance. In this way, the candidate alternatives can be narrowed down, reducing the time of the overall process. Practically, in this case the preliminary design is focused on the airfoil selection and it is achieved by means of two-dimensional

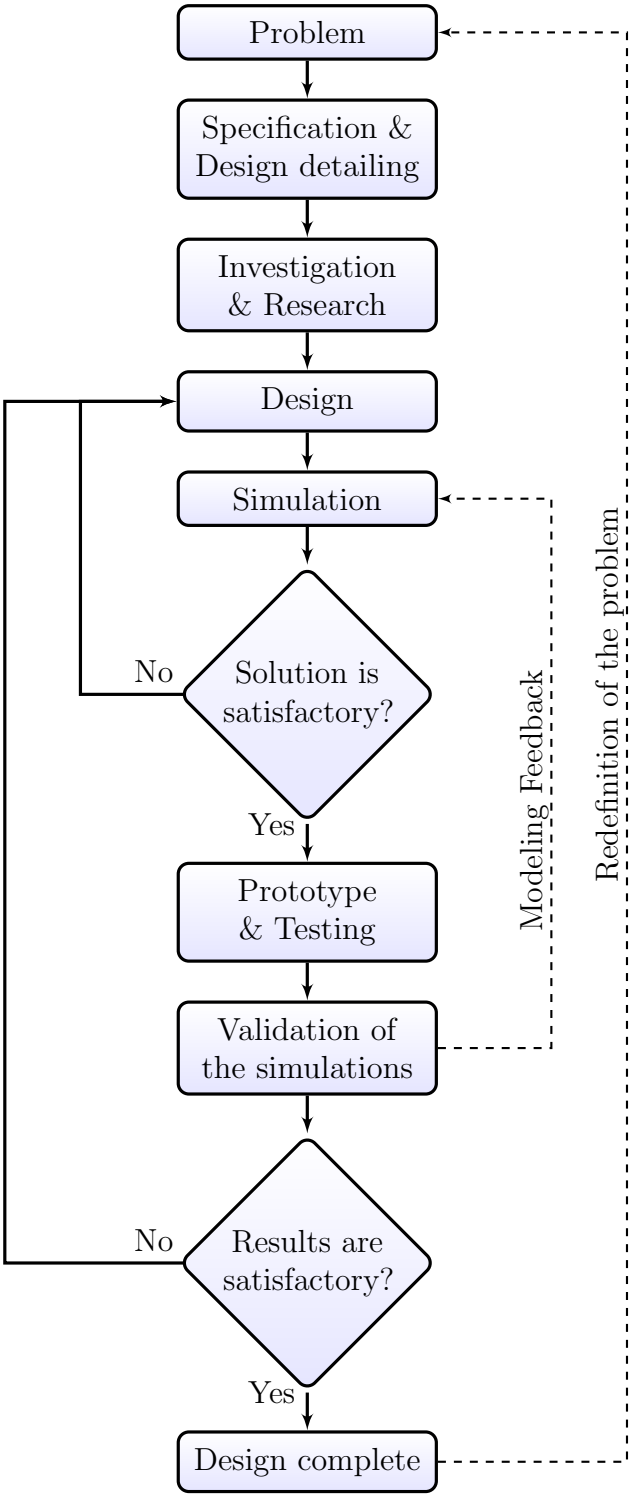

Figure 3.1: Design loop considered for the turbine design.

simulations of a section of the turbine, as it will be explained in Chapter 4. Then, once the available options have been reduced, more detailed aerodynamic simulations are performed and the details can be found in Chapter 5.

Unfortunately, as a consequence of a series of inconveniences that arose in the aerodynamic analyses and due to a lack of time, the structural verification was not carried out. Despite

this, Chapter 6 deals with considerations regarding the turbine structural design and in Chapter 7, a method to perform a preliminary estimation of the loads over the blades is presented.

In the following section, aspects related to the initial generation of possible solutions are presented, specially focused on the airfoil selection.

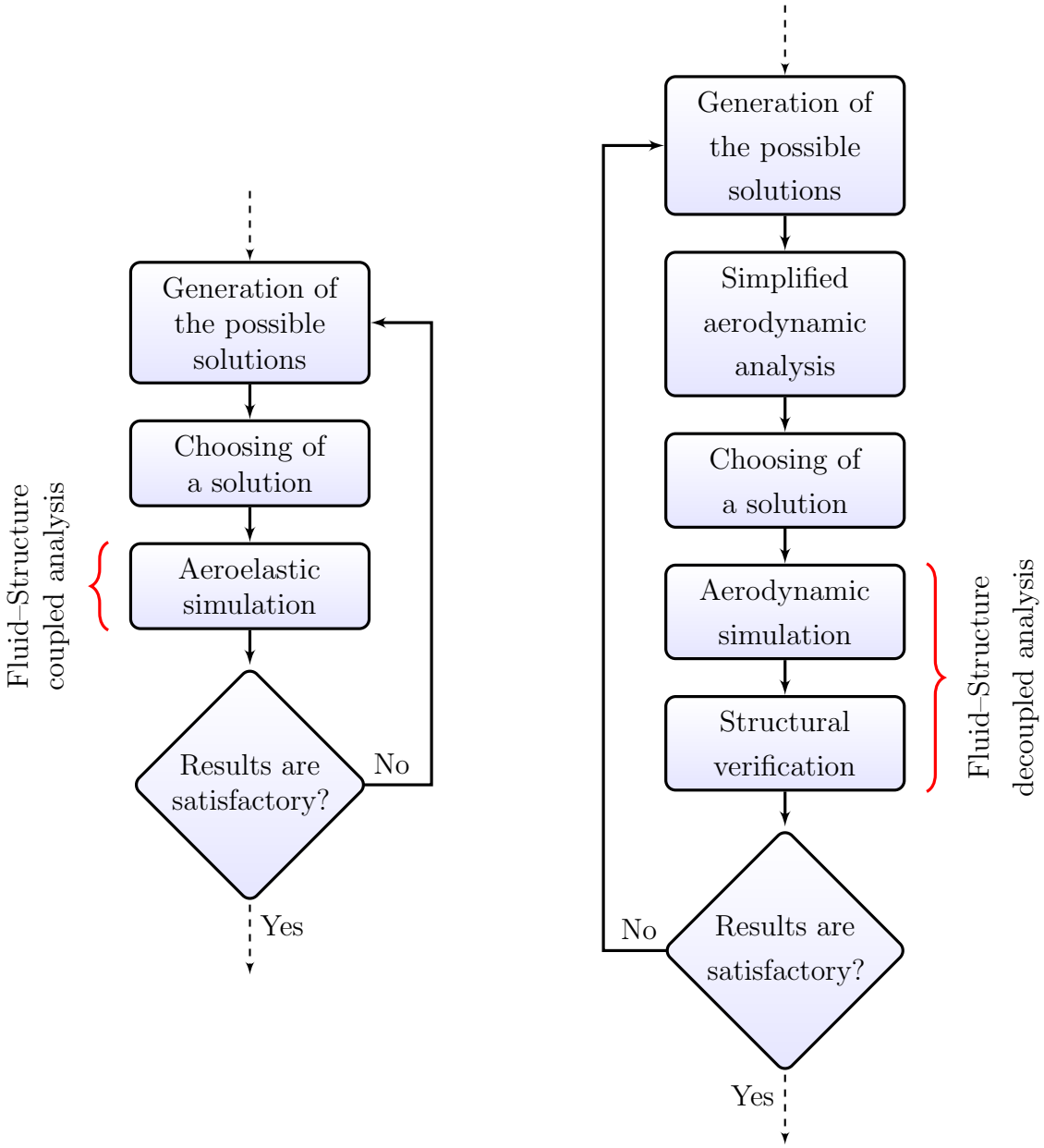

(a) Originally planned

(b) Implemented

Figure 3.2: Work flow for the Design and Simulation tasks.

3.3 Airfoil Selection

3.3.1 Criteria for the Selection

As it can be expected, the type of airfoil used in a wind turbine has a great impact on it and is, in many cases, responsible for the success or failure of the proposed design. Many different and varied aspects should be considered at the moment of selecting an airfoil shape and its material, which are briefly described as follows.

Aerodynamic performance It is directly related to the forces generated by the airfoils. The study can be divided in two parts:

Starting characteristics Behavior of the turbine at low rotational speed.

Operational performance Behavior at a steady operational condition.

Structural strength and stiffness The structure must withstand the loads without breaking or altering the performance of the turbine significantly.

Manufacturability The blades with the selected airfoil should be able to be produced at the scale of the project with well-known manufacturing techniques. The complexity and cost of the tooling, molds and matrices should be considered.

Maintainability The effect of surface damage, degradation or dirt that might deteriorate the performance of the turbine due to the loss of the initial characteristics will set the time between scheduled controls. The shape and material can also affect the possibility of making repairs to the blades.

Aeroelastic behavior Due to the flexibility of the structure, the aerodynamic loads will induce a change in the angle of attack of the airfoils, affecting therefore the aerodynamic behavior of the turbine and causing an important coupling between the structural and aerodynamic requirements (Popelka, 1982; Lobitz and Ashwill, 1985).

Noise generation Related to the aerodynamic of the turbine, the shed vortices will determine the noise emanated by the turbine. Works could be done to minimize it, as this reflects a loss of energy and a reduction in the power output.

Electromagnetic interference (EMI) Besides the fact that the power generator can be a source of EMI, it can be also affected depending on the shape, size and material of the turbine. The effect of this requirement should be evaluated in the final location of the device.

It is indeed evident that the requirements related to some of these items can be considered as being of secondary importance. In general, the selection of an airfoil can be based on

aerodynamic, structural, manufacturability and maintainability requirements and later on, any other criteria that is considered relevant can be verified.

In general, an aspect that should not be overlooked is the aeroelastic behavior, as it could have a great impact on the performance and reliability of the turbine.

3.3.2 Airfoil Performance Curves

Many investigations related to the performance of different airfoils have been performed over the years. In general, the information about the forces and moments and their variation with the angle of incidence of the flow is presented with nondimensional coefficients in curves known as polar diagrams. This concept has already been introduced in Subsection 2.2.2 when analyzing the forces over an airfoil.

The curves can be divided in different groups, depending on the information that is presented. The drag polar diagram plots the drag coefficient as a function of the lift coefficient. The lift polar diagram displays the lift coefficient as a function of the angle of incidence of the flow and, finally, the moment polar diagram is analogous to the lift polar, but for the aerodynamic moment coefficient. More information regarding this topic can be found in the works of Hepperle (1996–2008). Under certain conditions, the information provided by these curves could prove to be valuable for the preliminary design of an optimized turbine, as it will be explained in Subsection 4.1.2.

In Figure 3.3, the curve of the lift and drag coefficients versus the angle of incidence is presented for the airfoil NACA 0012, based on the work of Sheldahl and Klimas (1980).

3.3.3 Airfoil Design Methods

The design process of an airfoil is related to the knowledge of the properties of the boundary layer, as well as of the relation between its geometry and the pressure distribution over it. Two main approaches can be identified in the design method:

Direct Method With this approach, the geometry of the airfoil is specified and then the pressure distribution and the performance is calculated. If the results are not completely satisfactory, the shape can be modified to improve the performance.

Inverse Method Here the pressure distribution is chosen as the objective function and the corresponding geometry is to be obtained.

The design of tailored airfoils exclusively for use in VAWTs has always been a research topic of fundamental importance aimed at improving the efficiency of the turbines. Unfortunately, this type of approach exceeds the scope of this work due to the nature of the project and the airfoil will be chosen from existing designs, presented in the next section.

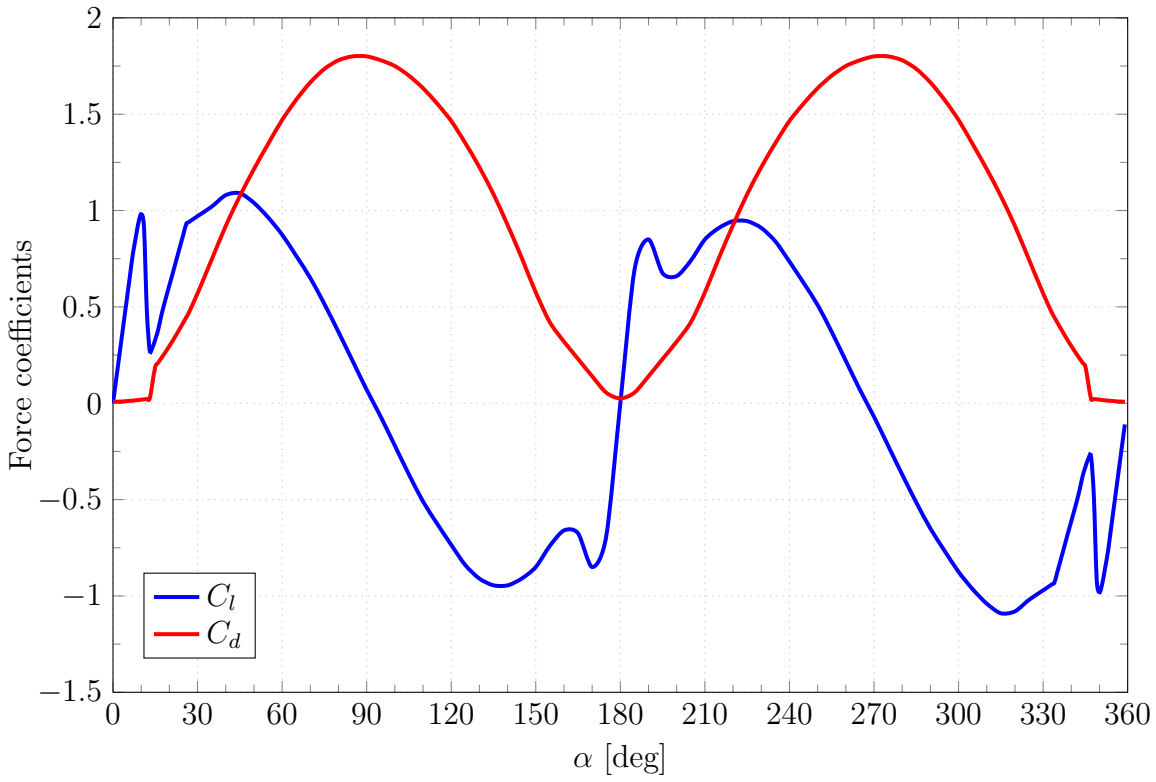

Figure 3.3: Force coefficients vs. incident angle. NACA 0012. (Sheldahl and Klimas, 1980)

3.3.4 Airfoil Types

In the field of airfoil design, many years of research and development have produced a wide range of airfoils suited for different needs. As expected, the first developments in the area were focused and oriented at airplanes. Later on this was extended to the field of wind turbines, especially for the HAWT family. In the following paragraphs, the main types of airfoils are described.

Conventional Airfoils

This denomination applies to the series of airfoils that were mainly developed for the aeronautical field, with the characteristic that even when the objective was always to maximize the lift to drag ratio, no particular flow condition was imposed. They can be mainly divided into two groups:

Four and five digits NACA Series In the 1930s, the U.S. National Advisory Committee for Aeronautics (NACA) introduced the systematization of profiles by developing and testing families of airfoils. Their main geometrical characteristics derived from the better existent airfoils of that time.

Many airfoils in the NACA four and five digit series were very successful and are still in use today for diverse applications.

Other non–NACA airfoils In parallel to the works performed by NACA, many other airfoils were developed with diverse degree of success. The theoretical bases used to justify the designs vary for each case. As examples, airfoils like the *Clark Y*, or families developed by the United Kingdom Royal Air Force (R.A.F. series) can be mentioned.

Laminar Airfoils

It is known that if the flow transition from laminar to turbulent regime can be delayed along the profile, lower drag forces can be achieved, with a significant increment in the lift to drag coefficient. Airfoils that are specifically designed to achieve this are referred to as laminar airfoils. They are characterized by the existence of a marked reduction in the drag coefficient for a range of values of the lift coefficient. In the polar diagram this can be observed with what is referred to as "drag bucket".

Six and seven digits NACA Series These families of airfoils in the NACA series were specifically developed to extend the laminar boundary layer over the profile to up to 60% of its chord. This is achieved by a displacement towards the aft of the profile of the minimum pressure zone and, therefore, delaying the generation of the adverse pressure gradient that encourages the transition to turbulent flow.

NREL Families

These type of sections are specifically targeted at HAWT applications. Developed in the U.S. by the National Renewable Energy Laboratory, they are designed in general to have a Cl_{max} which is largely insensitive to roughness effects. Another objective of the airfoils is to have soft stall characteristics, which results from a progressive flow separation from the trailing-edge (see Tangler and Somers, 1995).

VAWT Tailored Airfoils

Concerning the application of airfoils for VAWTs, there have been also efforts to introduce new sections that might improve the efficiency of the machine. It was not uncommon until recently that most of those developments were orientated to large turbines (see Sheldahl and Klimas, 1980; Klimas and Berg, 1983; Klimas, 1984; Saeed *et al.*, 2008). This tendency is now changing as the small and medium–sized turbines are becoming a more attractive alternative for remote or urban applications, fomenting a new series of studies in this area (Claessens, 2006).

3.3.5 Preselection of Airfoils

Based on the different sets of airfoils presented in the last Section, a smaller group will be selected and used as a case study for a series of two-dimensional models of the turbine.

As the information related to VAWT tailored airfoils is not abundant, this option will be discarded. In the same way, as the NREL airfoils are specifically targeted to HAWT, they were only presented on an informative basis. It remains then the selection between a conventional or a laminar airfoil from the NACA series.

It should be noted that all the research done when developing those airfoil families was oriented to aircraft design. Therefore, the performance and flow conditions considered were related to that field. When comparing an airfoil used in a VAWT with one used in an airplane, there are evident differences such as the permanent change in the angle of attack or the lower Reynolds number.

If it is taken into account that the interest of this work is placed on the design of a lift–type turbine, it is reasonable to consider that the airfoils with the higher lift to drag coefficient will pose as the better choice. In this case, the laminar airfoils match that condition but, however, there are several aspects related to the wind turbine operation that may affect this fact. First of all, there is a permanent change in the angle of attack of the profile that is inherent to the VAWT dynamics. This will obviously affect the performance of the airfoils that were designed to operate outside the stalled condition. In the case of laminar airfoils, it would be unlikely to have an acceptable laminar boundary layer as the flow is in a permanent transient state, with strong variations in the flow incidence. Moreover, as the turbine is expected to work for long periods of time in diverse environments with a minimum level of maintenance and cleaning, the surface rugosity of the airfoil, especially in the leading edge, might experience changes that will have a severe negative impact on the performance of the laminar airfoils. This last effect is not restricted to wind turbines and was also observed in airplanes when the presence of insects and dirt in the wing encouraged the boundary layer transition from laminar to turbulent.

Finally, another important factor that has a great impact on the airfoil selection is the manufacturing process. If the surface rugosity and final geometry of the built model differs greatly from the selected design, the performance will not be as expected. It also has a major impact on the cost and delivery time of the final unit and, in this aspect, a laminar airfoil must be processed under strict conditions to ensure that the desired characteristics are met.

Based on the previous discussion, it was decided to proceed with the design of the turbine with NACA airfoils of the four–digits family. In general, most of the existent VAWTs use symmetrical airfoils of this series (NACA 00XX), with thicknesses varying from 12% to 15% (Speral, 2009, Chap. 6).

It is important to preselect a series of airfoils in order to have a general view of the effect of the variation of the different parameters, such as the thickness or the curvature, in order to validate the phenomena described in Section 2.2. The final set of airfoils that will be studied in the next chapter can be found in Table 3.1. Three different thicknesses will be considered (12%, 15% and 18%) as well as four different curvatures (0%, 2%, 4% and 6%). For the cases of curved airfoils, the maximum curvature will be considered at 40% of the chord length. A graphical representation of the airfoils can be seen in Figure 3.4, based on the airfoil coordinates available at UIUC (1995–2011).

Table 3.1: Set of preselected four–digits NACA airfoils

Thickness	**Curvature**			
	0 %	**2 %**	**4 %**	**6 %**
12 %	NACA 0012	NACA 2412	NACA 4412	NACA 6412
15 %	NACA 0015	NACA 2415	NACA 4415	NACA 6415
18 %	NACA 0018	NACA 2418	NACA 4418	NACA 6418

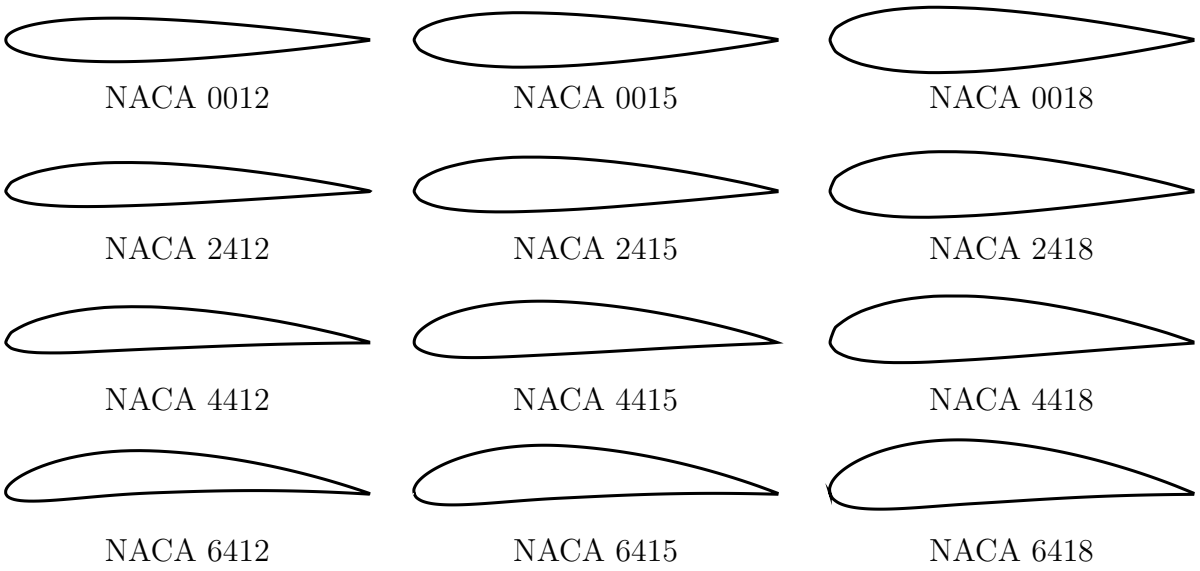

Figure 3.4: Set of preselected four–digits NACA airfoils.

3.4 Blade Support Structure: Interface Design

The links between the blades and the rest of the turbine are a fundamental part of the structure and two main roles can be associated with them. In the first place, they must withstand and transfer all the aerodynamic forces exerted over the blades so that the torque can be used in the generator. The other important role is related to the impact on the aerodynamic performance of the turbine as a consequence of the interaction between

the blades and the interface. The stage of the aerodynamic optimization is related to this last issue, as it was presented in Section 3.2.

Based on the same support structure introduced in the previous model, i.e. a tripod connecting the blades, two main design variants can be identified depending on their position with respect to the blades:

Interfaces placed at intermediate positions along the blades This concept was the one adopted in the first model of the turbine, as it was mentioned in Subsection 3.1.4. From the structural point of view, the bending moment on the links is reduced. However, from the aerodynamic point of view, two disadvantages can be mentioned. First, the presence of the tripod induces a local reduction of the forces due to the interference with the blades and secondly, the effect of the tip vortex is not addressed, leading to further reductions in the efficiency of the turbine.

Interfaces placed at the extremities of the blades Here the blades are connected to each other in their extremities. Depending on the configuration, it is possible to adapt the design with the objective of reducing the negative effects of the tip vortex in order to achieve better efficiencies. From the structural point of view, the bigger length between supports increases the loads on the interfaces and additional secondary supports along the blades might be required to absorb the radial forces and diminish the bending moment at the extremities.

In this case and related to the objective of optimizing the turbine, the interface was considered in the extremities and several design variants were proposed. Later on, the final selection can be made by means of analysis of their performance and other design criteria. Three design alternatives are presented here. The first one, seen in Figure 3.5, incorporates a transition between the blades and the tripods. The mechanical joint can be made independently of the shape of this interface and then a fairing can be used to obtain the desired aerodynamic behavior.

Another alternative consists in a smoother blending of the blades and the tripod, trying to keep the continuity in the surfaces for better flow characteristics (See Figure 3.6). The influence of the angle between the tripod and the blade in this area should be studied as another design variable in order to assess the effect in the overall performance.

Lastly, another possibility is to incorporate a fillet or chamfer in the interface, as shown in Figure 3.7. The effects of that particular geometry in the flow and in the pressure distribution in the tip area are to be studied.

Note that in all the figures the central shaft has been omitted.

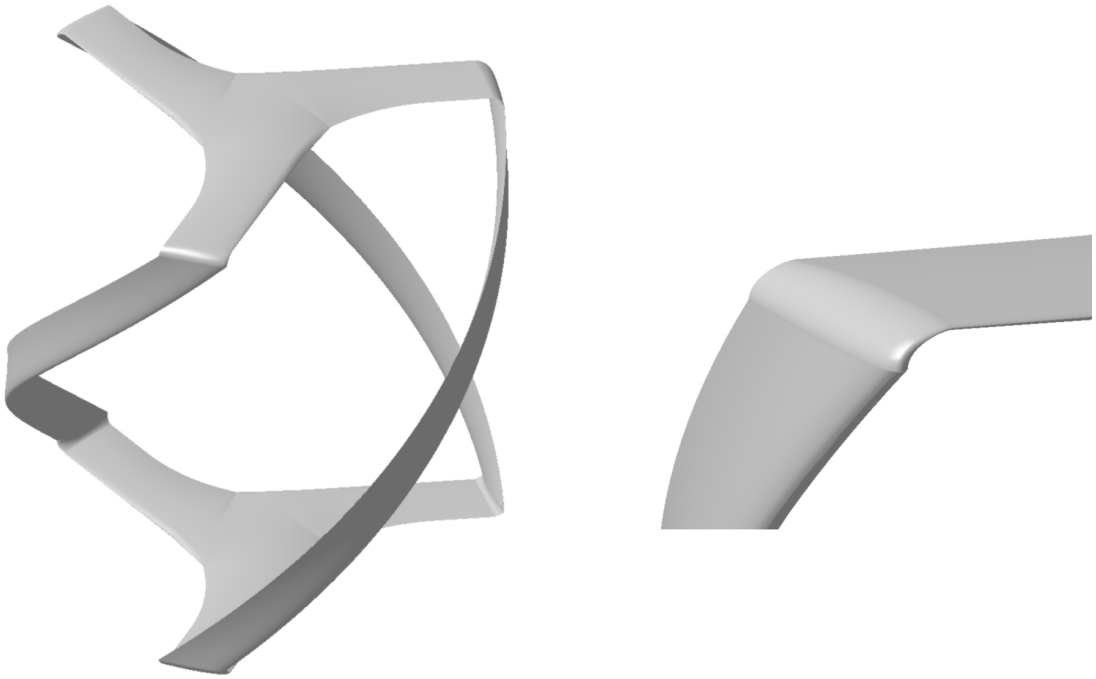

(a) General view. (b) Close up.

Figure 3.5: Blade–Tripod interface. Design with a transition element.

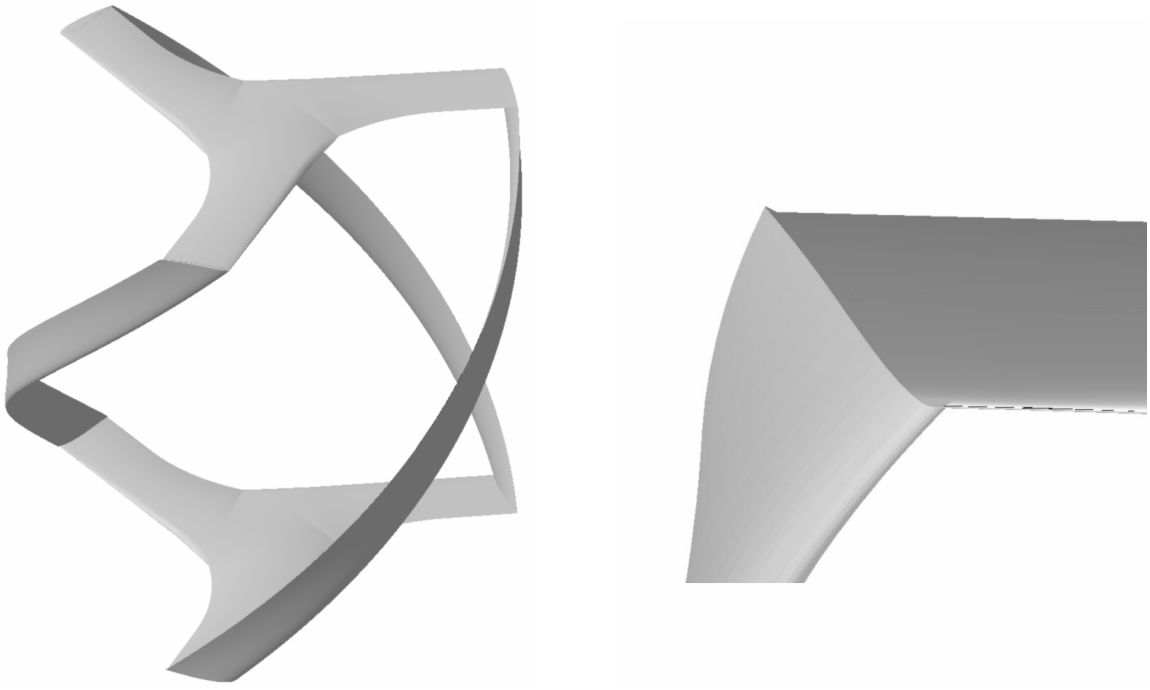

(a) General view. (b) Close up.

Figure 3.6: Blade–Tripod interface. Design with a smoothed joint.

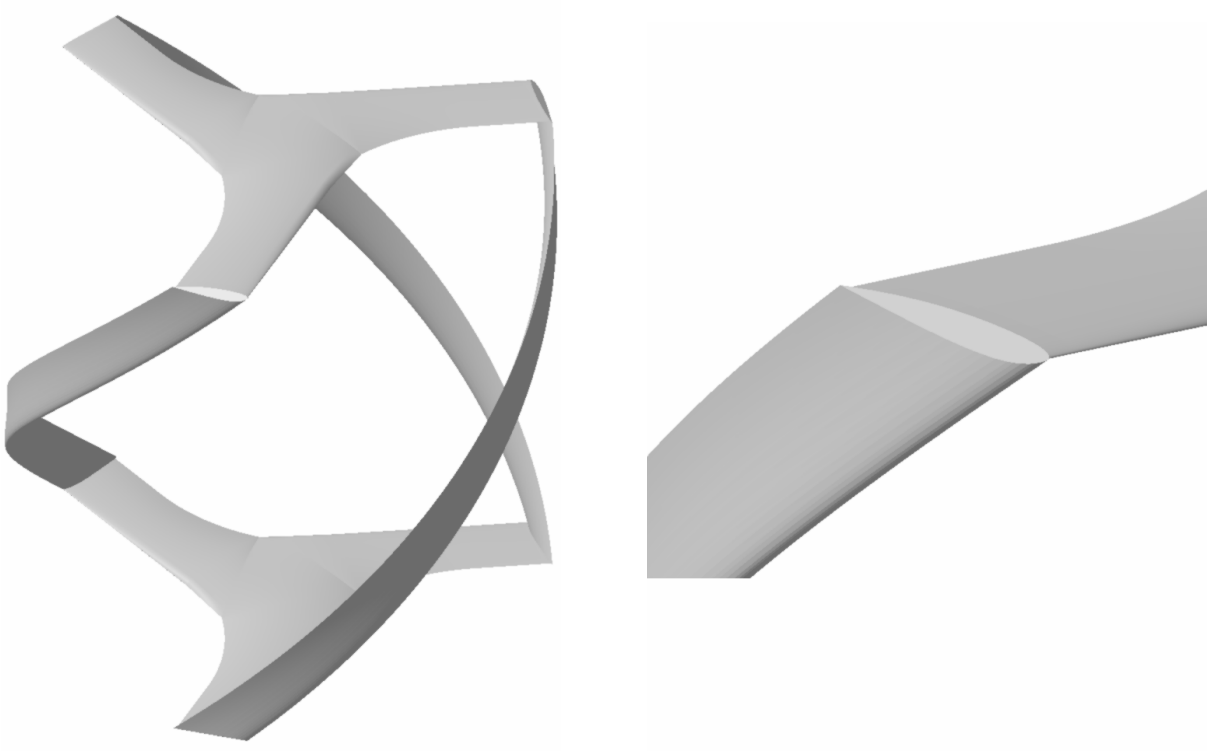

(a) General view. (b) Close up.

Figure 3.7: Blade–Tripod interface. Design with a chamfered edge.

Chapter 4

Two-dimensional Modeling of the Turbine

In Section 4.1, a preliminary simplified analysis of the dynamics of the turbine is performed based on the basic expressions presented in Chapter 2. Then, in Section 4.2, CFD simulations are used to perform a comparison among the preselected airfoils, reducing the list of candidate airfoils that are presented in Section 4.3.

4.1 Preliminary Analysis

As it was mentioned before, one of the most important aspects when facing a design project is the understanding of the physical phenomena involved in the problem. Based on the relations described in Section 2.2, a simplified analysis for a general airfoil is conducted considering the geometry of the turbine.

4.1.1 Angle of Incidence and Magnitude of the Relative Velocity

Taking into account what was discussed in Section 3.1, the studies were started considering a turbine with a diameter of $1.4m$. Moreover, as it has been mentioned in Section 2.1 referring to the wind characteristics, a velocity of $5m/s$ for the freestream is considered for the operational design condition. It is then possible to compute the evolution along a turn of the angle of incidence and the relative velocity of the flow in the airfoils, as plotted in Figures 4.1 and 4.2, respectively. Several curves can be found, corresponding to different tip speed ratios (λ).

It should be noted that in more detailed calculations than the ones presented here, the intensity of the velocity in the downwind half of the turbine will be slightly lower than in the upwind half as a consequence of the energy extracted by the blades in there. The same concept is used to derive the modified actuator disk method described in Section 2.3. As a consequence of this phenomenon, the angle of incidence in the downwind half will have also a lower magnitude.

The value of the local Reynolds number for the airfoil based on its dimensions and on the local velocity of the flow can be also plotted. In Figure 4.3, the variation along a turn

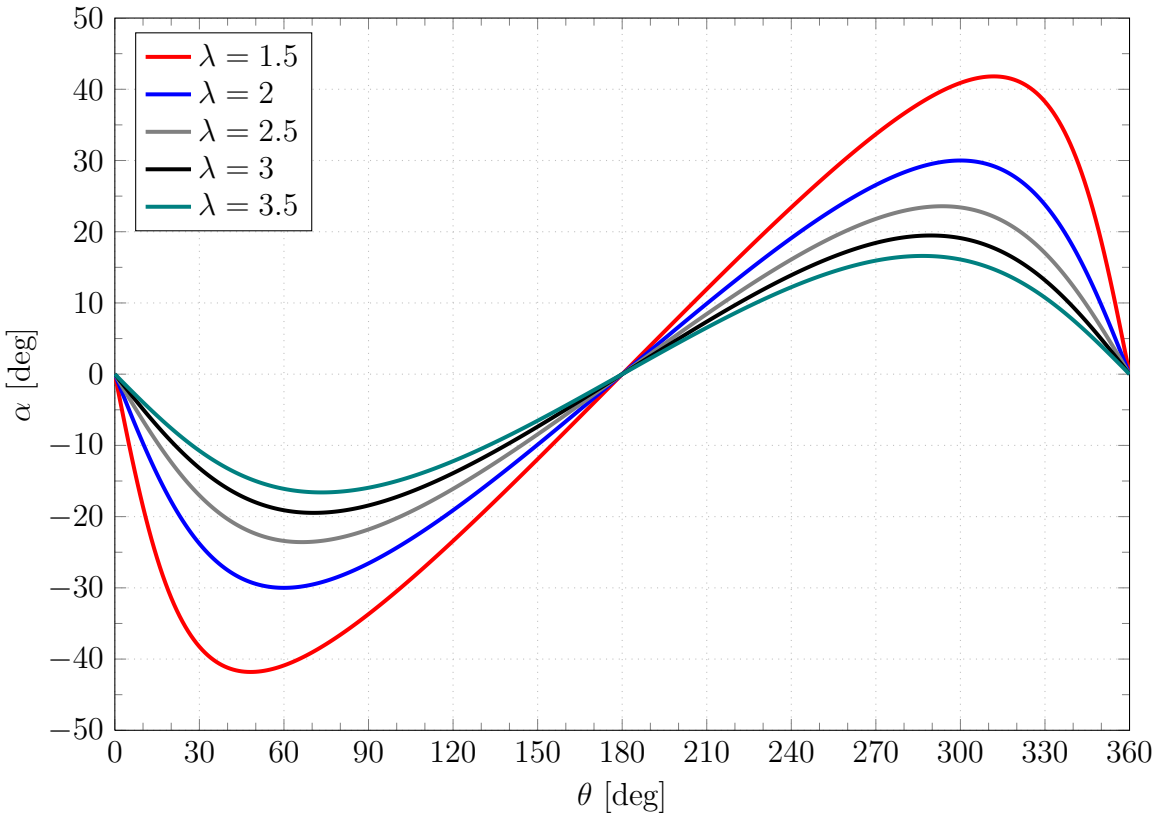

Figure 4.1: Angle of incidence of the flow along a turn for several tip speed ratios.

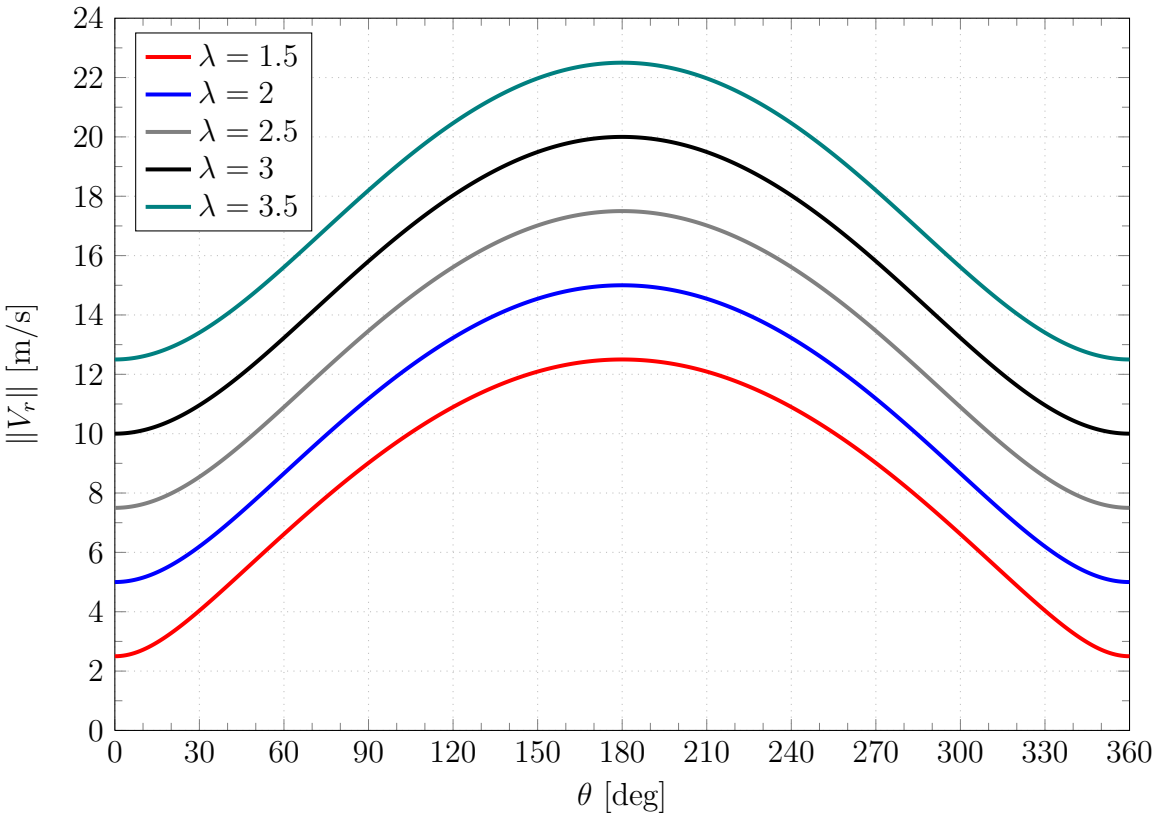

Figure 4.2: Relative velocity of the incident flow along a turn for several tip speed ratios.

can be observed for several tip speed ratios (λ). Logically, their variation along a turn is directly related to the variation of the relative velocity previously shown.

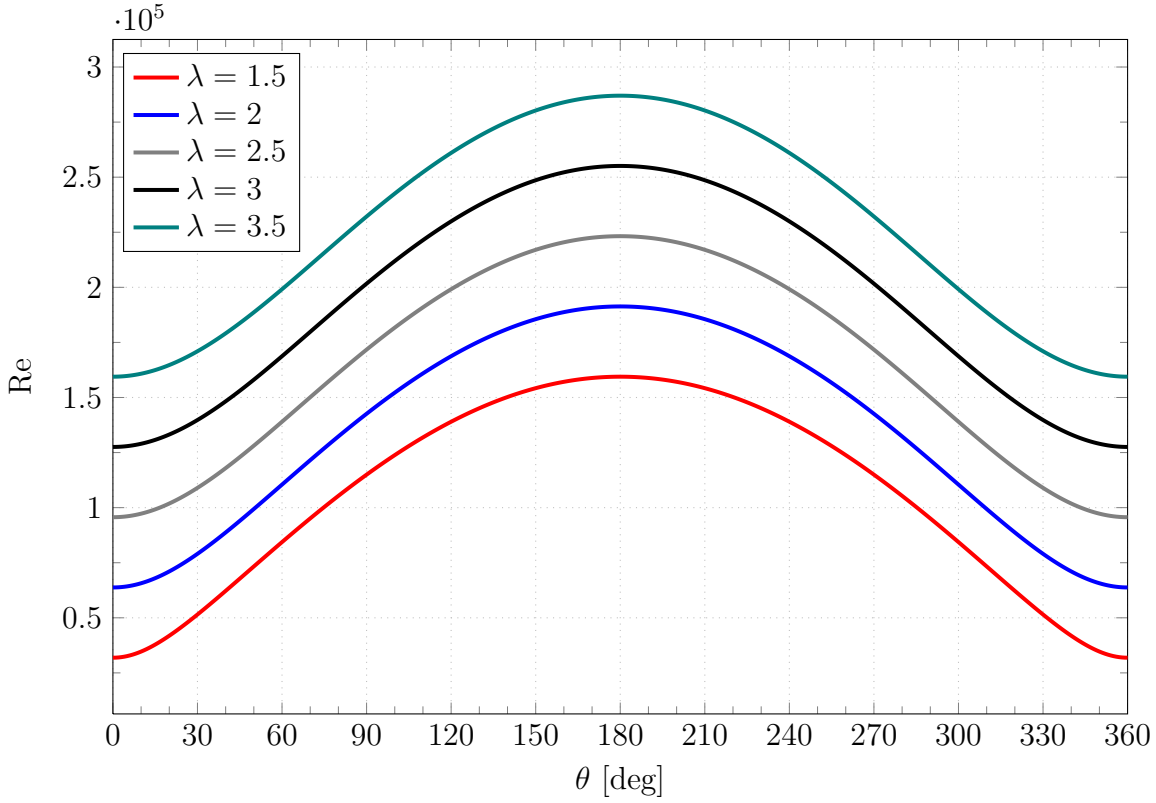

Figure 4.3: Local Reynolds number along a turn for several tip speed ratios. $V_\infty = 5m/s$.

It is possible now to analyze the previous figures in order to extract some information and have an insight of the problem. With respect to the angle of incidence, an antisymmetric behavior per each half turn can be observed. If it is also taken into account the relation between the angle of incidence and the aerodynamic forces generated by the airfoil (see Section 3.3.2), it is clear that the type of airfoil will have an impact on the overall performance along a turn.

Regarding the amplitude of the incident angle, it can be noted that it decreases as the rotational speed increases (increase of λ). This is logically related to the fact that the velocity component in the radial direction of the turbine is predominant compared to the freestream velocity. It is also interesting to observe how the maximum angle of incidence can easily be over 15°, which for many airfoils implies detachment of the boundary layer and the transition into a stalled condition.

With respect to the incident velocity, it is observed that the zone of maximum magnitude is obtained when the airfoil is moving from the downwind half to the upwind half of the turbine. As only the cases corresponding to $\lambda \geq 1.5$ are plotted, no inversions of the flow over the airfoil are observed.

4.1.2 Estimate of the Forces with Steady–State Airfoil Data

In early stages of the VAWT design, it might seem convenient to use the previous results in conjunction with information about the airfoil obtained from wind test tunnels to derive the forces on the blades. The main idea of this methodology is summarized in Figure 4.4.

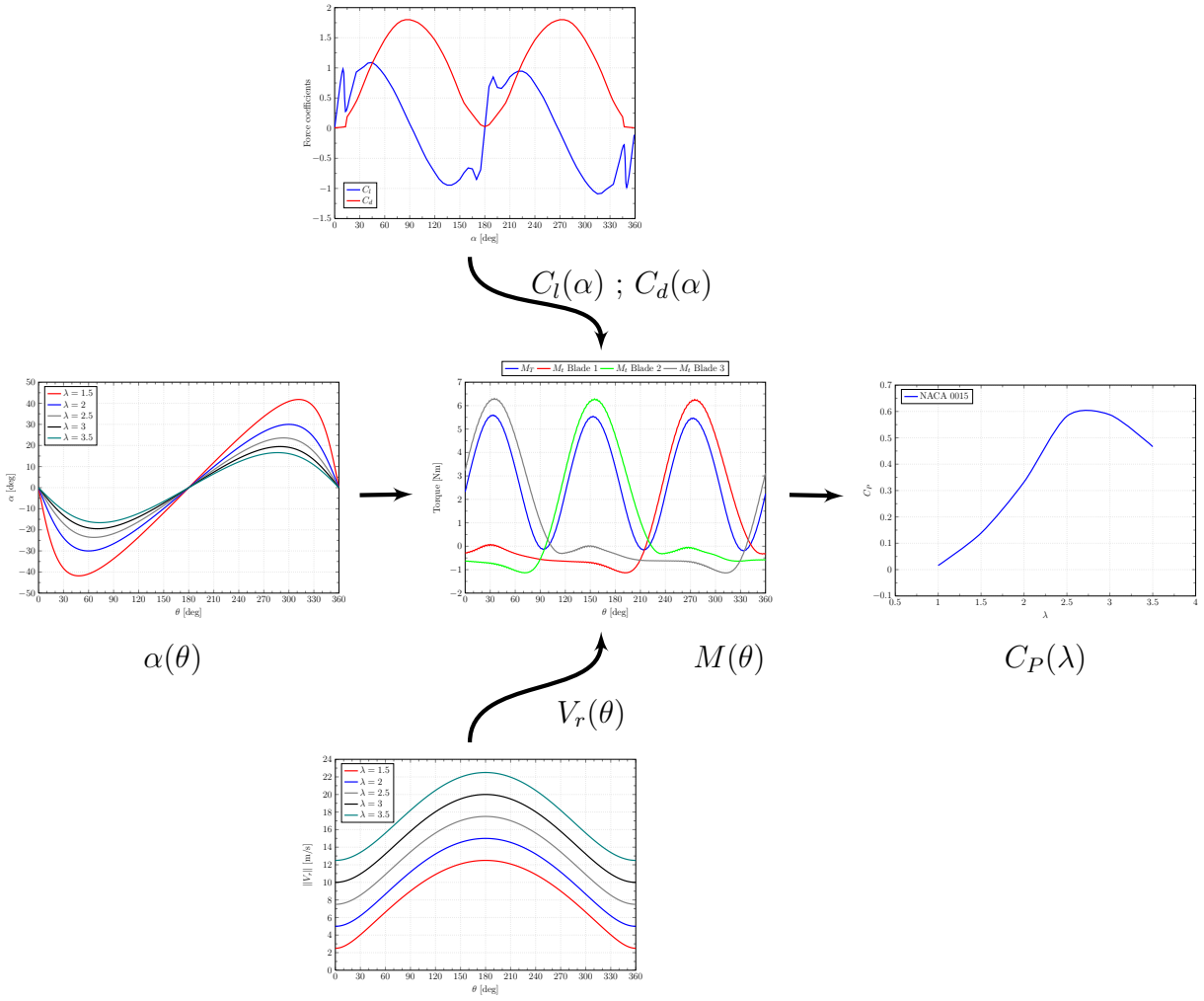

Figure 4.4: Scheme for the estimation of the turbine performance with airfoil data.

It should be noted however that, as stated by Speral (2009), there are several factors that raise doubts about the validity of this practice. First of all, the majority of the airfoil data does not extend for angles of incidence beyond stall but, however, this can be a normal operating condition for a VAWT. Nevertheless, it should be noted that airfoil tests specifically oriented to VAWTs and covering a wider range of angles can be found in the literature (Sheldahl and Klimas, 1980), as well as in predictions with numerical models.

Another aspect that can be questioned is the applicability of the steady–state airfoil data to the unsteady operating conditions of the VAWTs. Even though it appears that the

static data is valid for a non-stalled condition, caution is advised.

In relation to the previous point, the pitch rate[1] of the airfoil in a VAWT induces dynamic effects on the forces due to the existence of a pitching circulation of the flow. This can be seen as an offset between the static and dynamic force curves, inducing further error in the calculations.

Finally and due to the dynamics of the turbine, the blades moving through the downwind side of their trajectory will be affected by the wake of the airfoils moving through the upwind section. As this phenomenon is difficult to quantify and include in this simplified analysis, the validity of the results has to be critically analyzed.

4.2 CFD Analysis

In this section, two–dimensional CFD models for the set of preselected airfoils detailed in Table 3.1 are presented and their results are analyzed. The model description, hypotheses considered and the results obtained will be described in the following subsections.

4.2.1 Model Description

A section perpendicular to the rotation axis is studied. The models were created by means of the Computer Assisted Design (CAD) software SolidWorks using the corresponding airfoil coordinates and then exported to the software STAR CCM+. In this last one, the mesh or grid is generated and the equations for the conservation of mass, momentum and turbulence are solved. Once the numerical simulation of the flow characteristics is complete, it is possible to estimate the efficiency of the turbine with the considered airfoil. A workstation with a processor Intel Core 2 Quad Q9450 @ 2.66 GHz with 3.48 Mb is used for the calculations.

As it has been mentioned in subsection 2.3.7, the studies performed by means of CFD are very susceptible to diverse factors such as the grid quality, the imposed boundary conditions, the selected turbulence model and the difference scheme implemented. A description of these items in relation to the models is summarized below.

Grid Description

It is necessary to define a domain of study for the problem. In this case, a rectangular control volume (or area in a 2–D problem) is considered, as shown schematically in Figure 4.5. Its dimensions must be set in a way that the area of interest is far enough

[1]The pitch refers to the angle of incidence of the flow and the pitch rate to its change with time.

from the boundaries to avoid the potential problem of an unrealistic interaction that could affect the flow in the area of the turbine. In order to achieve this, the turbine diameter is taken as a reference dimension and in the lateral direction, the walls are set at one diameter of distance. The same distance is considered for the inlet and three diameters are considered to the outlet.

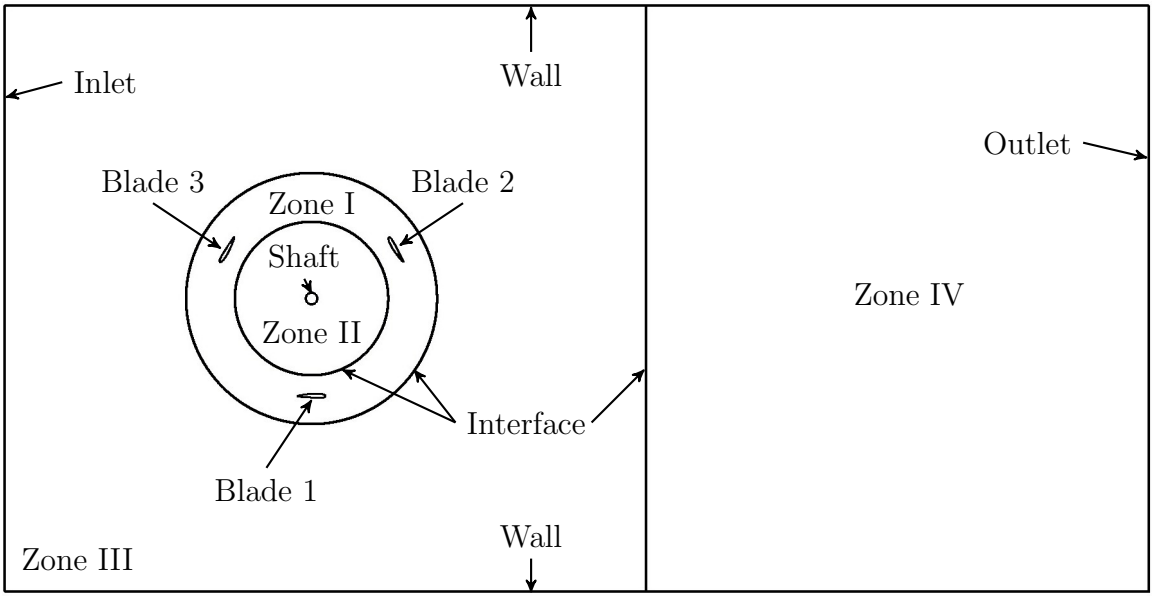

Figure 4.5: Schematic description of the domain under study. 2-D model.

The studied volume is divided into four zones, each one with different mesh density and characteristics. The zone containing the airfoils (Zone I) has an hybrid mesh with a structured region in the vicinity of the solid boundaries and composed by stretched quadrilateral elements. This is associated with the existence of the boundary layer and with its better simulation. In the remaining region, an unstructured mesh composed by polygonal elements is used. This zone has also the particularity of being a rotating or sliding mesh. In this way, the motion of the turbine can be simulated.

A compromise solution should be found for the mesh density, as it should be fine enough to adequately reproduce the geometry of the airfoils and to capture the flow field in the area, but not too fine to be solved with the available computing capacity.

Three other zones are defined with the purpose of reducing the overall number of elements of the model and with a mesh density that decreases away from the turbine area. Unstructured grids with polygonal elements are used in all of them.

The grid sensitivity of the solution is an important issue to be considered. In this case and based on the works on previous models of Brunellière and Bibard (2011), the used base sizes for the grid at different zones can be found in Table 4.1. As a result, the models have approximately 73 thousand cells.

In Figure 4.6, a general view of the mesh can seen and in Figure 4.7, a close up of the airfoil area can be observed, with the prismatic boundary layer elements.

Table 4.1: Grid base sizes for the different zones of the model

Zone	Base size [m]
I	0.008
II	0.015
III	0.1
IV	0.3

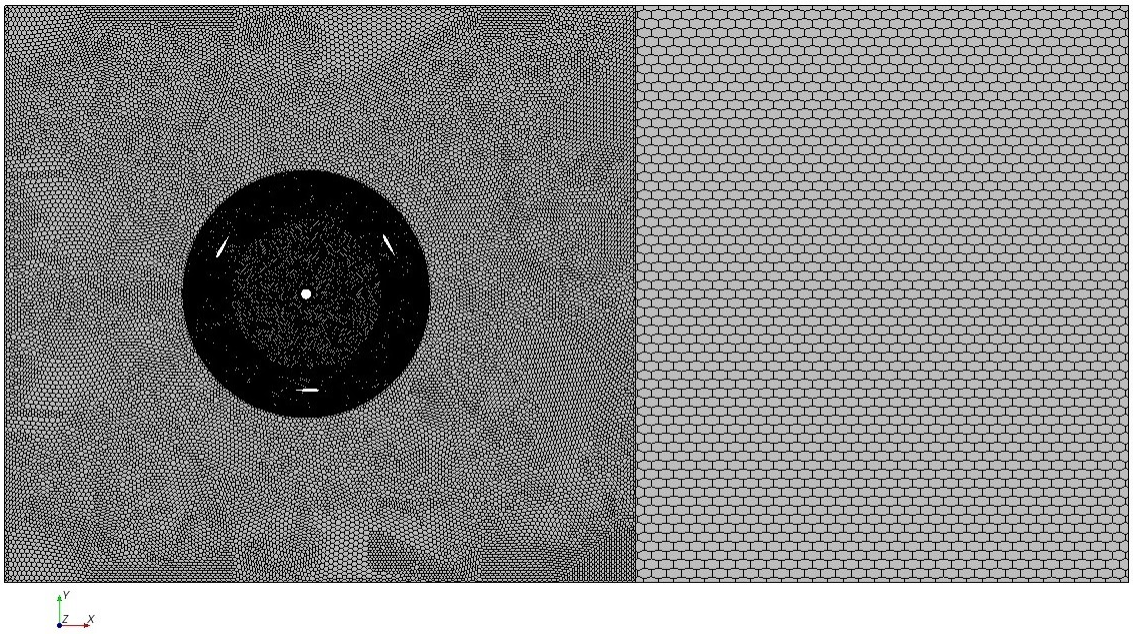

Figure 4.6: General view of the meshed domain. 2-D model. NACA 0015.

Boundary Conditions

Following up with the description of the flow domain introduced previously, the imposed boundaries conditions are discussed here.

The front face of the domain, upstream of the turbine, is defined as a velocity inlet. For the analyses described in this section, the flow is defined with a magnitude equal to $5m/s$ and with an intensity of turbulence of 1% to set the condition away from a perfectly aligned incident flow.

The back face of the domain, downstream of the turbine, is defined as a pressure outlet to allow the outflow.

Concerning the lateral faces of the domain, in this stage of the design the objective was not oriented to compare the numerical computations to experimental results in wind

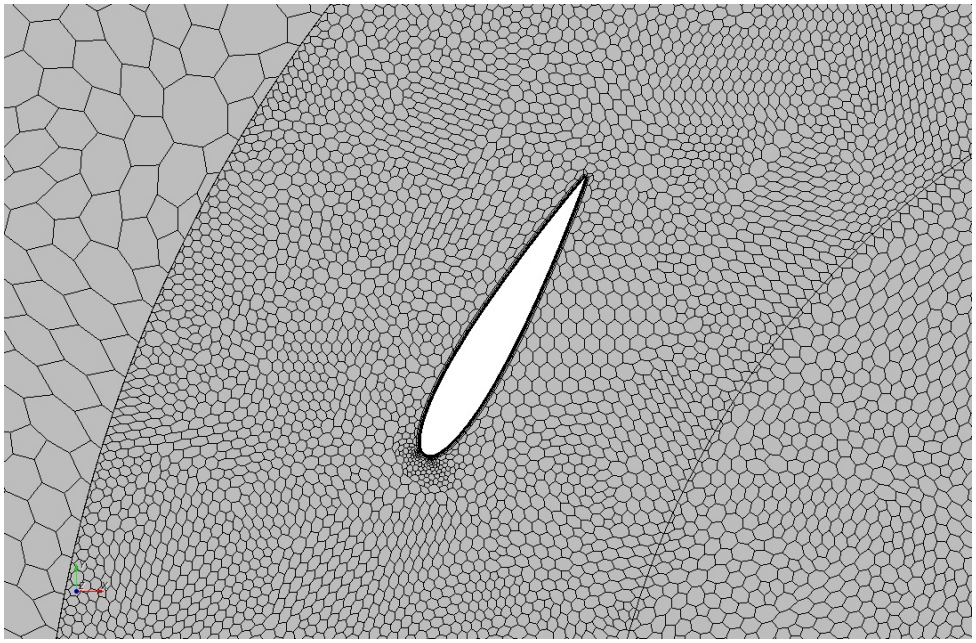

Figure 4.7: Detailed view of the mesh around the airfoils. 2-D model. NACA 0015.

tunnel and, therefore, the effect of the wall friction was not considered establishing a slip condition.

With respect to the blades, they are defined as non slip walls, with a wall treatment that will be described in the next section.

One last type of internal boundary had to be set due to the existence of multiple zones in the domain. In order to ensure the continuity of the flow variables across the meshes, interfaces are defined in the limits of each zone, either static or rotating.

Turbulence Modeling

The simulation of the flow field turbulence constitutes one of the most critical issues when performing a CFD model. This area has been an object of research for a long time. The details of the different models will not be discussed here as it is a topic widely discussed in the bibliography (Launder and Spalding, 1974; Ferziger and Perić, 2002; Wilcox, 2006; CFDORN, 2005–2012).

In this case, taking into account the available computational resources and the number of simulations to be performed, the flow field was modeled with the Reynolds Averaged Navier–Stokes equations (RANS) complemented by a turbulence model and wall functions to give closure to the problem. Logically, the choice of the turbulence model will have an effect not only in the resultant flow field but also in the computational cost of the simulation.

From the two-equation turbulence models, one of the most widely used is the k–ϵ model,

that uses a transport equation for the kinetic energy k and another one for the turbulence dissipation rate ϵ. In general, this is a robust model with an acceptable accuracy for a wide set of turbulent flows. Another variation of this model, the *Realizable* $k - \epsilon$ model developed by Shih *et al.* (1994), incorporates mathematical constraints on the Reynolds stresses, in consistence with the physics of the turbulent flows. In general, this implies a better performance for flows with rotation, detachment and recirculation. From the models available in the software, this last one is used to perform the calculations.

A *Two-Layer* approach with *All y+ Wall Treatment* is also implemented. This is a hybrid treatment that is expected to give reasonable results for intermediate meshes like the one used here.

Solver Details and Calculation Parameters

Once the models for the different preselected airfoils of Table 3.1 are built according to the previously discussed characteristics, it only remains to set the simulations parameters and conditions in order to proceed with the calculations.

One of the most important parameters is related to the simulation time step. If its value is too large, the model will not be able to capture certain flow structures whose time of development is much smaller than it. An analogy of this can be made up to certain degree with the sampling theory, where the effect of the aliasing can result in misleading results.

On the other hand, a time step that is too small will significantly increase the computational cost of the simulation, to the level of making it impractical for the case of study. There are also other effects which lay behind the scope of this work regarding the dependence of the selected turbulence model with the time step.

Many previous works dealt with the CFD modeling of VAWTs (Strickland *et al.*, 1980; Allet *et al.*, 1999; Ponta and Jacovkis, 2001; Ferreira *et al.*, 2007a; Dixon, 2008, among others) and the where effect of the time step was analyzed. In this case and based on previous works performed at ICAM in the context of the project (Brunellière and Bibard, 2011), a time step corresponding to one degree of azimuthal rotation of the turbine was determined to be an adequate value with an acceptable calculation time. As the rotational speed can change among simulations, the time step will also change, as it can be observed in equation (4.1).

$$\Delta t = \frac{1^\circ}{\omega}\,\frac{\pi}{180^\circ} = \frac{0.01745}{\omega} \tag{4.1}$$

It should be noted, however, that as it was shown by Ferreira *et al.* (2007b), the chosen value for the time step can lead to an underestimation of the generation and evolution of the vorticity over the airfoils, depending on the adopted turbulence model. As the objective of these simulations is to compare a series of airfoils, it was decided to proceed

with the adopted value in this preliminary stage of the design.

Concerning the simulation time, it should be assured that the effect of the initialization of the solution is not affecting the results. In relation to this problem, the results corresponding to the first turn of the turbine are not reliable and should be disregarded. If the influence of the turbulence of the incident flow is considered, the results will vary at each turn. It is reasonable to perform a simulation comprising several turns and then obtain an averaged value of the parameters of interest. In this case, due to the time constraints of the project and taking into account the objective of this series of tests, the results for the third turn of the turbine are considered for the analysis.

Considering N_T number of turns, the total time for the simulation, t_{sim}, can be expressed as in equation (4.2).

$$t_{sim} = \frac{2\pi N_T}{\omega} \tag{4.2}$$

The last important parameter that will be discussed here, the rotational speed of the turbine, was introduced in the previous equation. As it was mentioned, the simulation is done imposing a rotational speed to the blades and then analyzing the flow and performance characteristics of the turbine. As the parameter that is being considered as a reference for the rotational speed is the tip speed ratio (λ), it is possible to isolate ω as a function of this parameter from equation (2.3) of Chapter 2. The final expression can be found in equation (4.3).

$$\omega = \frac{V_\infty \lambda}{R} \tag{4.3}$$

In this case, six different rotational speeds are analyzed for each airfoil. The recovered information will be then used to build the curve of the efficiency versus the tip speed ratio (C_P vs. λ) as shown in subsection 2.2.3.

In Table 4.2, the calculation parameters employed for the simulations are summarized.

Convergence Criteria

As CFD problems are generally non–lin

In this case, the presence of turbulent flow that is inherently unstable deems necessary to establish a convergence criteria for the iterations within each time step, in an attempt to obtain the best solution possible.

The convergence will be measured by the level of residuals, as they give an indication of the amount by which the discretized equations are not satisfied. The parameters chosen as indicators of convergence are the momentum in the x and y direction, the turbulent kinematic energy and the turbulent dissipation rate. Previous works (Brunellière and Bibard, 2011) determined the acceptable value for the residuals as $1{\times}10^{-3}$.

Table 4.2: Calculation parameter for the simulations.

λ	ω [rad/s]	ω [RPM]	$\Delta t \times 10^{-3}$ [s]
1	7.14	68	2.44
1.5	10.71	102	1.63
2	14.29	136	1.22
2.5	17.86	171	0.97
3	21.43	205	0.81
3.5	25.00	239	0.69

4.2.2 Simulation Results and Analysis

The models described previously were solved by the CFD software and the obtained results are presented here taking into account two different parts, one concerning the generated torque and the consequent efficiency of the different airfoils and another one related to the pressure distribution around the airfoils.

Efficiency Evaluation

To proceed with the analysis, for each simulation the torque for each blade was extracted in order to obtain the overall torque of the turbine. As it has been detailed in Subsection 2.2.3, from that information it is possible to obtain the average value for the torque and the extracted power.

As twelve different models were simulated at six different rotational speeds, the obtained information is represented here for a particular case and the main results are summarized for the rest. Detailed results can be found in Appendix C.

In Figure 4.8, the torque variation along a turn for the airfoil NACA 2415 is represented for a rotational speed corresponding to $\lambda = 3$. The contribution of each individual blade to the overall torque can be observed. As expected, each blade has a similar behavior, with a phase shift of 120° between them.

Taking into account the available energy in the freestream, the efficiency for all the simulated cases is computed according to equation (2.19) and the results are summarized in Table 4.3. In the same way, it is possible to present the same results graphically to have a global view of the performance of all the airfoils, as shown in Figure 4.9.

In order to present the results more clearly, the effect of the curvature and the thickness will be analyzed separately focusing on the shapes of the curves but not in the absolute value of the results.

First of all, the influence of the curvature is considered. In Figure 4.10, the curves for

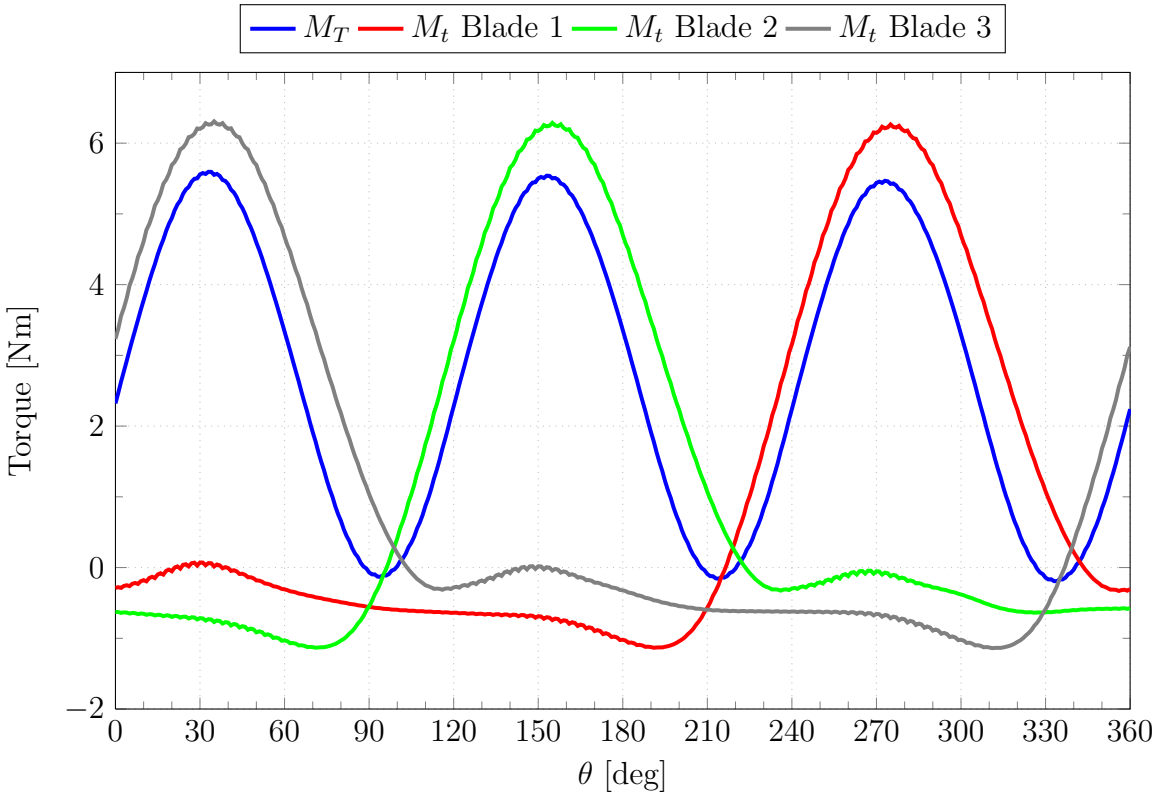

Figure 4.8: Torque along a turn. 2–D model, NACA 2415, $\lambda = 3$.

Table 4.3: C_P as a function of λ for the selected NACA airfoils. 2–D model.

λ	**0012**	**0015**	**0018**	**2412**	**2415**	**2418**	**4412**	**4415**	**4418**	**6412**	**6415**	**6418**
1	0.003	0.016	0.013	0.003	0.002	-0.012	-0.001	-0.017	0.006	-0.021	0.005	-0.003
1.5	0.057	0.139	0.152	0.042	0.089	0.141	0.033	0.029	0.082	-0.013	0.148	0.050
2	0.200	0.332	0.334	0.177	0.273	0.245	0.066	0.201	0.238	0.059	0.244	0.189
2.5	0.464	0.582	0.577	0.432	0.505	0.522	0.304	0.362	0.392	0.263	0.384	0.286
3	0.593	0.587	0.548	0.585	0.567	0.530	0.513	0.516	0.479	0.373	0.511	0.396
3.5	0.498	0.466	0.416	0.493	0.453	0.400	0.452	0.399	0.336	0.299	0.397	0.250

the four different curvatures for an airfoil with a thickness of 12% can be found. It can be observed that as the curvature increases, the peak value tends to decrease. In the same way, a similar behavior can be seen in Figure 4.11 and Figure 4.12 for airfoils with a thickness of 15% and 18% respectively.

Regarding the effect of the thickness in the airfoil behavior, in Figure 4.13 the curves corresponding for the symmetric airfoil and the three different considered thicknesses can be found. Similarly, in Figure 4.14, Figure 4.15 and Figure 4.16 analogous curves can be found for the airfoils with a curvature of 2%, 4% and 6%, respectively. However, in this case it is not possible to detect a marked trend in the effect of the thickness and, therefore, the results are inconclusive.

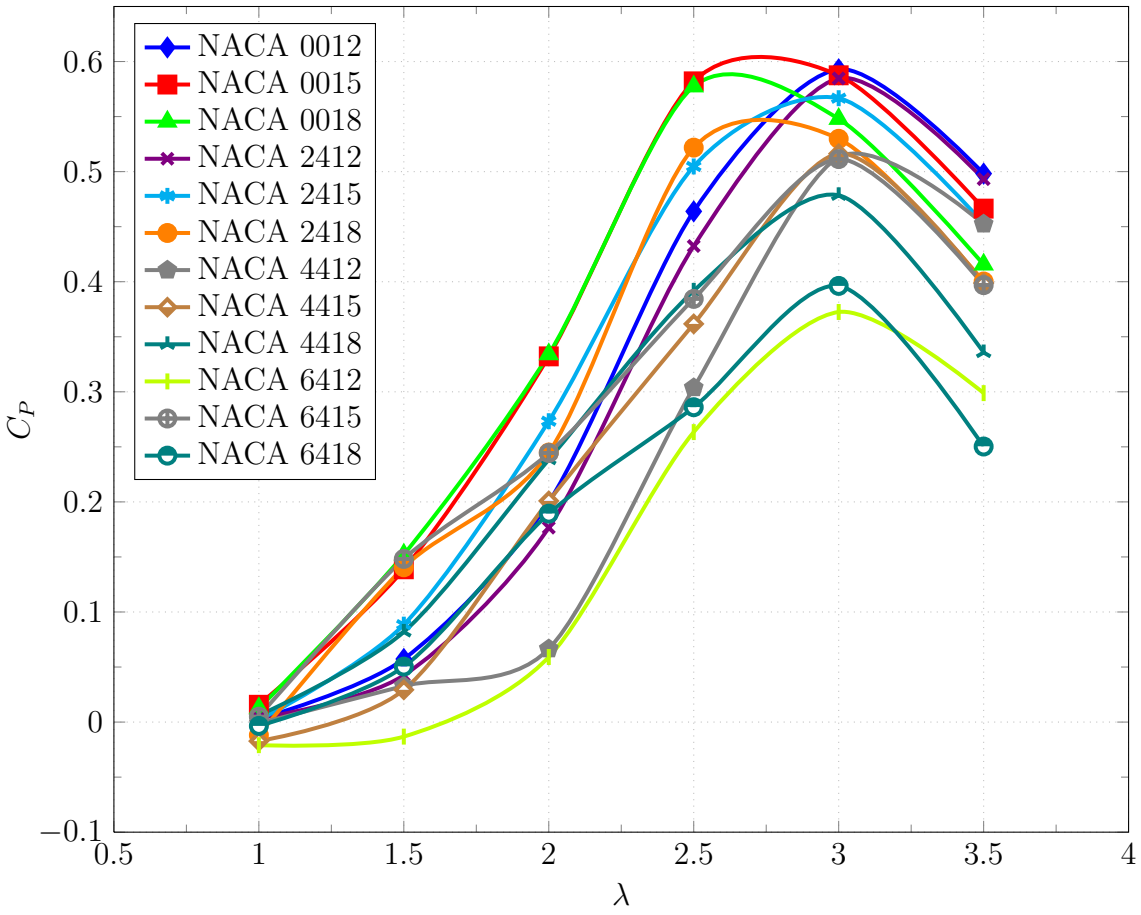

Figure 4.9: C_P as a function of λ for the selected NACA airfoils. 2–D model.

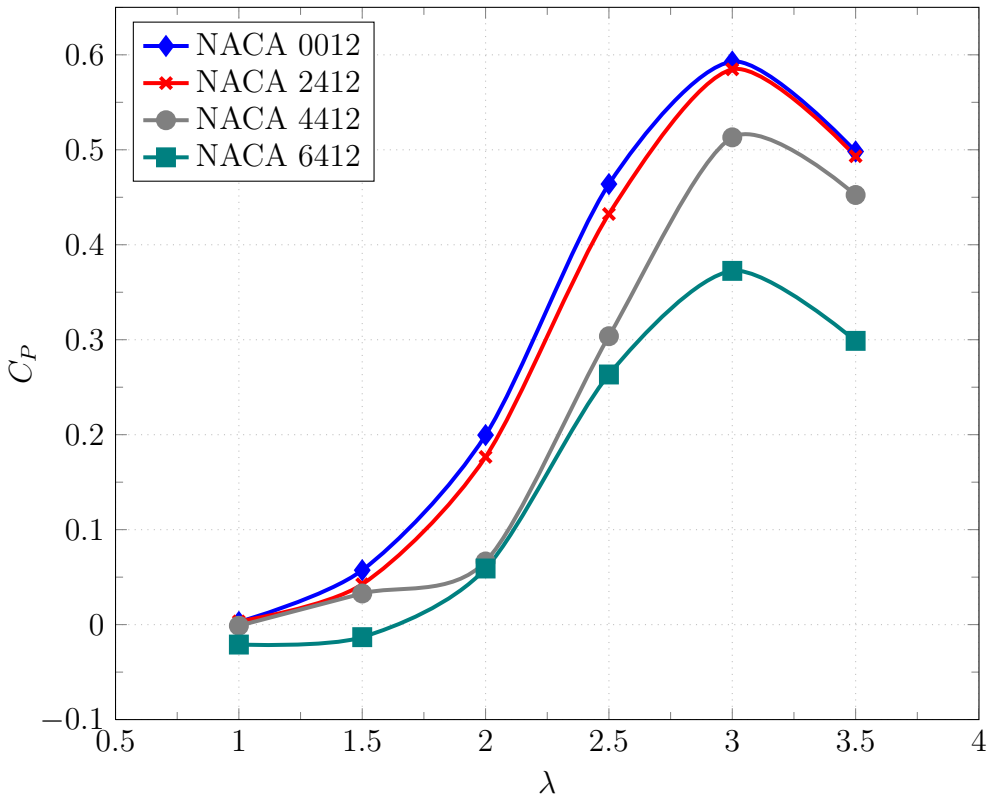

Figure 4.10: Effect of the airfoil curvature in C_P. NACA XX12. 2–D models.

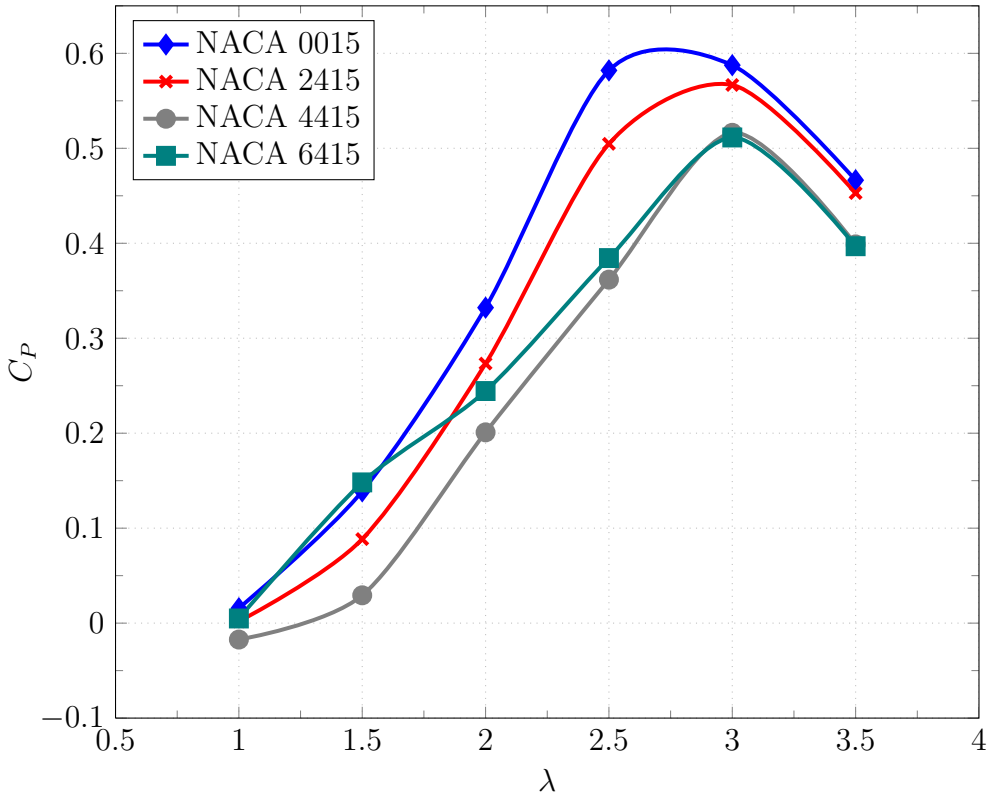

Figure 4.11: Effect of the airfoil curvature in C_P. NACA XX15. 2–D models.

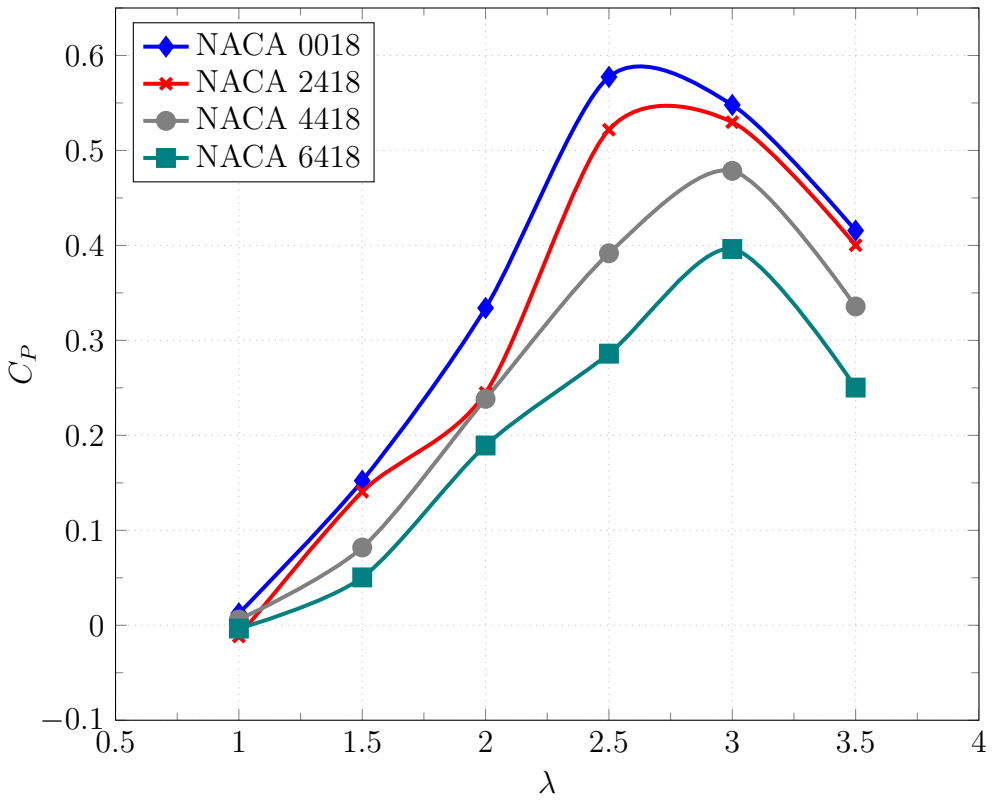

Figure 4.12: Effect of the airfoil curvature in C_P. NACA XX18. 2–D models.

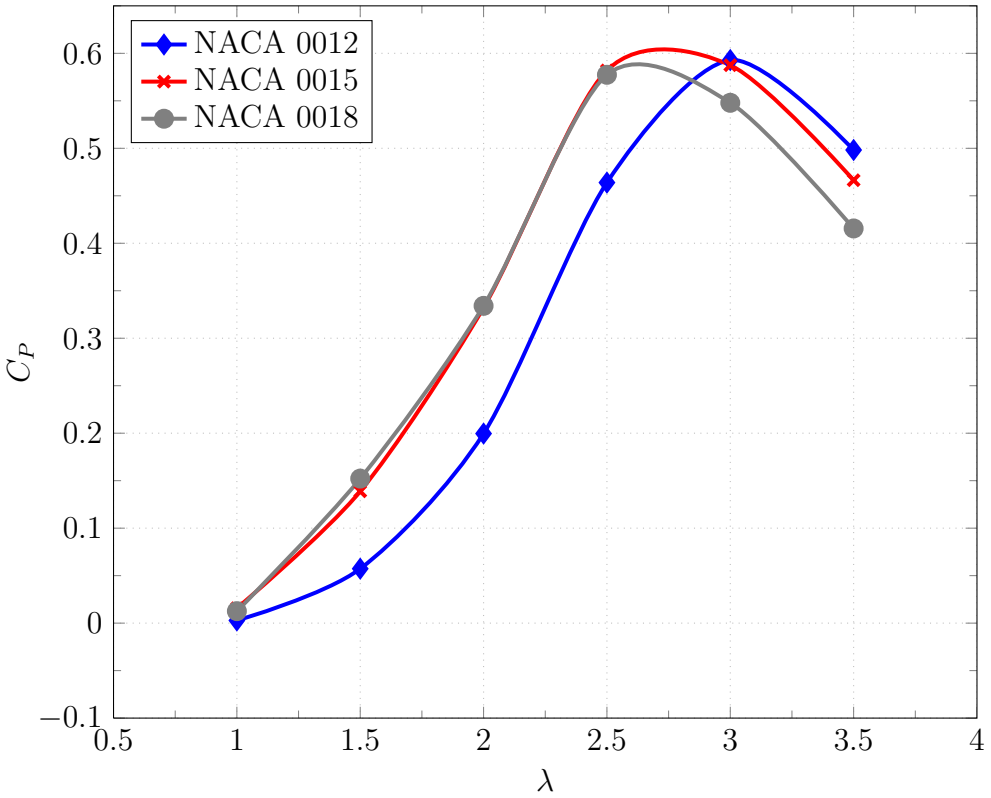

Figure 4.13: Effect of the airfoil thickness in C_P. NACA 00XX. 2–D models.

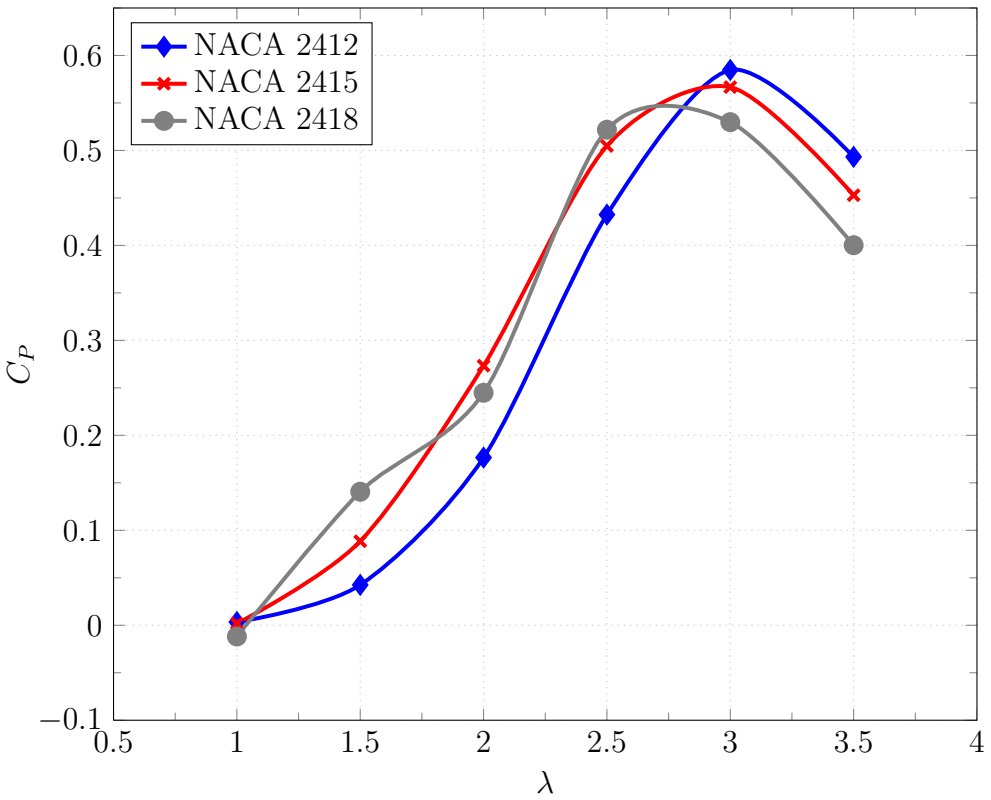

Figure 4.14: Effect of the airfoil thickness in C_P. NACA 24XX. 2–D models.

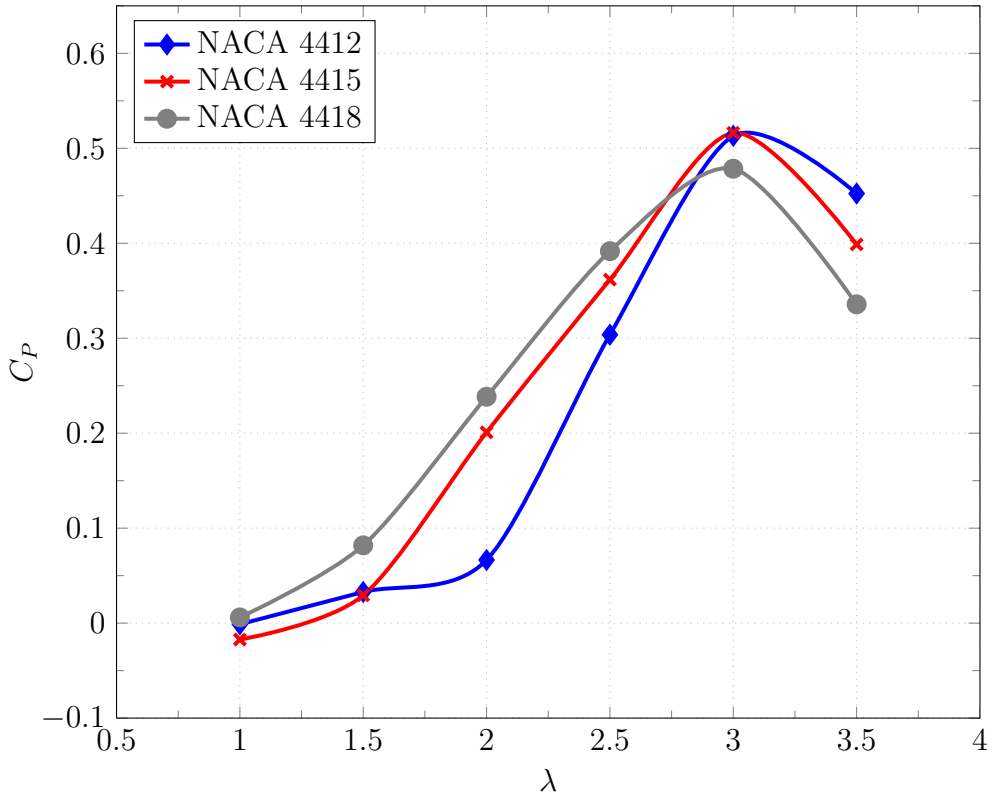

Figure 4.15: Effect of the airfoil thickness in C_P. NACA 44XX. 2–D models.

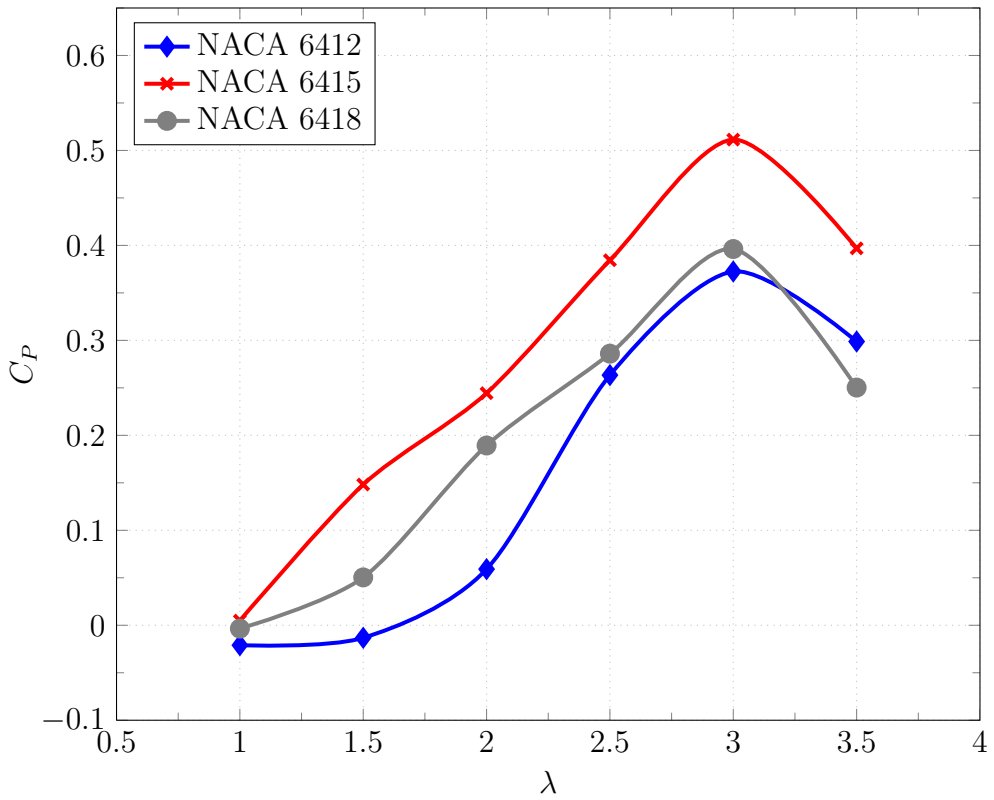

Figure 4.16: Effect of the airfoil thickness in C_P. NACA 64XX. 2–D models.

To sum up, the analysis of the previous figures leads to the conclusion that it is not possible to observe a clear effect caused by the change of airfoil thickness, more than a tendency of the efficiency to improve when the thickness is increased from 12% to 15%. Regarding the effect of the curvature, as it increases the maximum peak in the efficiency curve is reduced in what should be the operational range of λ for the turbine. Considering the range of lower values of λ, a consistent change in the curves is not observed.

Before proceeding, the previous analysis raised questions concerning the validity of the results and, therefore, a deeper analysis is deemed necessary. In order to do that, the curves will be analyzed considering two different zones separately: low and high rotational speed.

For the high rotational speeds of the turbine (high λ), one of the first things that can be noted is the peak values of the curves. As it has been mentioned in Section 2.3, the maximum efficiency for an actuator disk is found to be 59.3%, which is equivalent to have $C_P = 0.593$. If the derivation for the maximum efficiency specifically developed for VAWTs with the double actuator disk theory is considered, the limit corresponds to $C_P = 0.64$. In this case, the maximum values of some of the curves are close to this limit. Despite the fact that the simulation corresponds to an ideal case of a turbine of infinite length and, therefore, higher efficiencies than the real case are expected, it was shown by many authors (Ferreira *et al.*, 2007b; Howell *et al.*, 2010; Dragomirescu, 2011, among others) that the maximum efficiency for VAWTs is far from the theoretical maximum. Therefore, the results in this area should be considered qualitatively.

In the low rotational speeds (low λ), an unusual behavior is observed. As it has been discussed in Subsection 2.2.8 regarding the self–starting characteristics of VAWTs, the use of symmetric airfoils in a straight bladed turbine (equivalent to the infinite model simulated here) results in a non self–starting turbine. As the efficiency is related to the generated torque, this corresponds to negative values of C_P at low rotational speeds. However, the results of the simulations are not in accordance with the expected physics of the problem and most of the airfoils present positive values of C_P for $1 < \lambda < 1.5$. Even more interesting is the fact that one of the airfoils with greater curvature and, therefore, better self–starting characteristics, the NACA 6412, is one of the few whose results correspond to negative values of C_P for low values of λ.

Looking closely at the conditions of the flow for the low range of λ, it is not difficult to find an explanation for the misleading results of the simulations. As it was shown in Figures 4.1 and 4.2, as the rotational speed decreases, the angle of incidence of the flow increases whereas the incident velocity decreases. The first has an effect on the aerodynamic behavior of the airfoil, with flow detachment and highly turbulent flow. The last implies a reduction of the local Reynolds number, which could lead to the generation of laminar separation bubbles, as explained in Subsection 2.2.7.

To have a better understanding of the results, the evolution of the total torque along a turn for an arbitrary airfoil (NACA 2415 in this case) at different rotational velocities is presented in Figure 4.17.

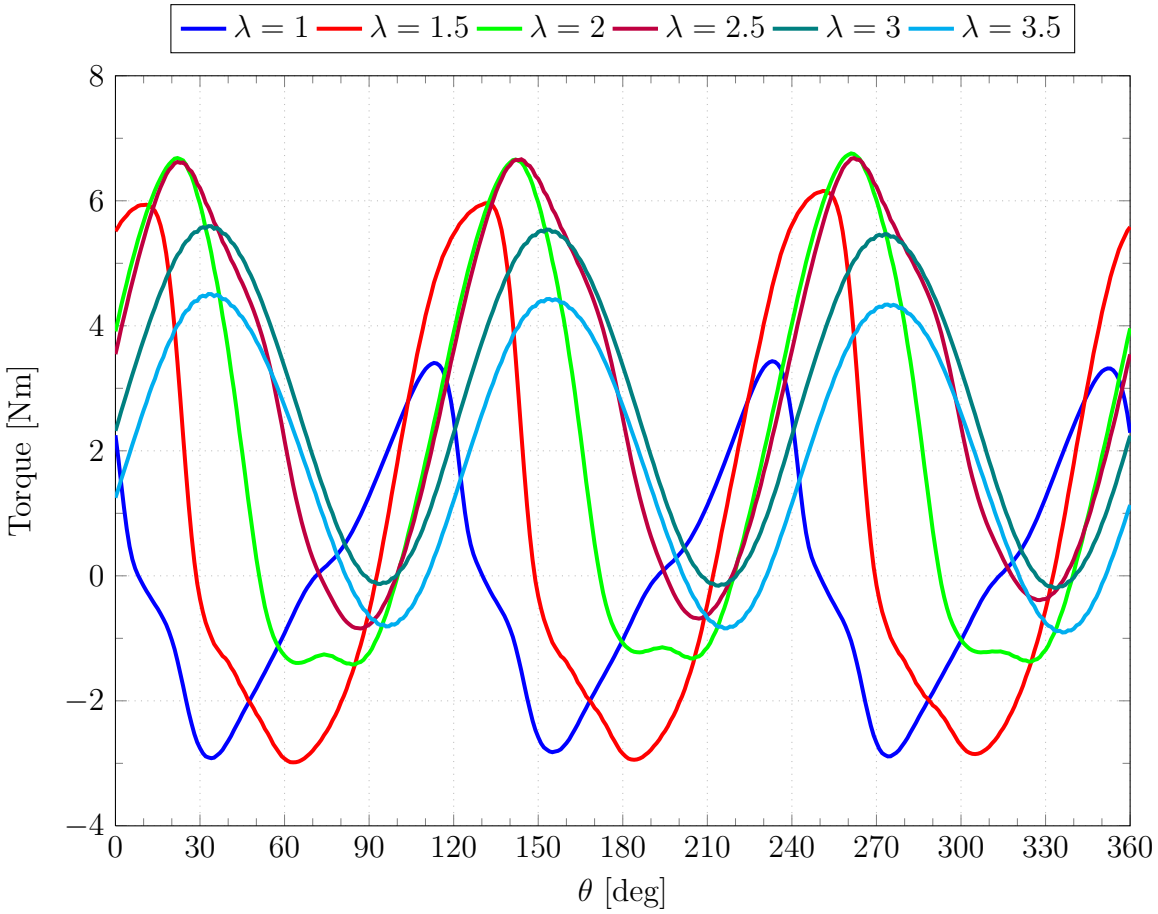

Figure 4.17: Total torque along a turn for different λ. 2–D model, NACA 2415

It can be observed that, for $\lambda \leq 2.5$, the curves present more oscillatory shapes, associated with the increase in the vortex shedding during the simulation. This can also be verified if the flow pattern is observed. As an example, in Figure 4.18 the flow pattern based on the pressure distribution at $\lambda = 1$ for six different intervals along a turn can be observed.

Analyzing the case of low rotational speed of the turbine (Figure 4.18), it can be observed in (a) how for the airfoil in the upwind section the high angle of attack of the flow encourages the generation of a low pressure zone, leading to the separation of the boundary layer due to the adverse pressure gradient. Subsequently, in (b) the vortex detaches from the airfoil's extrados. In (c) it can be seen how a second vortex is shed from the trailing edge. From (d) to (f), the vortices travel downstream. As the airfoil is also moving downstream, they affect its pressure distribution, even when their intensity is progressively decreasing. This phenomenon has already been described in Subsection 2.2.5 when discussing the doublet of counter rotating vortices traveling downstream as they increase in size, product of the dynamic stall.

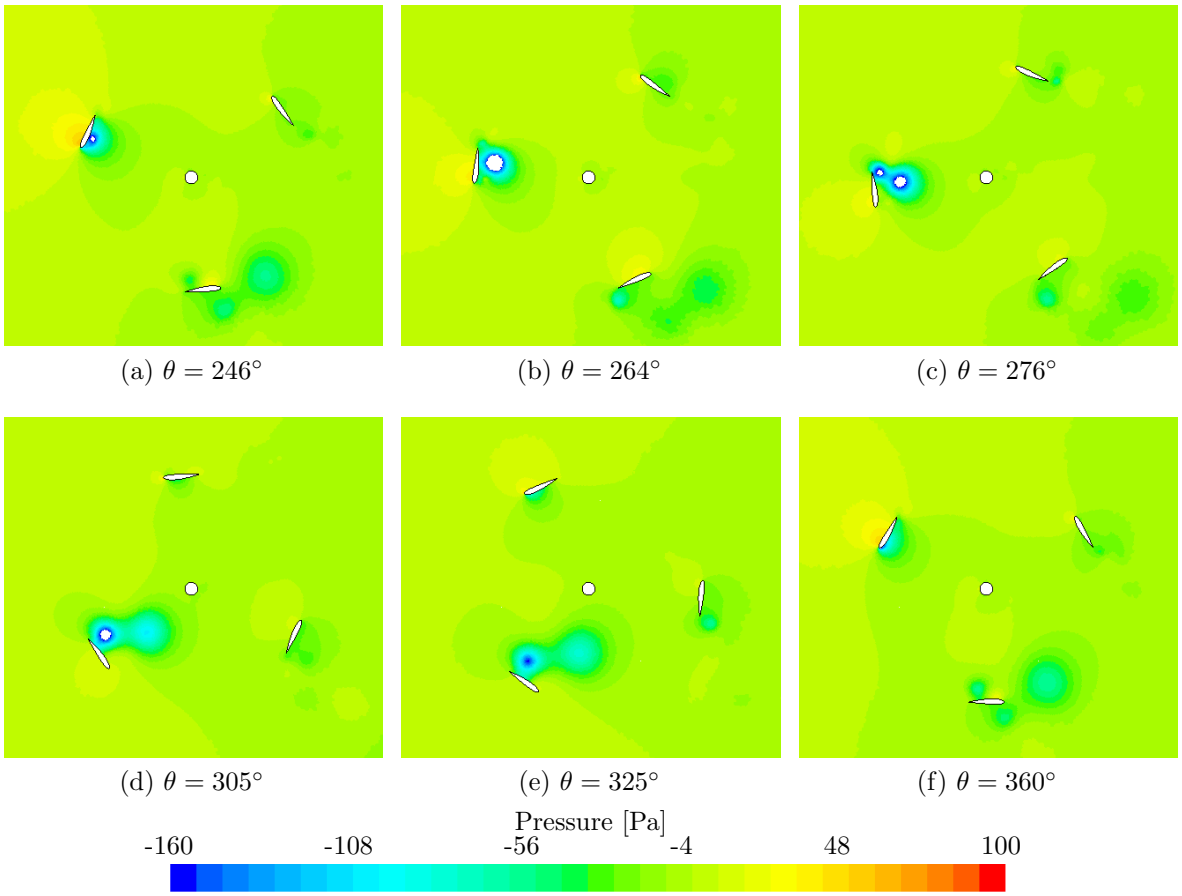

Figure 4.18: Pressure field along the simulation. 2-D model, NACA 2415, $\lambda = 1$.

As mentioned before, the generation and shedding of the vortices can be observed in the total torque curve of Figure 4.17 as oscillations or sudden changes of its intensity.

Recalling what has been discussed in Subsection 4.1.2, it is evident now how the vortex shedding can alter the moment produced by the blades in the downwind side of the turbine, making the estimation of the performance by means of steady–state airfoil data unreliable.

If now the case for the same airfoil at $\lambda = 3$ is considered (Figure 4.19), the differences that can be observed in the flow pattern are evident. In the sub-figures (a) to (c), the low pressure zone in the extrados of the upwind airfoil can be distinguished. However, as the angle of incidence is lower than in the previous case (see Figure 4.1), the detachment of the boundary layer is not as evident. In the following time intervals, as the airfoil moves towards the downwind section of the turn ((d) to (f)), the pressure difference between the intrados and the extrados decreases and vortices can be observed traveling downwind.

Recalling the description of the turbulence model used in these simulations (Subsection 4.2.1), there are obviously limitations on the particularities of the flow that can be properly detected and represented here, especially at the lower Reynolds number range. This was also shown by Ferreira *et al.* (2007b), remarking the unsuitability of using a single turbulence model scheme for the numerical simulation of a 2-D Darrieus turbine at

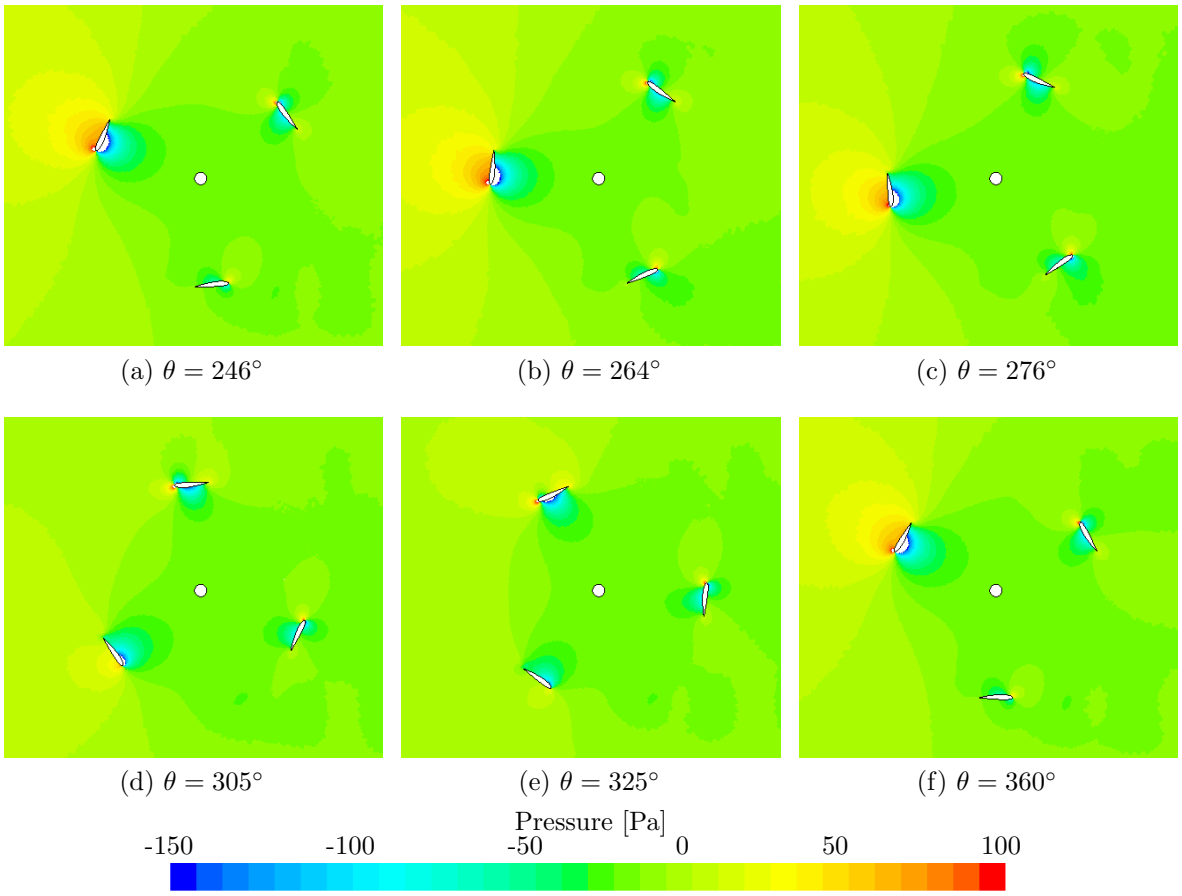

Figure 4.19: Pressure field results. 2–D model, NACA 2415, $\lambda = 3$.

low tip speed ratios due to the presence of dynamic stall.

If the hypothesis that the uncertainty in the simulation affects all the cases similarly is adopted, the zone of the graph corresponding to $\lambda \geq 2$ could be used for a comparative analysis between the profiles. However, at the lower Reynolds numbers, this hypothesis lacks foundations as it is possible to be in the limit of applicability of the turbulence model and therefore, the small variations in the mesh characteristics in the vicinity of the different airfoils could have an important effect on the way the solution converges. As a consequence of this, that zone of the curve will not be considered as a valid representation of the physics of the turbine.

Another aspect that could be affecting the results is related to the grid characteristics. As it has been mentioned, it was decided to use similar mesh sizes as the ones employed in previous works at ICAM. However, as it is possible that this factor is affecting the results, an attempt to validate the selected grid with the study of one particular design was performed and the details can be found in Appendix B. Although the results of the analysis are not conclusive, further studies in the area are deemed necessary to assure the grid–independence of the solution.

Pressure Distribution over the Airfoils

In the previous analysis, the pressure distribution of the fluid was used as a tool to observe the flow pattern along the simulation. Another logical step consists in observing the pressure exerted on the blades by the fluid. Even though these analyses do not take into account the coupling between the fluid and the structure as mentioned in Section 3.2, this information can be used to estimate the loads on the blades or to proceed with further analysis, as the one described in Chapter 7.

4.3 Selection of Airfoils for Further Analysis

Based on the results of the previous analyses, it was decided to continue the three-dimensional analyses with airfoils having a thickness of 15%. That value showed to have an adequate performance and it is also more convenient from the structural point of view, as will be discussed in Chapter 6. With respect to the curvature, the net effect in the self–starting characteristics of the turbine could not be identified and, therefore, curvatures of 0% and 2% will be further studied. All in all, the range of airfoils is reduced to the NACA 0015 and the NACA 2415.

Chapter 5

Three-dimensional Modeling of the Turbine

Based on the results of the previous chapter, a simplified three-dimensional CFD model of one of the designs of the turbine is presented in Section 5.1, along with the analysis of its results. Section 5.2 focuses on the discussion about the modeling of a more detailed model.

5.1 Study of a Simplified Model of the Turbine

In this case, the CFD model of the three-dimensional turbine is performed. Based on the conclusions of the previous chapter, a single airfoil, the NACA 0015, is chosen to illustrate the procedure. However, in this first stage, certain simplifications are introduced to the geometry in order to reduce the complexity of the model. Further discussion is presented in the following subsection.

5.1.1 Model Description

In order to evaluate the three-dimensional characteristics of the flow during the operation of the turbine, the main simplification that is introduced is the absence of a support structure of any kind for the blades. As it has been discussed in Section 3.4, there are many options to be considered and the simulation and analysis of the selected alternatives should be performed as part of the optimization design process. Further discussion on this topic was presented in Section 3.2.

A similar process as the one presented in Chapter 5 was followed to create the three-dimensional model. The geometry was created with the Computer Assisted Design (CAD) software SolidWorks and the CFD modeling and resolution was done in the software STAR CCM+.

Concerning the details of the construction of the model, a description of the different aspects involved is presented as follows.

Grid Description

The domain under study is a parallelepiped in which the turbine is contained, as shown schematically in Figure 5.1. As an experimental validation of the simulations is planned for future stages of the project, the transversal area of the control volume should be coincident with the test area of the wind tunnel in which the test will be performed. However, as that information is not yet available, the same criteria used for the two-dimensional simulations will be used and its dimensions are set so that the influence of the boundaries with the turbine is minimized. As a consequence, the lateral boundaries and the inlet are set at one turbine diameter of distance from the blades and the outlet is placed at approximately four diameters. For the upper and lower limits, the distance to the turbine is set to 70% of the turbine diameter.

The studied volume is geometrically divided into twelve zones, depending on particular conditions and on the grid density, of which there are four. The zone in which the blades are contained (Zone I) has an hybrid mesh with a structured region in the vicinity of the solid boundaries composed by stretched prismatic elements. As explained before, this is due to the existence of the boundary layer. The rest of the region has unstructured polyhedral elements. Logically, this zone is the sliding one, simulating the motion of the turbine.

Another of the main reasons to divide the control volume in several regions is related to the need of reducing the overall number of elements of the model. In this way, the mesh density by zones decreases as the distance to the turbine increases. Specifically in this case, reducing the size of the model is particularly important in the three-dimensional study as the available computational power is limited.

An attempt to find a compromise solution concerning the mesh density was made but it should be noted that, due to a limitation in the available time and computational resources, it was not possible to perform a study of the sensitivity of the solution with the mesh size. Based on the work of Brunellière and Bibard (2011), (Le Sourne, personal communication) suggested the adoption of similar grid densities as the ones adopted in the aforementioned work during the construction of a previous model of the turbine. The grid base sizes can be found in Table 5.1.

As a consequence, the resultant model has approximately 1.4 million cells and a general view of the mesh can be seen in Figure 5.2. In Figure 5.3, a close up of the airfoil area can be observed, with the prismatic boundary layer elements.

Table 5.1: Grid base sizes for the different zones of the simplified 3-D model.

Zone	**Base size [m]**
I	0.018
II	0.028
III	0.06
IV	0.2

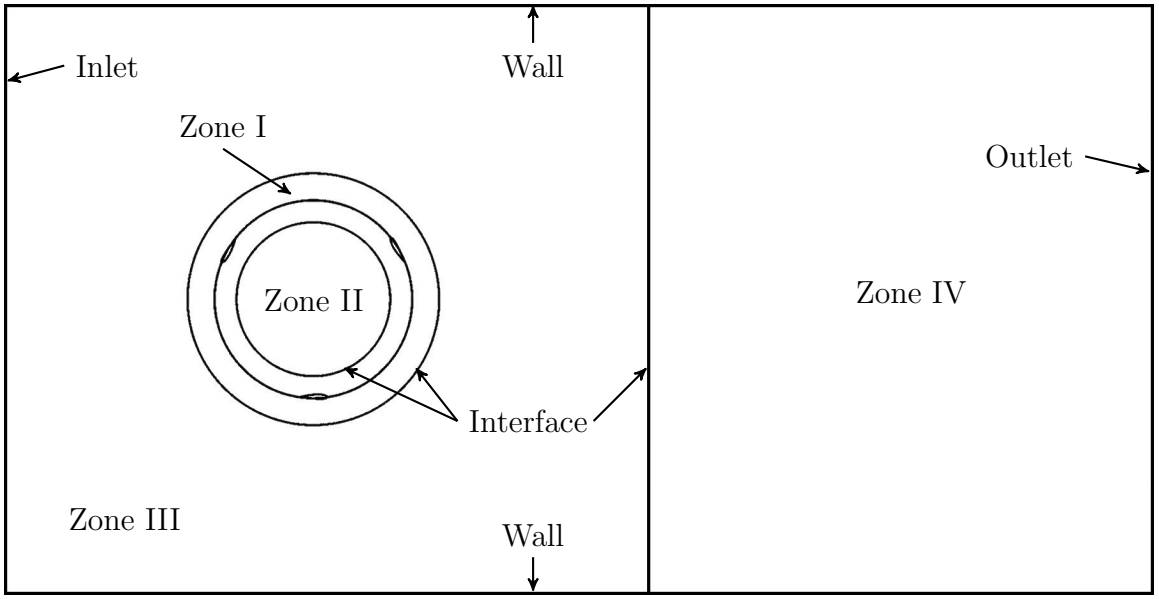

Figure 5.1: Schematic description of the domain under study. 3-D model.

Boundary Conditions

With respect to the boundaries conditions imposed to the control volume, the front face of the domain, upstream of the turbine, is defined as a velocity inlet. Its magnitude is set to $5m/s$ with an intensity of turbulence of 1%. A pressure outlet is set at the back face of the domain, downstream of the turbine.

Concerning the lateral, up and bottom faces of the domain, a slip condition is considered. As it has been mentioned previously, in the case of future simulation for which an experimental validation will be performed, a slip condition with an adequate wall treatment should be adopted. Logically, the blades are defined as non slip walls, whose wall treatment is described in the next section.

Finally, as the domain was split in several regions, internal boundaries had to be set to have continuity in the different flow variables across zones.

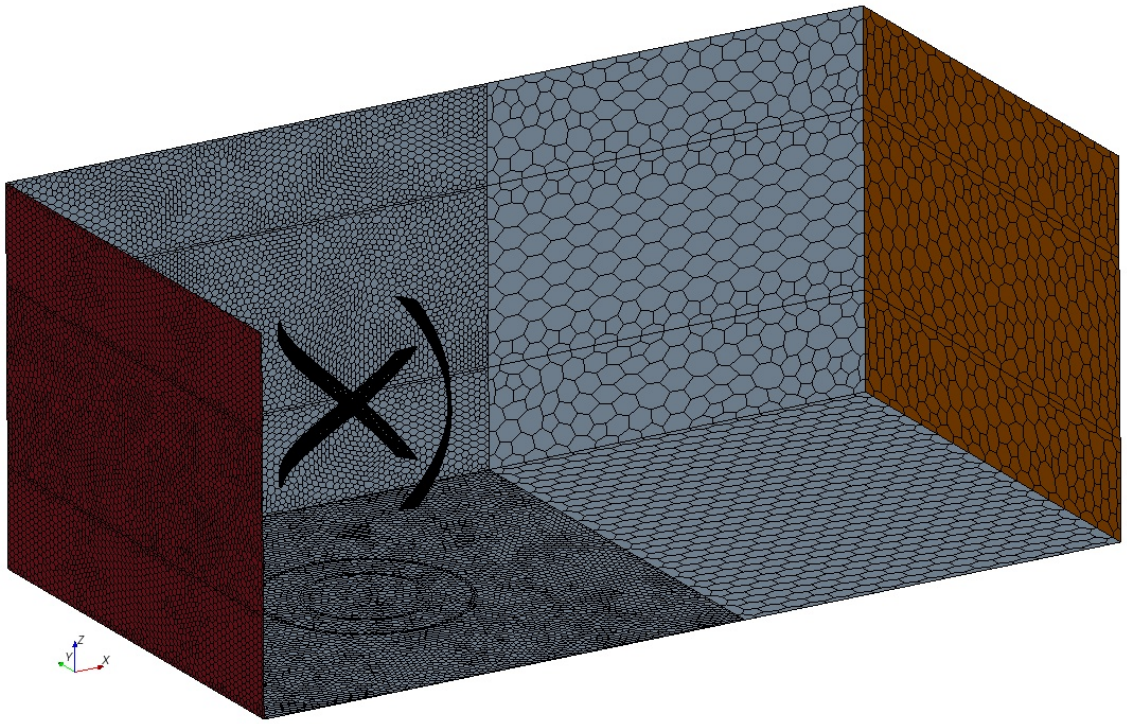

Figure 5.2: General view of the meshed domain. 3-D model. NACA 0015.

Turbulence Modeling

As shown in the previous chapter, the adopted turbulence model is not able to adequately capture the flow phenomena associated with the low rotational speeds of the turbine. Two alternatives that could prove to give more accurate results are available for three-dimensional simulations (See Wilcox, 2006). One of them is the direct numerical simulation (DNS) in which no turbulence model is adopted and, therefore, the solution of the Navier–Stokes equations governing the problem must be done resolving the complete range of temporal and spatial scales of the turbulence. The main disadvantage of this method is, of course, the extremely high computational cost associated with the necessary grid and time steps characteristics. In normal industrial applications like the one concerning this work, implementing this type of modeling is not feasible, being reserved for studies and research in turbulence itself. Another alternative is the use of the model known as large eddy simulation (LES), that separates the treatment of the turbulence into two groups: the large scales and the small scales. As the large scales of the eddies are considered dependent on the geometry of the problem, they are directly simulated. On the other hand, as the smaller scales are considered universal, they are modeled with the consequent reduction in the simulation cost in comparison to DNS. With this type of models, it is possible to solve typical industrial problems like a wind turbine (Iida *et al.*, 2007) wherever a supercomputer is available, as the demand of computational resources is still high. It is due to this last aspect that it was not possible to implement the LES model in this simulation and the combination of Reynolds Averaged Navier–Stokes equations with the

Figure 5.3: Detail view of the mesh around the blades. 3-D model. NACA 0015.

Realizable $k - \epsilon$ model selected for the two-dimensional simulations had to be used.

A *Two-Layer* approach with *All y+ Wall Treatment* is also implemented, expecting to have reasonable results for intermediate meshes like the one used here.

Solver Details and Calculation Parameters

Regarding the different parameters that have to be set to perform the simulations, the ones adopted for the two-dimensional models of Section 4.2 will be also implemented for this model and summarized as follows.

The time step is set as the time required to have an azimuthal rotation of the turbine equal to one degree per calculation step and it is expressed as a function of the rotational speed in equation (4.1). It should be noted that the remarks about the relation between

the time step and the possible variations in the resultant turbulent patterns are still valid but until experimental results are available for comparison, it is not possible to judge the adequacy of the selected time step.

Concerning the rotational speed of the turbine, five different rotational speeds are considered for the simulation to derive its efficiency curve.

Convergence Criteria

The convergence will be measured by the level of the residuals. The parameters chosen as indicators of convergence are the momentum in the x, y and z direction, the turbulent kinematic energy and the turbulent dissipation rate. The limit value is taken as 1×10^{-3}.

5.1.2 Simulation Results and Analysis

Following an analogous procedure to the one used for the two-dimensional simulations, the models were solved by the CFD software and the results are presented as follows.

Efficiency Evaluation

The instantaneous torque values were extracted from each simulation in order to obtain the average value for the torque and the extracted power. As an example, in Figure 5.4 the torque variation along a turn for a rotational speed corresponding to $\lambda = 2.5$ is presented. The contribution of each individual blade to the overall torque and the phase shift of 120° between the peak values of the blades can be observed. Compared to the torque distribution found for the two-dimensional cases (Figure 4.8), it can be seen that the peaks are slightly wider. Regarding the magnitude of the curves, it is not possible to compare them directly as, in this case, the real turbine with a height of $1.4m$ is modeled, whereas in the two-dimensional case the height was of $1m$. Despite this, it can be noted that the relative magnitude of the last curve is lower, what is related to the effect of the blade shape in distributing the loads more evenly along the turn. Detailed calculations and results concerning each simulation can be found in Appendix D.

Taking into account the available energy in the freestream, the efficiency curve can be computed according to equation (2.19) and the results are presented graphically in Figure 5.5. In order to compare the results with the previous analyses, in the same figure the corresponding curve but for the two-dimensional case is also plotted.

In Figure 5.6 the wake of the blades can be observed by means of the vorticity contours in planes perpendicular to the turbine axis at three different positions along the blade.

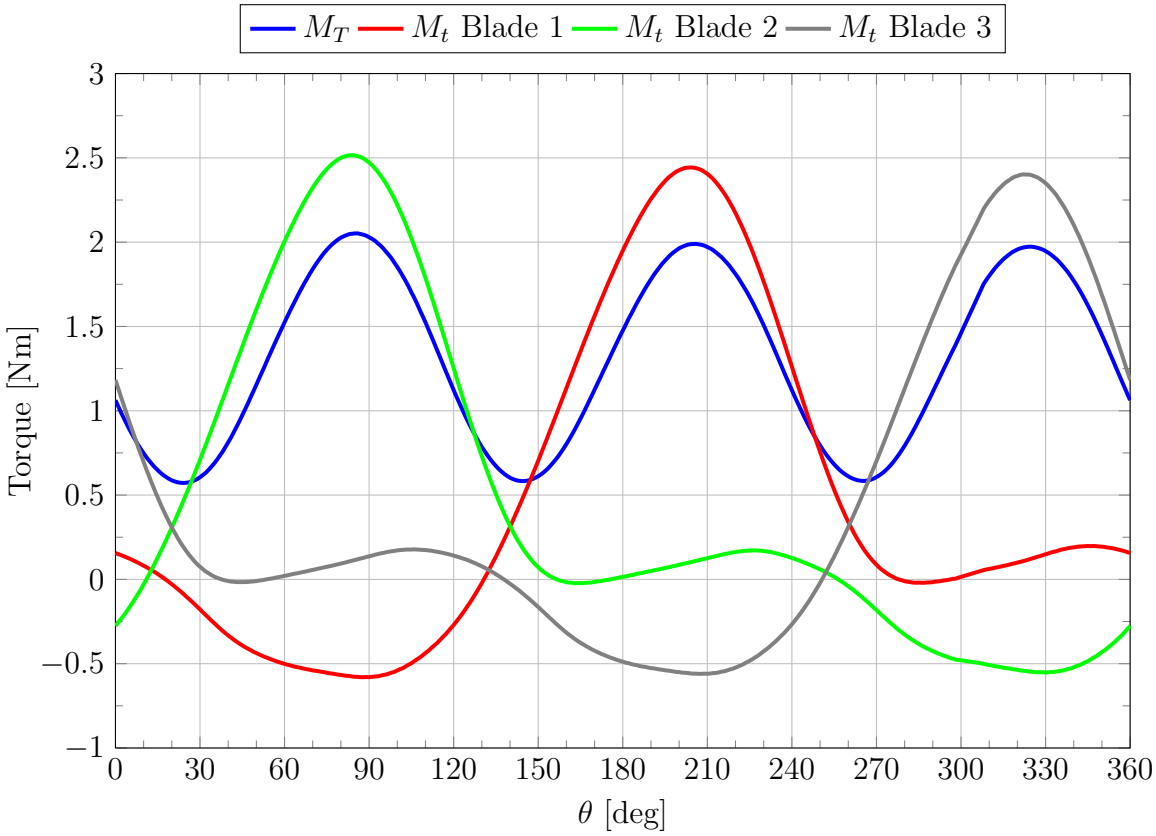

Figure 5.4: Torque along a turn. 3-D model, NACA 0015, $\lambda = 2.5$.

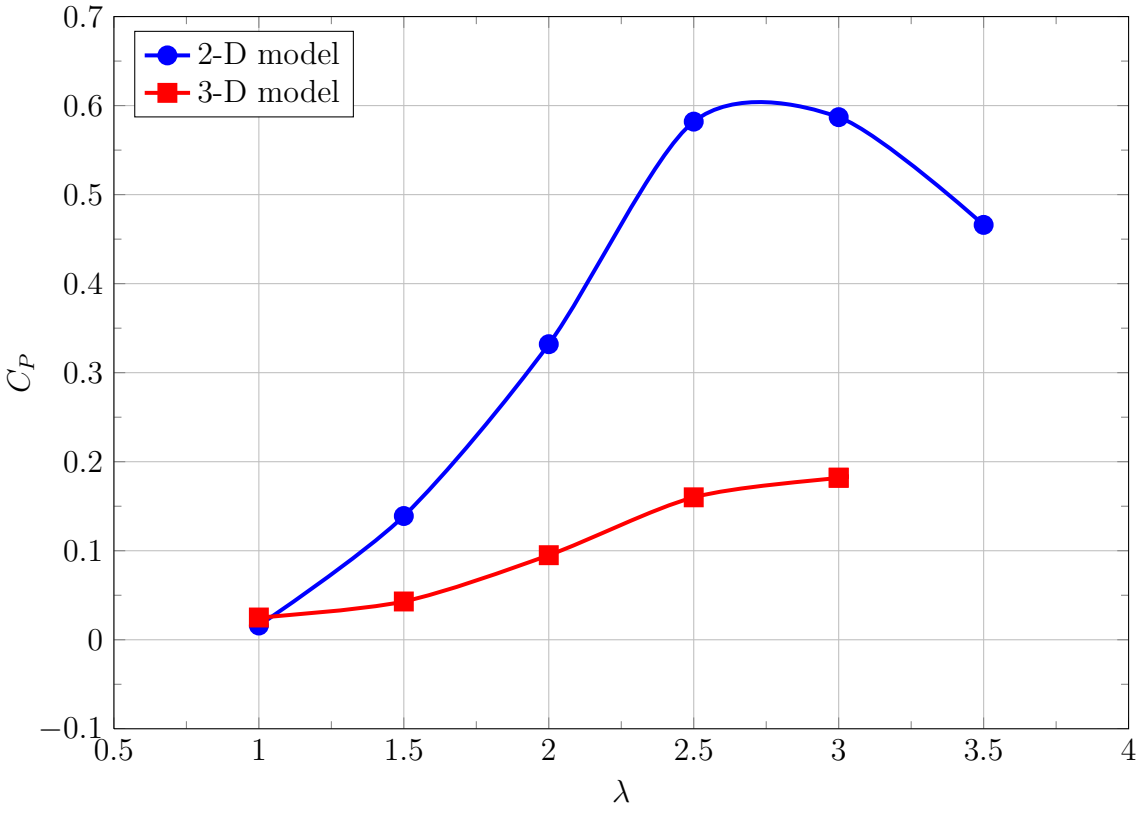

Figure 5.5: C_P vs. λ. Comparison of the 2-D and 3-D models, NACA 0015.

As discussed in Subsection 4.2.2, the peak value for the C_P *vs* λ curve was not realistic. It can be seen here how in the three-dimensional simulation the maximum value is lower. This reduction in the performance of the turbine is associated mainly with the three-dimensional flow pattern that develops in the blade extremities. This phenomenon is not exclusive to VAWTs but is associated to all types of wings with finite span. The pressure difference between the blade's intrados and extrados, responsible for the generation of the aerodynamic forces, must be at equilibrium in the blade extremities. Physically, this is achieved by the generation of tip vortices as the air in the high–pressure zone flows and mixes with the air in the low–pressure zone. In Figure 5.7, contour plots of the flow vorticity at several planes perpendicular to the freestream direction can be found. The effect of the blade tip can be clearly observed for one of the blades, in the lower right corner of the images. It should be also noted that as the support structure between the blades was not modeled, the interaction between both components and the consequent effect on the turbulent structures are not captured.

Pressure Distribution on the Blades

The variation of the pressure distribution along the blades as the turbine turns is very important to assess the structural behavior of its different components. In this case and following what was introduced in Subsection 4.2.2, this information can be used to evaluate the structural response of the turbine and to perform further analyses as the ones discussed in Chapter 7.

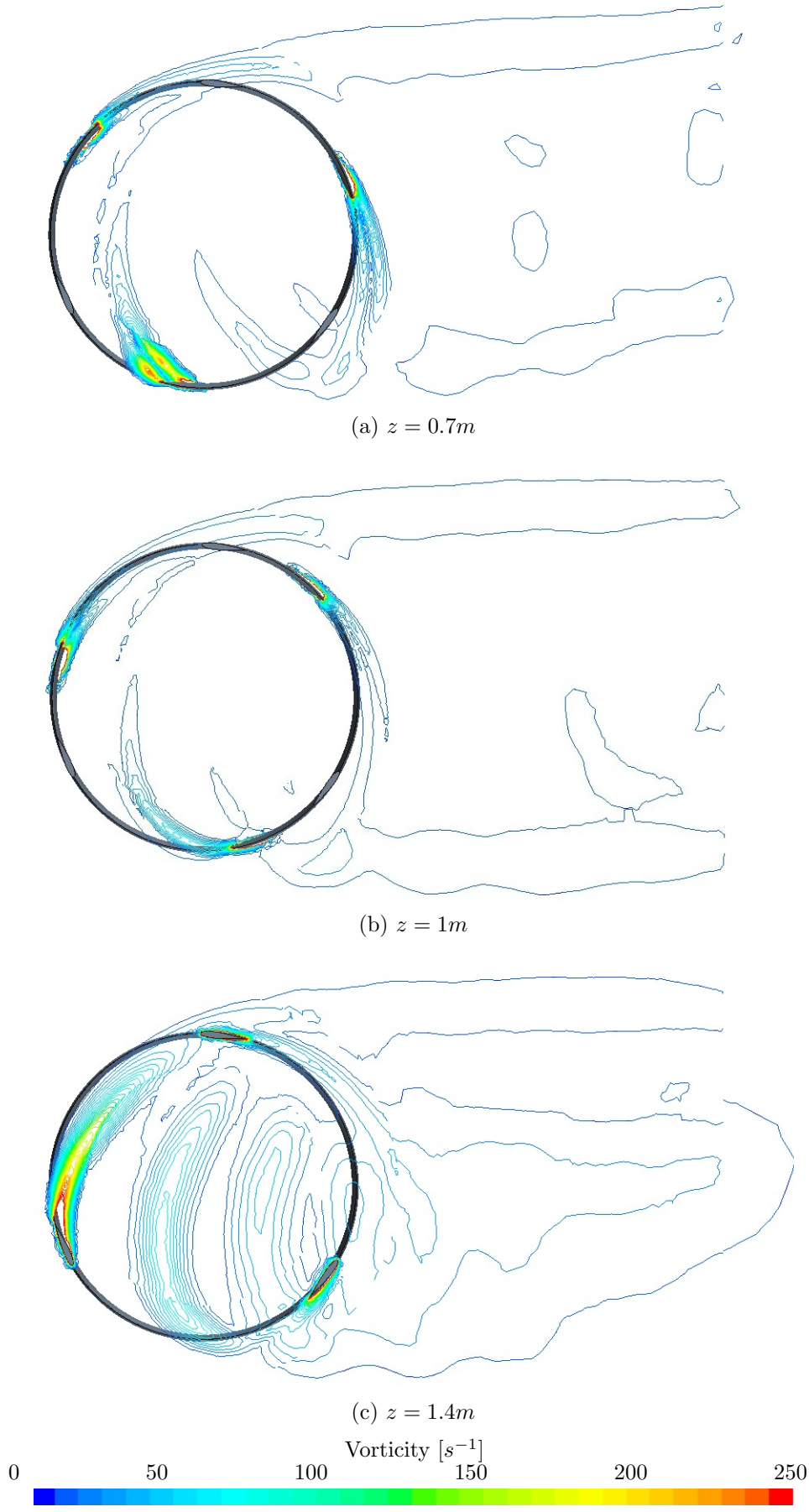

(a) $z = 0.7m$

(b) $z = 1m$

(c) $z = 1.4m$

Figure 5.6: Vorticity contours showing the wake. 3-D model, NACA 0015, $\lambda = 2.5$.

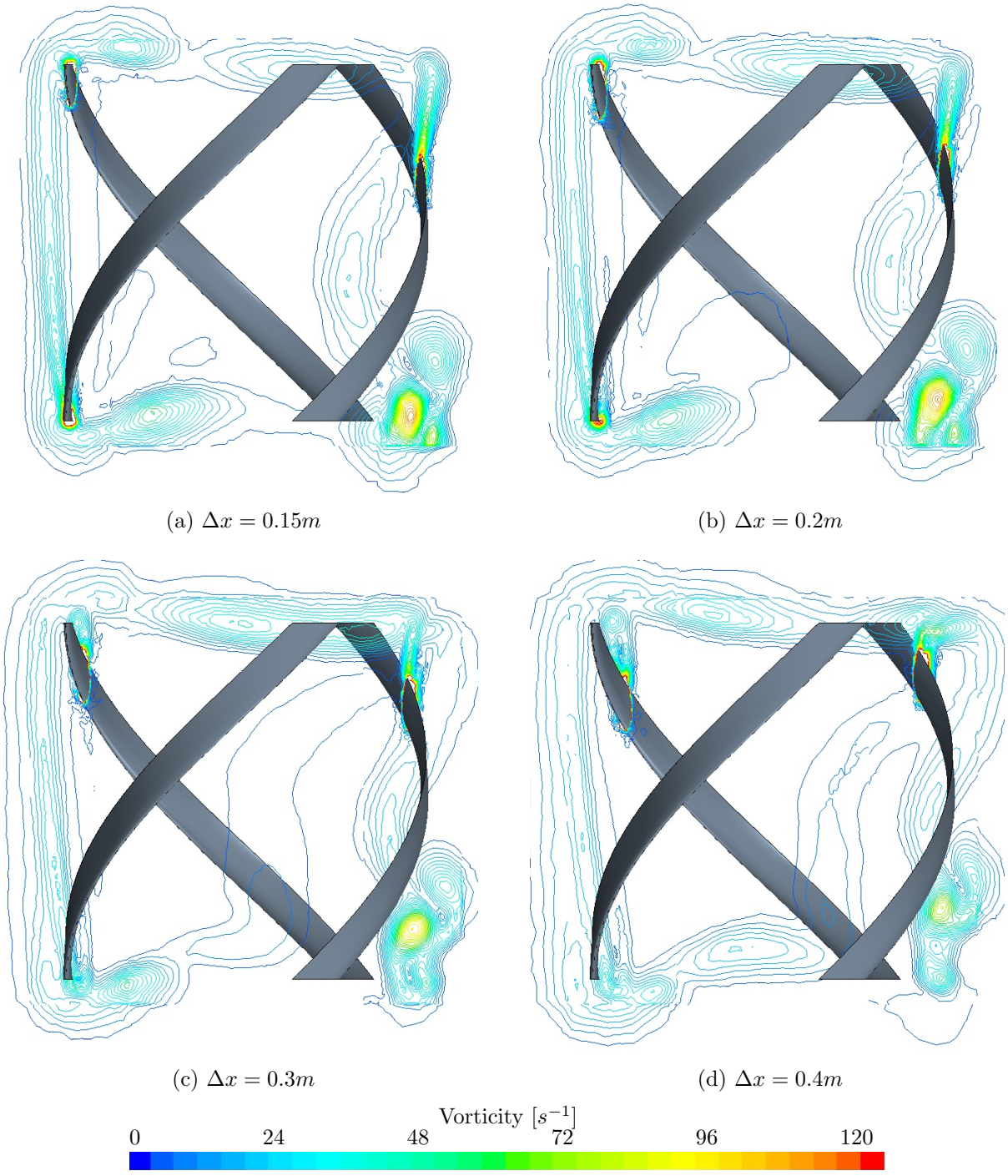

(a) $\Delta x = 0.15m$

(b) $\Delta x = 0.2m$

(c) $\Delta x = 0.3m$

(d) $\Delta x = 0.4m$

Figure 5.7: Vorticity contours showing the tip vortices. 3-D model, NACA 0015, $\lambda = 2.5$.

5.2 Study of a Detailed Model of the Turbine

The next logical step in the simulation process of the turbine is the incorporation of the blades support structure into the models. In that way, a better understanding of the flow dynamics and of the variation of the performance of the turbine for each design can be achieved. Logically, this also implies an increase in the complexity of the model.

In the following subsection, the characteristics adopted for a model including the support structure are detailed.

5.2.1 Model Description

The assessment of the three-dimensional characteristics of the flow for the turbine with the support structure is very important in order to select an adequate design of the interface with the blades. As many alternatives can be used, the model presented here was developed with the idea of allowing switching among different configurations in an easy way, reducing the time of model set up and configuration. It should be noted that even when the model was presented considering a support structure at the blades extremities, it can be easily adapted to alternate locations of the supports as described in Section 3.4.

Concerning the creation of the model, as in the previous simplified version, the geometry was created with the Computer Assisted Design (CAD) software SolidWorks and the CFD modeling and resolution was done in the software STAR CCM+.

Grid Description

Once again, the domain under study is a parallelepiped in which the turbine is contained. The main difference with the case described in Section 5.1 is the presence of the support structure. The lateral boundaries and the inlet are set at one turbine diameter of distance from the turbine and the outlet is placed at approximately four diameters. The upper and lower limits are at distance of 70% of the turbine diameter from the support.

Regarding the division of the domain into different zones, as it is shown schematically in Figure 5.8, the differences with the previous model are evident. In this case, the studied volume is divided into nineteen zones, depending on particular conditions and on the grid density, of which there are five.

As a fundamental condition to perform the simulation, the zone containing the turbine (Zone I) is the sliding one. It also has an hybrid mesh with a structured region in the vicinity of the solid boundaries composed by stretched prismatic elements. The rest of the region has unstructured polyhedral elements.

In order to reduce the overall number of elements of the model, the region at the center of the turbine (Zone II) has a coarser mesh. In the other zones, the mesh density by zones decreases as the distance to the turbine increases.

As the domain was split in several regions, internal boundaries had to be set to have continuity in the different flow variables across zones. Regarding this aspect, during the first attempts to build and run the model, it was noted that there were some problems when interfaces were placed across surfaces of different size. In order to avoid this problem, the final domain had to be divided as shown in Figure 5.8.

The mesh densities had to be slightly modified with respect to the previous model in order to reduce the overall numbers of cells. The grid base sizes can be found in Table 5.2. As a consequence, the final model has approximately 1.4 million cells and a general view of the mesh can be seen in Figure 5.9. A view of the blades and support structure can be observed in Figure 5.10.

Table 5.2: Grid base sizes for the different zones of the detailed 3-D model.

Zone	**Base size [m]**
I	0.023
II	0.028
III	0.06
IV	0.14
V	0.2

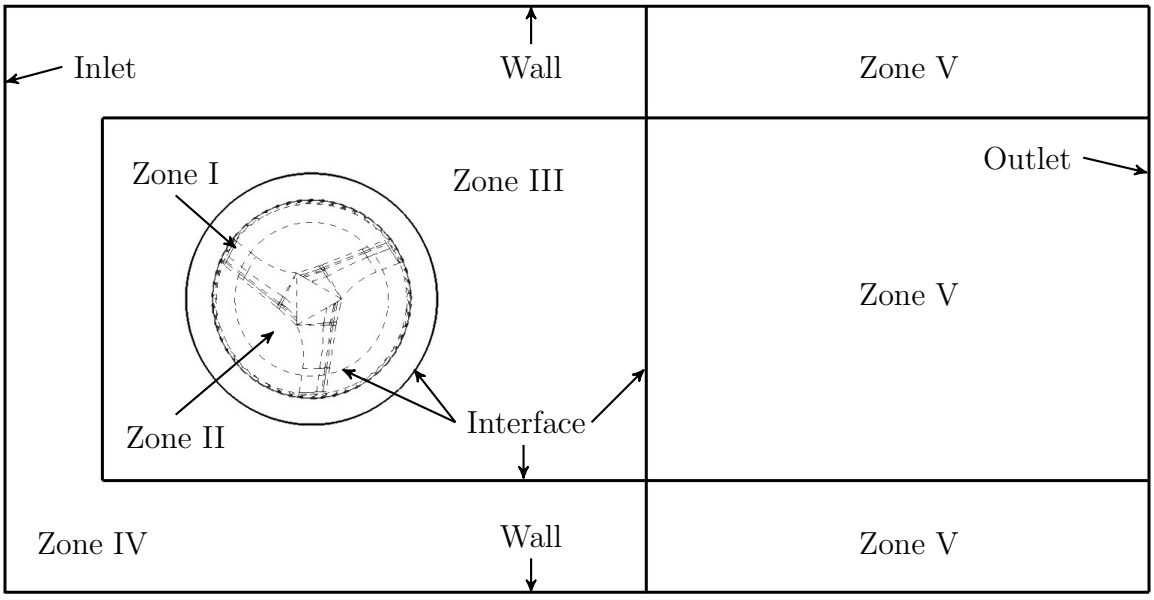

Figure 5.8: Schematic description of the domain under study. 3-D detailed model.

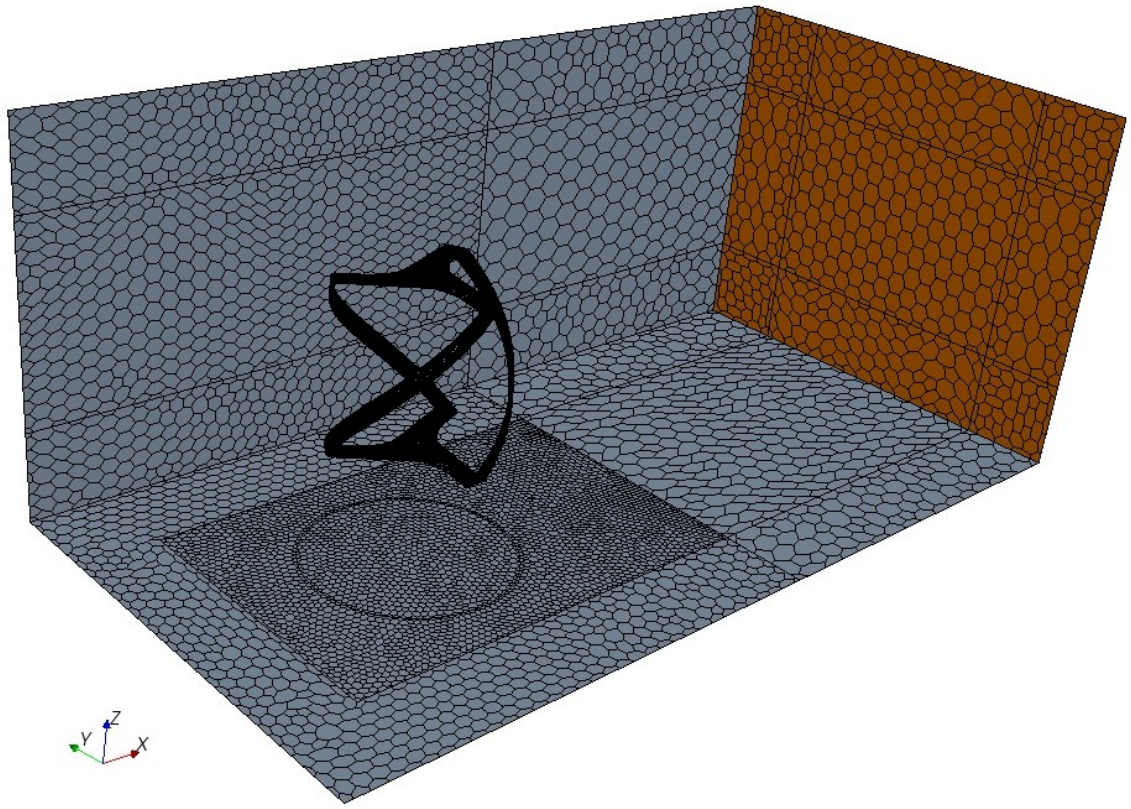

Figure 5.9: General view of the 3-D meshed domain. Detailed model.

Boundary Conditions

As for the boundaries conditions of the domain, the front face upstream of the turbine, is defined as a velocity inlet with a magnitude of $5m/s$ with an intensity of turbulence of 1%. A pressure outlet is set at the back face of the domain, downstream of the turbine.

In the lateral, up and bottom faces of the domain, a slip condition is considered whereas the blades and the support structure are defined as non slip walls, whose wall treatment is described in the next section.

Internal boundaries were set in the interfaces of the different volumes to ensure the continuity in the flow variables.

Turbulence Modeling

The same discussion detailed in 5.1.1 is valid here and, therefore, the approach based on the use of the Reynolds Averaged Navier–Stokes equations with the *Realizable* $k - \epsilon$ model is implemented.

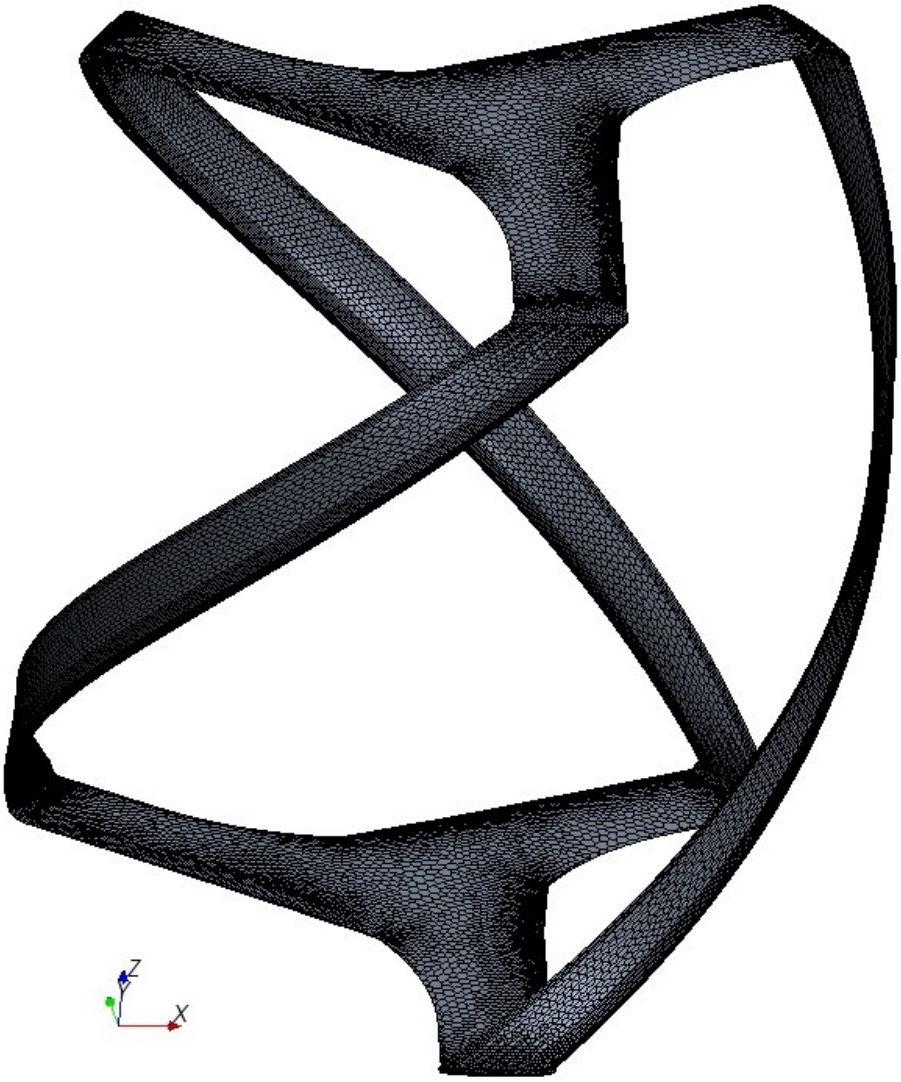

Figure 5.10: Detail view of the 3-D mesh around the blades. Detailed model.

Solver Details, Calculation Parameters and Convergence Criteria

Due to the similarity of this model with the one described in Section 5.1, the same parameters are applied here, and are summarized as follows.

The time-step is set as the time required to have an azimuthal rotation of the turbine equal to one degree per calculation step and it is expressed as a function of the rotational speed in equation (4.1).

Concerning the rotational speed of the turbine, six different rotational speeds are considered for the simulation to derive its efficiency curve. The residual of the momentum in the x, y and z direction, the turbulent kinematic energy and the turbulent dissipation rate are chosen as indicators of convergence. The limit value is taken as $1{\times}10^{-3}$.

5.2.2 Simulation Results and Analysis

The model described previously was run in STAR CCM+ to find a solution. Different rotational velocities were set for the turbine but, unfortunately, it was not possible to find a converged solution for the problem in any of the cases.

The problem was traced to a divergence of flow variables in the vicinity of the support structure, in the interface with the blades. Apparently, a combination of the employed turbulence model, the complex geometry and the mesh characteristics in the proximity of the turbine were thought to be the main reasons for the divergence in the solution.

As mentioned in the discussion regarding the available turbulence models in 5.1.1, that parameter could not be changed. An attempt to reduce the complexity of the interface between the blades and the support structure was made, introducing the different variations presented in Section 3.4 and shown here in the meshed domains of Figure 5.11 and Figure 5.12. However, once again the model failed to converge to a solution.

The last alternative considered was related to the mesh characteristics in the vicinity of the interface. It was decided to increase the mesh density in that area, but due to the lack of computational resources, this approach was infructuous.

As the tasks related to this problem were performed in the last stages of the involvement with the project, it was not possible to continue with the work on other alternatives or configurations that could lead to a functional detailed model of the turbine. However, based on the experience acquired while performing these tasks, new personnel at ICAM will continue working towards a satisfactory model.

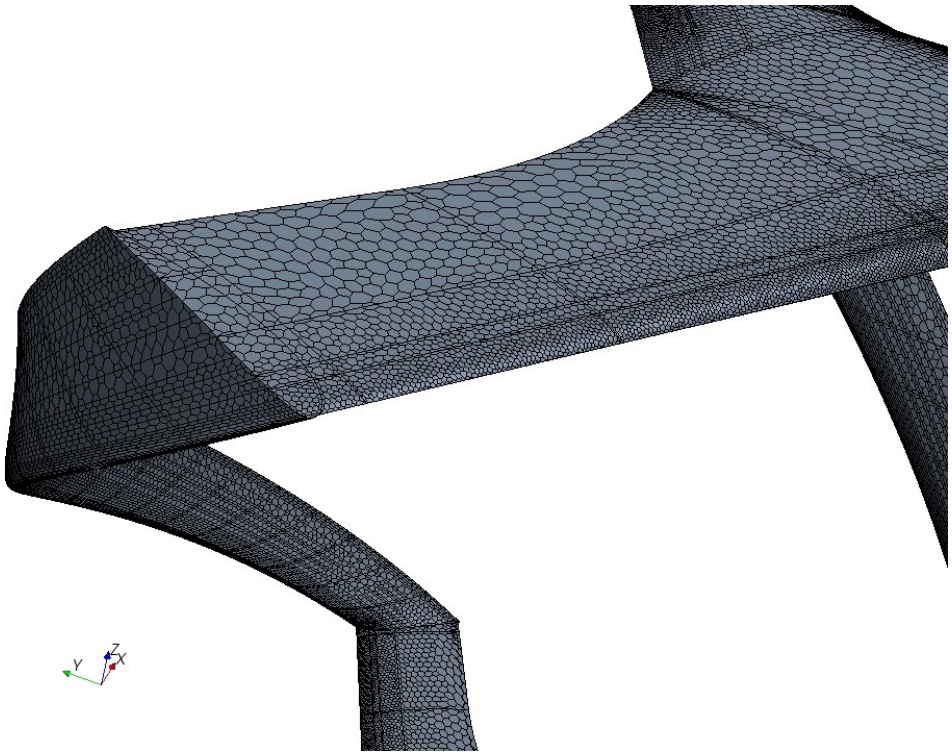

Figure 5.11: General view of the 3-D meshed domain. Alternative design #1.

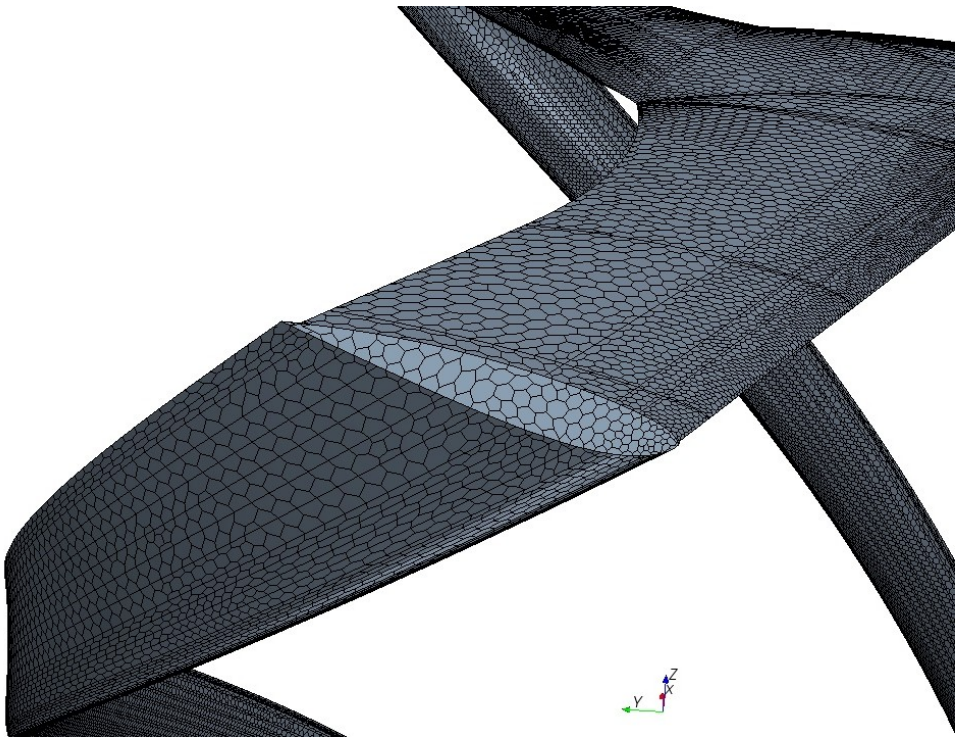

Figure 5.12: General view of the 3-D meshed domain. Alternative design #2.

Chapter 6

Structural Analysis of the Turbine

An introduction to the structural design is presented in Section 6.1. Then, a description of the loads affecting the turbine during its lifetime is done in Section 6.2. Finally, in Section 6.3 the characteristics of the material configuration for the blades are discussed.

6.1 General Considerations

In the previous chapters, the analysis of the turbine was centered on the aerodynamic performance with the objective of maximizing the power extracted from the wind. Here, the focus is set on the structural design, analysis and verification. As it has been mentioned before, it was not possible to perform the tasks associated with this topic during the period of involvement with the project. However, an introduction to this important stage in the design loop will be presented here with the objective of setting the foundations for future works in the area.

The main objective of the activities related to the structural design is to guarantee that the turbine will be able to withstand the loads exerted during its operational life and in any other stages of the construction or manipulation without risks of material or human losses and without sacrificing the energy capture. In relation to the optimization of the structural design, the objective is to perform that basic task maximizing the efficiency and minimizing the resources employed to the construction. In the following sections, the different aspects related to the structural design will be presented.

6.2 Load Assessment

One of the fundamental steps in the structural design is related to the identification and quantification of the different loads that will be exerted on the turbine along its life, either in operational or non–operational conditions.

In this case, the loads will be analyzed based on a classification according to their nature, leading to a division into three main groups: aerodynamic loads, inertial loads and accidental loads. A discussion about each one of them will be presented as follows.

6.2.1 Aerodynamic Loads

These are obviously the loads exerted by the fluid over the structure. It is possible to identify two situations for which these load should be considered, as detailed below.

Operational Condition

In this condition the turbine is turning to produce energy. The aerodynamic loads are then related to the existence of a time–dependent pressure distribution over the blades, caused by the wind as the turbine extracts energy from the flow. This concept was previously introduced in Chapters 4 and 5 and further analyses will be done in Chapter 7. The oscillatory nature of these loads makes them a main concern with respect to the fatigue life of the structure.

Non–operational Condition

This condition corresponds to any situation not related to the power production, with the turbine in a stationary position. The most critical one happens when the turbine is exposed to heavy winds beyond the operational condition, inducing large drag forces. In this case and according to the adopted design guidelines, a wind speed of $30m/s$ should be considered. Different wind incidences should be analyzed in order to identify the worst loading condition. Here not only the loads on the blades are important, but also the bending moments in the interface between the turbine and the power generator.

With regards to the wind loads during the transport and installation, it is assumed that adequate precautions will be taken in order to avoid loads greater than the ones mentioned before.

6.2.2 Inertial Loads

In this category, the loads deriving from known accelerations imposed to the turbine will be considered. As for the aerodynamic loads, these ones can be also separated according to the operational status of the turbine.

Operational Condition

It is in this condition where the main inertial loads can be found. Their origin is logically related to the rotation of the turbine and manifest themselves as centrifugal forces applied to the different elements, proportionally to their distance to the rotation center.

In the range of small and medium–sized wind turbines, the forces exerted by the gravitational acceleration are of secondary importance during the operation in comparison with the ones previously mentioned.

It should be also noted that inertial forces play an essential role in the dynamic analysis of the turbine, affecting the aeroelastic behavior or the response to changes in the wind characteristics.

Non–operational Condition

Unlike the previous case, here gravity is the main inertial load in play and the structure should be able to maintain its integrity while not turning. As it has been mentioned before, in small and medium–sized turbines, this is not one of the critical loading conditions.

Special considerations should be taken in order to avoid damage to any parts during the transportation and installation of the turbine. In general, the effect of the transport–induced loads can be mitigated by adequately designed ground support equipment (GSE).

6.2.3 Accidental Loads

This category includes all the loads that cannot be associated to a normal operational or non–operational condition of the turbine. Particularly, impacts of foreign objects are likely to be the main source of accidental loads. Depending on the size of the object and the energy in play during the impact, the consequences might vary from deterioration of the blade's surface to the complete loss of the turbine.

The structural analysis involving high energy impacts exceed the scope of this work but, however, the effect of the blade degradation due to minor impacts must be taken into account when selecting the material and its external protective layer, if any.

Other accidental load might arise as a consequence of the transport or installation operations, and in that case the necessary precautions should be taken in the procedures and in the design of the GSE to minimize the risks.

6.3 Turbine Materials

Once the geometrical design of the turbine and the loads applied on it have been identified, the next logical step consists in selecting the material to build the structure. There are several aspects that must be considered when selecting the materials:

- Structural strength and rigidity

- Blade manufacturing
- Worker health and safety
- Recyclability
- Health monitoring
- Blade – Support connection
- Cost

Typically, wind turbine blades are built using metallic materials such as aluminum or steel, composites materials or a combination of them. In the field of small and medium–sized turbines, it is possible to find straight blades in extruded aluminum or wood composites. However, due to the tendency to reduce the composite materials cost, it is becoming more and more common to find laminate blades and structures, as it also allows to easily obtain more complex geometries.

A composite material consists of a reinforcement element in combination with a binder. The characteristics and properties of the final material are superior to those of the individual elements that compose it. The main advantages of composites are the previously mentioned ease of fabrication into the desired shapes, a high strength and a high stiffness to weight ratio. Obviously, the final characteristic will depend on the type of reinforcement and binder used, as well as of the selected arrangement.

Concerning the reinforcements for wind turbines (Manwell *et al.*, 2009), fiberglass, carbon fiber, and wood are typically used. E–glass fabrics have low cost with a reasonably good tensile strength. In the glass fiber family it is also possible to find the S–glass, with a tensile strength around 30% higher than that of E–glass but significantly more expensive, doubling its price. Another common type of reinforcement is carbon fibers, with price eight times higher than glass fibers but with higher stiffness and strength.

In relation to the binder or matrix of the composite, the resins that are commonly used are in the liquid form during the lay up of the composite but when they are cured they become solid. Three main types can be identified. The polyester resins have a short cure time and low cost, but with the disadvantage of having a high shrinkage upon curing. Epoxy resins are stronger, have better chemical resistance, good adhesion, and low shrinkage upon curing, but they are also more expensive and have a longer cure time than polyesters. Finally, the vinyl esters resins are epoxy-based resins with similar properties than epoxies, but at a lower cost and with a shorter cure time. Its good environmental stability made them very popular in marine applications.

As mentioned in Subsection 3.1.5, the material was defined in early design stages as a laminate of E–glass – epoxy composite.

In works performed previously by Brunellière and Bibard (2011) in relation to the structural analysis of the turbine, several simplifications were done. One of the main one was related to the modeling of the composite as an isotropic material. As an unidirectional fiber–reinforced layer of composite material presents an orthotropic behavior, in reality it is indeed possible to combine layers in multiple directions to obtain a laminate with quasi–isotropic behavior. Logically, this is done at the expense of an ineffective use of the material. As this is not in accordance with the optimization of the turbine not only geometrically but also on its material, a discussion towards the definition of an adequate layup for the blades will be presented in the following paragraphs. It should be noted that a detailed explanation of the theory behind composite material analysis will not be provided here, and the reader may refer to the works of, for example, Jones (1999), Kollar and Springer (2003) or Daniel and Ishai (2006).

6.3.1 Composite Layup

The structural design of the blades must assure not only that it will be able to withstand extreme loads while having an adequate fatigue life, but also that its deformation will not degrade significantly the aerodynamic performance of the turbine.

For blades of larger turbines, a structural core composed of shear webs and spar caps can be used as the main element, attaching to it the trailing and leading edge shape sections. In this case, however, a monocoque design is implemented and, therefore, the whole blade section plays a structural role. It is possible, however, to adapt or distribute the different types of reinforcements according to the effort distribution on the section. For future references, the fiber orientation angle will be defined with respect to the longitudinal axis of the blade.

The loads applied on the blades will determine the nature of the efforts present on them, that will fall in one of the following types:

- Global bending along the main axis
- Global bending along the secondary axis
- Torsion
- Local effects

Unlike the case of a HAWT blades in which the inertial centrifugal loads induce mainly axial loads on the them, for a VAWT the effect of the rotation is absorbed by bending of the blades. Considering that the airfoil thickness is the smallest dimension of the blade, the global bending around the main axis will be one of the critical state to define the layup. In order to obtain a blade with an adequate section modulus and compensating for the lack of height of the section, layers with the fiber oriented in the longitudinal direction

of the blade (0°) should be placed in the outer regions of the airfoil.

Taking into account that the pressure distribution over the airfoil is not uniform, a torsional moment will be applied on the section, generating shear stresses that will add up to the bending–induced ones. As the layers oriented longitudinally present a low shear strength and stiffness, it is necessary to have layers with a ±45° fiber orientation placed all around the airfoil.

Finally, to account for the local effect of the pressure and other possible temporary loads, layers of fibers with an orientation of 0°/90° should also be present around the airfoil.

A central core made of foam material can also be also used, depending on several factors. For example, related to the final manufacturing technique employed, a core might be needed to laminate over it, using it as a mold. Another reason for which the core might be required is related to stability considerations of the blade. In advanced stages of the structural calculations it should be verified that local buckling does not happen in sections of the blade under compressive loads, which could cause delamination and eventually collapse of the entire structure. The presence of a core might help to mitigate this effect, increasing the local buckling stresses.

To sum up, an schematic view of the described layer distribution can be seen in Figure 6.1, but it should be noted that the final layup configuration including type, quantity and orientation will depend on the diverse load cases analyzed, on the material properties and on the manufacturing technique, as it will be explained in the following subsection.

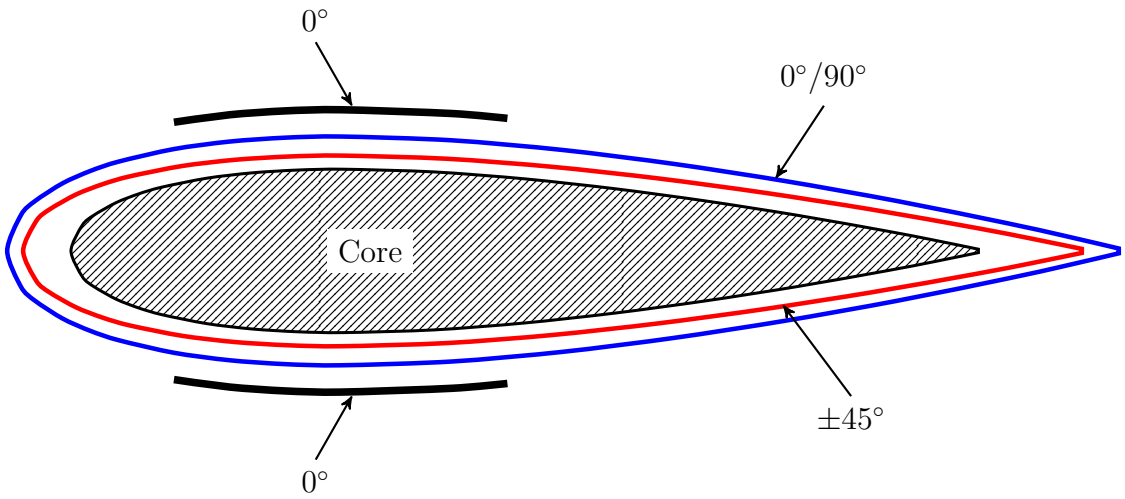

Figure 6.1: Schematic layer distribution around the airfoil.

6.3.2 Manufacturing Technique

The way in which the blades are manufactured will have a significant impact on the final cost and, more critically, on the final material properties. As it is known, the mechanical

characteristics of composite materials can vary greatly depending on several factors such as fiber to resin ratio, percentage of voids, curing scheme, among others.

Concerning the techniques to lay the material and as it is mentioned by Watson and Serrano (2010), manual layup was traditionally used to manufacture blades but this technique has the inconvenience of being highly dependent on the ability of the worker to obtain an adequate impregnation and fiber to resin ratio. When vacuum infusion was introduced, it took the blade manufacturing technology to a higher level, improving the general consistency and performance of the blades. With this technique it is possible to achieve better fiber to resin ratios, and with an adequate implementation, the lack of impregnation can be minimized or even eliminated. The pressure on the laminate also reduces the presence of voids and consequently improves the mechanical performance of the material. Later on, the use of pre–impregnated fabrics (prepreg) further enhanced the blade performance by combining resins and reinforcements in a more rigorously controlled manner before placement in the blade mold.

In this case, the manual layup technique will be used for the prototype manufacture and once the final design is defined, vacuum infusion will be implemented in the series production of the blades.

Concerning the cure process, it is an important factor that can greatly improve the overall performance of the material. The use of chemical catalyzers and accelerators allow the matrix to cure at ambient temperature. However, if the curing is done in an oven, it should be noted that other factors such as the time of curing and the temperature profile implemented will have an impact on the possible residual deformations and stresses after the curing process. For the case of the epoxy resins selected for these blades, the time of curing could be significantly reduced by curing at higher temperatures.

Chapter 7

Preliminary Assessment of Pressure Loads

In Section 7.1, an introduction to the factors that motivated the development of this analysis is presented. Then, in Section 7.2, the methodology is presented along with its possible limitations, concluding in Section 7.3 with its application to a test case.

7.1 General Discussion of the Problem

As discussed in Chapter 6, the loads exerted by the fluid over the blades are fundamental to define and assess the structural design of the different components, especially the blades. Ideally, a fully coupled analysis taking into account the interaction between the fluid and the structure should be made but, as it has been mentioned in Section 3.2, that type of analysis was not possible in the context of this project.

From the structural point of view, the decoupled analysis consists in the study of the response of the structure subjected to the loads exerted by the fluid, without contemplating any alteration of the loads as the structure is deformed. This is the main reason for presenting the pressure distribution on the blades in the CFD simulations of Chapters 4 and 5, as they serve as a basis for the structural analysis. Another important factor that was noted during the three-dimensional CFD simulations is the amount of time required to obtain reasonable results with modest computational resources, as in this case. This means that, even when an uncoupled analysis is performed, the time delay required in order to proceed with the structural analysis of the design is considerable.

Logically, a design loop, as the one presented in Section 3.2, is necessary to optimize the design. However, its implementation in the preliminary stages of the design when the geometries and configurations are being defined, might prove to be impractical due to the time constraints of the project.

It is clear then that even when the optimization loop is fundamental in the essence of the tasks being developed here, both the time–constraints and the modest computational resources encourage searching for an alternative work scheme, at least in the initial phases of the design. Due to this, a simplified analysis method is proposed in order to predict the aerodynamic loads for the structural analysis of the blades.

7.2 Method Description

7.2.1 General Considerations

As previously discussed, there are many parameters that can affect the performance and behavior of the turbine. In Chapter 4, simplified two-dimensional CFD models were used as a tool to narrow down the set of airfoils to be studied by means of detailed three-dimensional CFD models. In this way, the complexity of the aerodynamic analysis is reduced in early stages of the design. It should be noted though, that the described procedure is valid as long as certain hypotheses regarding the effects of the three-dimensional flow are made. This means that if those effects are considered either negligible or having a similar impact on all the designs, that approach can be followed. If a similar reasoning can be applied to the assessment of the aerodynamic loads over the blades, it could be possible to estimate in early stages of the design the impact of the different designs on the structural response of the turbine.

The work flow for the Design and Simulation stages of the turbine design loop presented in Figure 3.2b can be modified as shown in Figure 7.1 to incorporate this new intermediate analysis. It can be seen that the simplified aerodynamic analysis (two-dimensional CFD models) is now followed by tasks related to the structural verification performed on a three-dimensional model with a simplified load estimation. This allows having the first iteration loop in the design process, either for the aerodynamic or the structural aspects, in which certain type of problems could be detected and solved before investing a great amount of time and effort in the more advanced simulations.

As this new series of analyses imply the use of the pressure distributions obtained from the two-dimensional CFD model in a three-dimensional structural model, it is necessary to analyze under which hypotheses this could be done or what extra considerations should be taken into account.

In this case, it is possible to identify two main design aspects affecting the flow three-dimensionality and, therefore, the pressure distribution over the turbine. One is related to the blades of finite length and the presence of an interface between them and the support structure. The other one is linked to the helicoidal shape of the blades. A brief explanation will be given here concerning the effect of these two aspects based on stationary aerodynamics, as described by Clancy (1975) and McCormick (1979), among others.

Concerning the helicoidal shape, its effect on the flow can be associated with that of the sweep of a subsonic aircraft wing causing the streamlines to be curved towards the sweep direction. Near the extremes of the blades, this will have an impact on the pressure distribution.

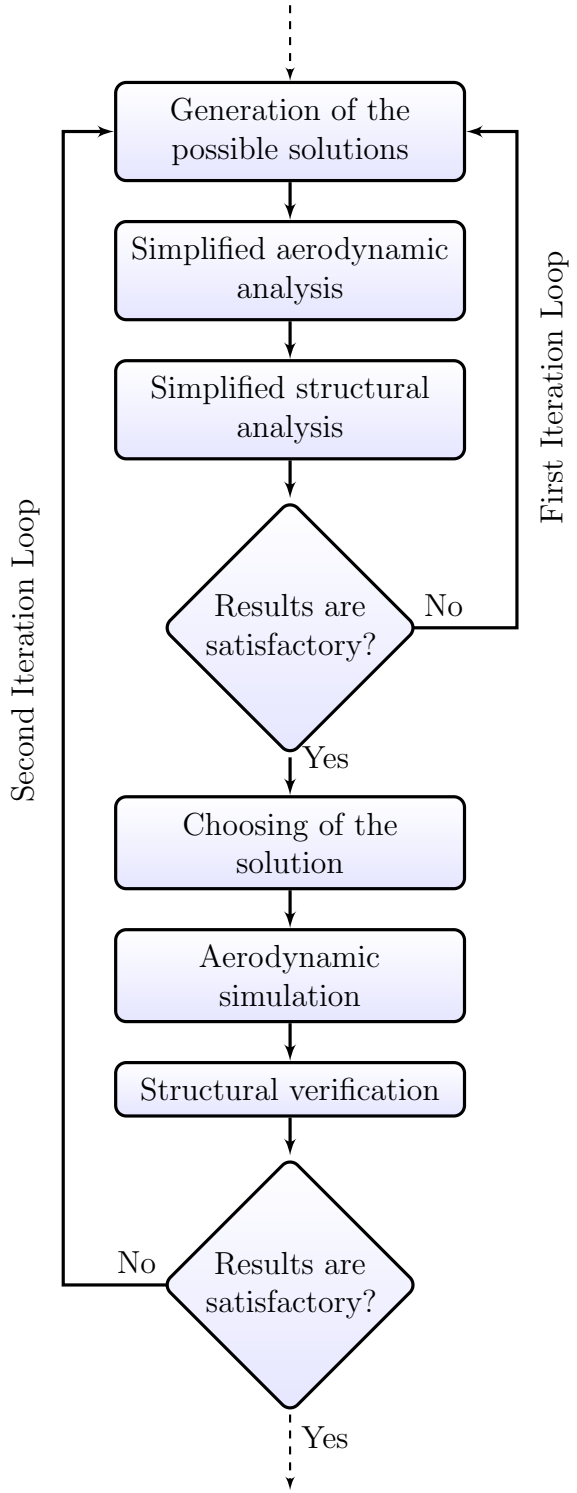

Figure 7.1: Modified work flow for the Design and Simulation tasks.

With respect to the blade length, the change in the performance of a wing with finite span is well known and is extensively studied in aerodynamics. A local variation of the span–wise pressure distribution along the wing will be induced by its shape. For the case of non–tapered wings like the blades, the greatest variation is found in their extremes. In this aspect and motivated by research in the aeronautical industry, most of the information available applies to flows of rather high Reynolds numbers, over 1×10^6. Depending on the

rotational speed of the turbine, lower Reynolds numbers can be found and therefore, it is necessary to search for research works related to lift distributions in low–Reynolds flows, like the one of Sathaye (2004).

In the following subsection, a way to obtain a simplified pressure distribution along the blades based on two-dimensional simulation data is explained, along with its limitations and assumptions.

7.2.2 Implementation

When dealing with the application of the two-dimensional pressure distributions to the three-dimensional models, two variables should be taken into account: the time dependence and the position along the blade. In the case of straight–blade turbines, it would only be necessary to make a correction in the distribution along the blades to take into account the effect of the finite blade span. In the case of helicoidal blades, however, the airfoils located at different stations have a different angle of incidence with respect to the flow and, therefore, a different pressure distribution. If the effect of the blade shape on the pressure distribution is neglected, it is possible to relate the change with the position of the airfoil along the blade with a time variation of the pressure. This is possible due to the relation existing between the time variation and the azimuthal position of the airfoil. This also implies that the discretization of the pressure along the blades will be linked to the discretization employed to obtain the two-dimensional data, 1° of azimuthal angle in this case.

As has been mentioned in Section 3.1, the turbine height is set to $1.4m$ and the blade spans over 120° of the turn. It is then possible to relate the blade angle with the position along the blade considering a linear evolution, as shown in equation (7.1).

$$\theta(z) = \frac{120^\circ}{1.4m}\, z \tag{7.1}$$

As the solution to the problem is found at discrete intervals, the last equation can be used to relate the increment of height with the angle. Isolating z and expressing the variables as increments, equation (7.2a) is shield. Considering the discretization previously used to derive the results of the CFD simulations ($\Delta\theta = 1^\circ$), the value corresponding to the discretization along the blade can be obtained (equation(7.2c)).

$$\Delta z = \frac{1.4m}{120^\circ}\, \Delta\theta \tag{7.2a}$$

$$= \frac{1.4m}{120^\circ}\, 1^\circ \tag{7.2b}$$

$$= 0.01175m \tag{7.2c}$$

The next step consists in defining the relation between the pressure distribution in the two and three-dimensional cases. The expression corresponding to that relation will be defined for a blade having the airfoil at its base ($z = z_0 = 0$) in the same position as the initial position of the two-dimensional airfoil. Additionally, as the pressure distribution along the airfoil is also discretized based on the grid employed during the calculations, the following expressions will correspond to a particular point on the airfoil, with the focus placed on the distribution along the blade. The same methodology can easily be applied to obtain the complete three-dimensional distribution for all the point of the blade.

First of all, it is necessary to define the position along the blade. As z is considered to be a continuous function, its expression can be obtained with an analogous process as the one used to derive equation (7.1). As in this case the solution is discrete, the position of the different stations along the blade can be expressed as in equation (7.3).

$$z_k = z_0 + k\,\Delta z \qquad\qquad k = 0, 1, 2, \ldots, n_Z \tag{7.3}$$

In the previous expression, z_k represents the position along the blade. Here, the total height of the turbine is discretized into n_Z sections, based on the selected azimuthal step and the blade helix angle. In this case, its general expression is found in equation (7.4).

$$n_Z = \frac{120^\circ}{\Delta\theta} \tag{7.4}$$

Based on the two-dimensional pressure distribution, it is now possible to write the expression for the approximate pressure for a point i over the blade depending on the azimuthal position of the reference section, θ_j, and on the indicator of the position along the blade, k, as seen in equation (7.5).

$$P'_{3\mathrm{D}i}(\theta_j, z_k) = P_{2\mathrm{D}i}(\theta_j \pm k\,\Delta\theta) \tag{7.5}$$

From the last equation it can be seen that when $k = 0$, $P'_{3\mathrm{D}i}(\theta_j, z_0) = P_{2\mathrm{D}i}(\theta_j)$ or, in other words, the reference section has the same pressure distribution as the two-dimensional results. Another thing that can be noted is the presence of the uncertainty in the contribution of the term $k\,\Delta\theta$ in the pressure shift. The reason for this is linked to the direction of the helix used to shape the blades. A positive sign should be consider when the blade evolves towards the sense of rotation, whereas the negative sign applies for the case of the blade leaning in the opposite direction of the rotation.

The approximation for the three-dimensional pressure distribution that was presented can be certainly used to proceed with the structural modeling and analysis of the turbine. However, some things are to be noted. First of all, the effect of the interfaces was ignored as if the blades had infinite length. Expanding what has been mentioned in the previous section, the effect of the interface is associated with a decrease on the pressure in its

proximity. This implies that, if no modifications are made to the pressure distribution, the structural analysis based on it will be conservative, as the loads were overestimated. However it is also possible that, depending on the Reynolds number, the presence of a tip vortex could lead to a local increase of the pressure on the blade, as shown by Sathaye (2004). As this phenomenon is closely linked to the characteristics of the interface, it is unknown whether the magnitude of the local pressure will be higher or lower than in the unaffected zone. Therefore, it is not possible to draw conclusions about the simplified structural analysis. Taking into account the complexity involved in the interference between the blade and its supports, further analyses in the topic are not in accordance with a simplified method as the one presented here.

In order to improve the pressure distribution to make it more realistic concerning the finite span, it is possible to multiply the results by a correction or shape function. The idea behind this is inspired by the observation of the actual lift distribution curves over wings of finite span, as it was introduced in Subsection 7.2.1 and mentioned by Schlichting and Truckenbrodt (1979). In that way, the corrected pressure distribution can be expressed as follows:

$$P''_{3\mathrm{D}i}(\theta_j, z_k) = P_{2\mathrm{D}i}(\theta_j \pm k\,\Delta\theta)\, f_C(z) \tag{7.6}$$

If it is based on the concept of lift variation for a finite wing, the expression of the shape function could be complex and dependent on the wing dimensions. On the other hand, a simple correction could be applied defining it as linear intervals, like the ones shown in Figure 7.2. There it can be seen that the correction only produces the reduction of the pressure towards the tip and several alternatives can be proposed.

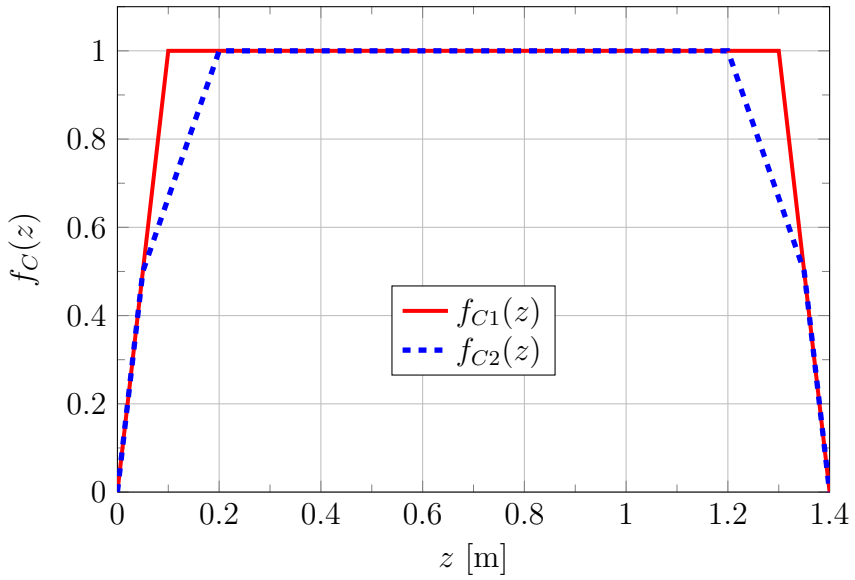

Figure 7.2: Examples of shape functions to correct the 3-D pressure distribution.

Another effect that can be mentioned in relation to the hypotheses considered in the analysis is that the simplified pressure distribution will have as a resultant of its action

over the blades an incorrect value of the torque applied on the turbine. This could affect the results of the structural analysis in case of performing a study of the dynamic response, as the accelerations and, consequently, the inertial loads induced by the torque variations will not be realistic.

A more general expression than the one given in equation (2.15) can be derived for the torque generated by each blade and is obtained by integration of the pressure, taking into account the distance to the turbine axis. Its expression can be found in equation (7.7).

$$\mathbf{M_{t\,3D}}(\theta) = \int_S \left(P_{3\mathrm{D}}(\theta, x_c, z)\,\hat{\mathbf{n}}\right) \times \mathbf{r}\, dS \tag{7.7}$$

If the discrete case is considered, equation (7.8) can be shielded from the last expression.

$$\mathbf{M_{t\,3D}}(\theta_j) = \sum_{k=0}^{n_Z} \sum_{i=1}^{n_c} \left(P_{3\mathrm{D}i}(\theta_j, z_k)\,\hat{\mathbf{n}}_i\right) \times \mathbf{r}_i\, \Delta x_i\, \Delta z \tag{7.8}$$

If information about the pressure distribution is available from three-dimensional CFD analyses, it could be possible to propose a shape function dependent of certain coefficients that could be determined in such a way that the approximate pressure distribution produces the same torque as the actual distribution. Then, for new models that do not present radical changes with respect to the reference model, the same shape function could be used to estimate the structural loads more accurately. This last approach has the limitation of deciding for which models the function is valid and for which ones it is not, as well as requiring the construction of a three-dimensional CFD model as reference, what could not be possible in early stages of the design. It should be also noted that it is difficult to define an appropriate shape function only based on the total torque that, in the end, represents the global averaged behavior of the turbine.

7.2.3 Remarks

As a conclusion to all the previous discussions regarding the approximate pressure distribution and its corrections, even when most of the bibliographical references are based on stationary aerodynamics, the effect of the reduction of pressure towards the blade tip is directly related to an equilibrium condition. However, there are no solid bases to affirm that the pressure will be reduced in the same way for all the points along the airfoil in the vicinity of the tip and even less, in the same way as a in another design. Therefore, for the purpose of preliminary structural analyses it could be convenient to use the simplified pressure distribution without any corrections as it, a priori, overestimates the loads on the blades. As the aerodynamic design evolves and more representative three-dimensional CFD models are available, the structural calculation could be made with the correct

pressure distributions extracted from the new simulations.

7.3 Application and Analysis of the Results

In order to have a better understanding of the methodology explained in the previous section, an example will be analyzed here. The model selected to proceed with the analysis corresponds to the turbine with an airfoil NACA 0015, rotating at a velocity equivalent to $\lambda = 2$.

As it has been previously described, it is possible to extract the pressure values for many points along the airfoil according to the employed mesh density. In order to make the presentation of the method as clear as possible, the analysis will be carried out for a specific point over the airfoil, as shown in Figure 7.3, but the same process should be performed for all the points in order to obtain the complete three-dimensional distribution.

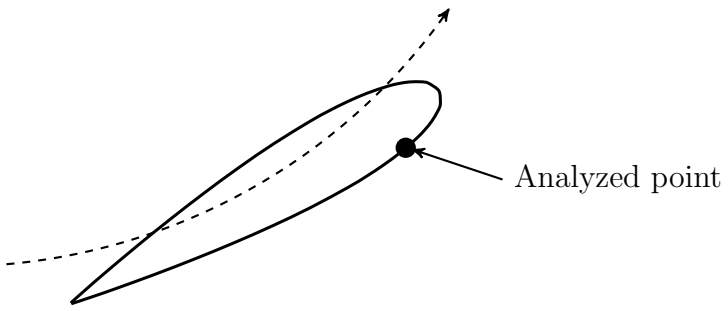

Figure 7.3: Schematic localization of the point selected for the calculations.

In Figure 7.4, the variation of the pressure for a point over the extrados of the airfoil belonging to one of the blades can be observed as a function of the azimuthal angle of the turbine. It can be noted that there is an oscillation of the curve in certain intervals. The source of these components of higher frequencies could be a product of the selected time-step for the solution or could be related to other numerical reasons, such as the convergence criteria or the turbulence model used. On the other hand, if the physical phenomena have associated such an effect, it is not being adequately captured as its apparent frequency is in the order of the sampling determined by the time-step. Despite what has been previously mentioned, it is very clear that from the point of view of a simplified structural analysis, the effect in the higher frequencies is not of particular interest. In advanced stages of the design, however, this effect should be considered regarding the induced vibrations and the dynamic loads on the turbine.

In order to proceed with the calculations and based on the previous discussion, a low–pass filter is applied to the data. In this case, a moving average filter with a span of nine values was selected and the resulting curve is also plotted in Figure 7.4.

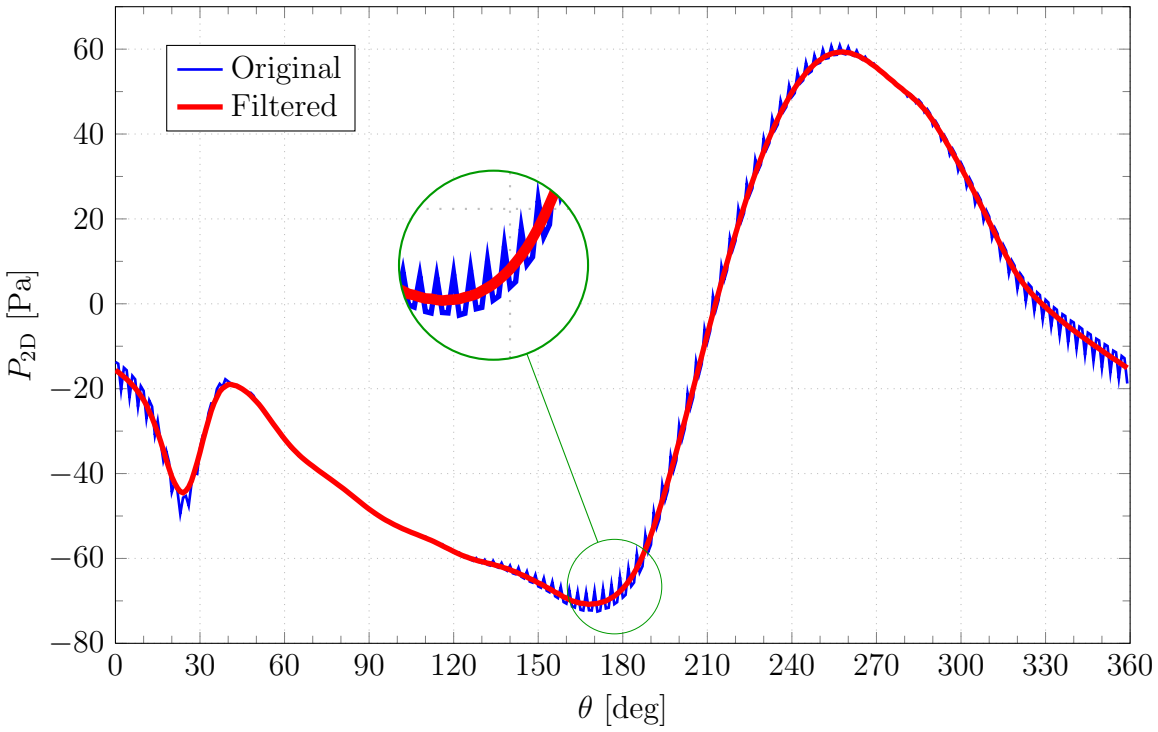

Figure 7.4: Pressure for a point over the airfoil vs. the azimuthal angle. NACA 0015.

Once the curve for the two-dimensional pressure distribution has been conditioned, it is possible to proceed with the estimation of the three-dimensional distribution. As it was shown in equation (7.5), the pressure for the same point over the airfoil in different positions along the blade is directly related to a shift in time or equivalently, in azimuthal angle of the initial curve. This is graphically shown in Figure 7.5, where the original curve is plotted together with the curves for three other positions along the blade. As in this case the selected time-step is equivalent to $\Delta\theta = 1°$, the value of the index k corresponds also to the shift in degrees of the curves with respect to the initial one.

It is possible to have a global view of the time variation of the pressure distribution by means of the three-dimensional plot of Figure 7.6. A contour plot of the same results is presented in Figure 7.7 to provide a better view of the variation along the blade.

If the corrected pressure distribution is considered (equation (7.6)) using the shape function defined as $f_{C1}(z)$ in Figure 7.2, the results can be observed in Figures 7.8 and 7.9.

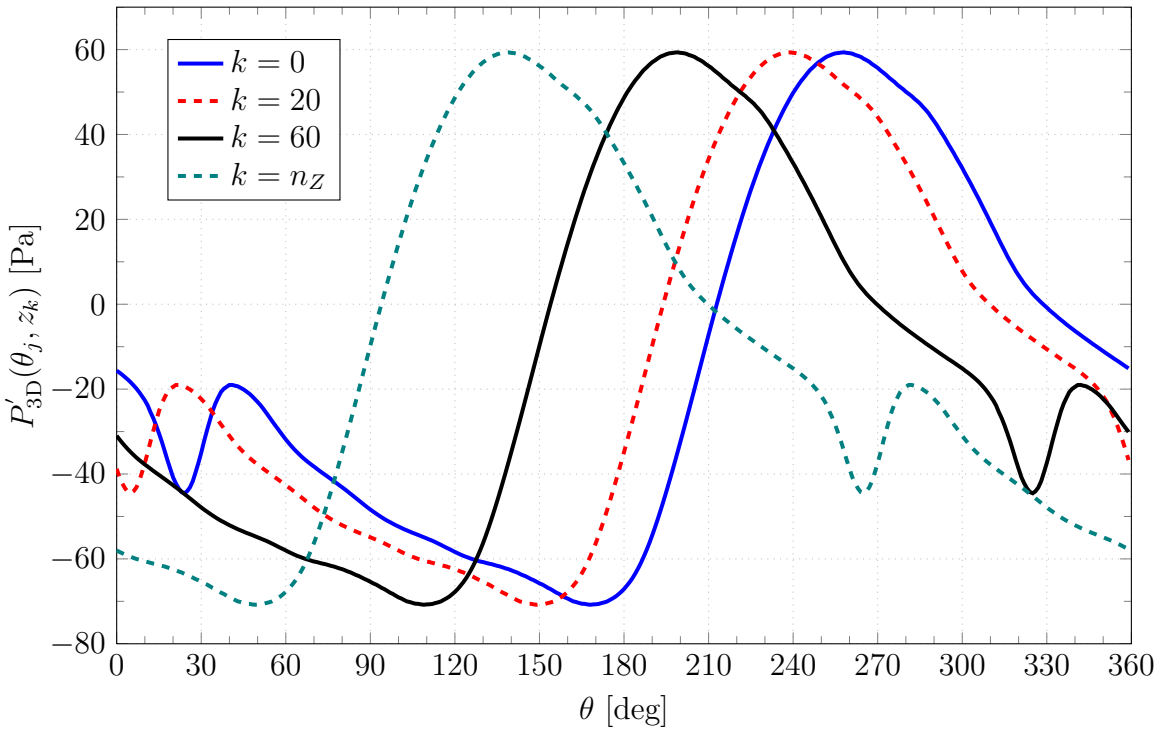

Figure 7.5: Shift in the pressure variation for different positions along the blade.

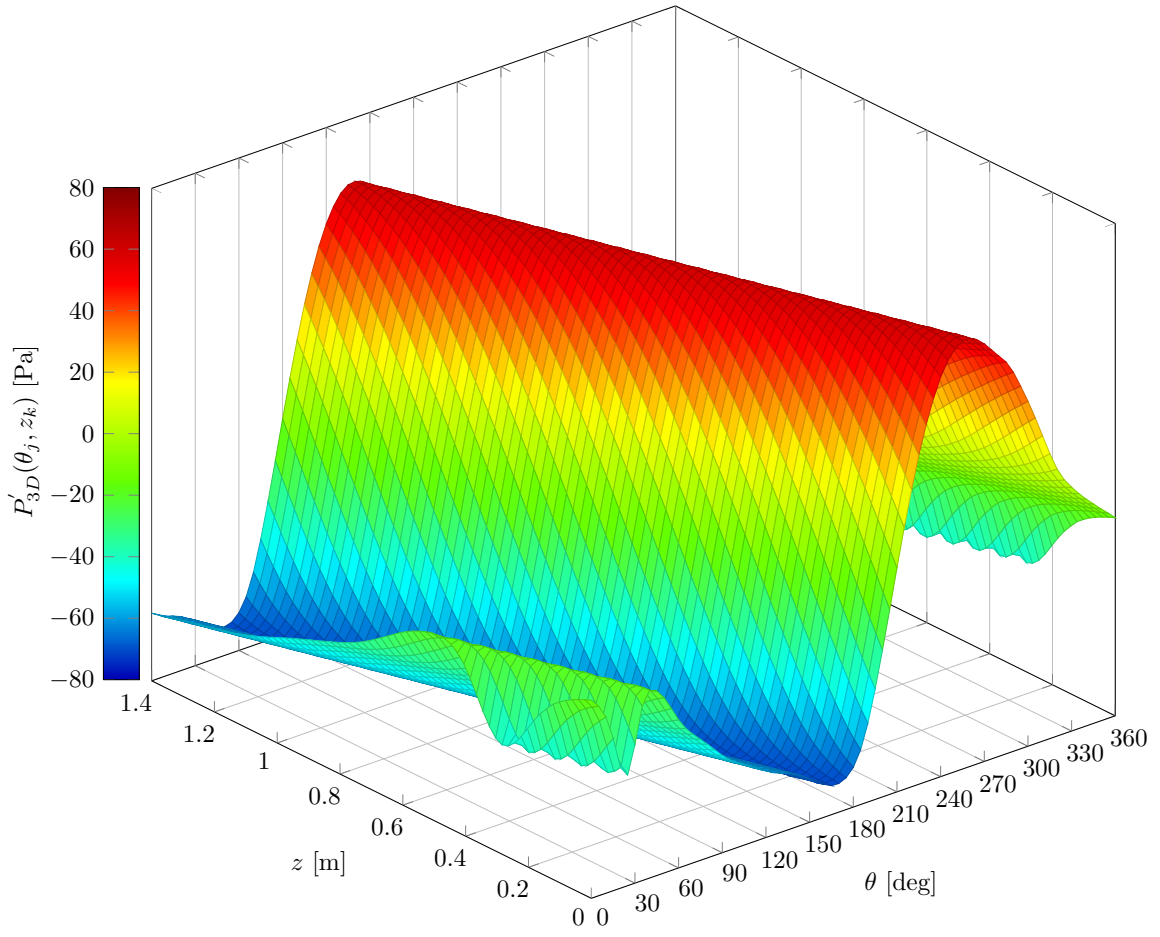

Figure 7.6: Simplified 3-D pressure distribution for a point over the airfoil.

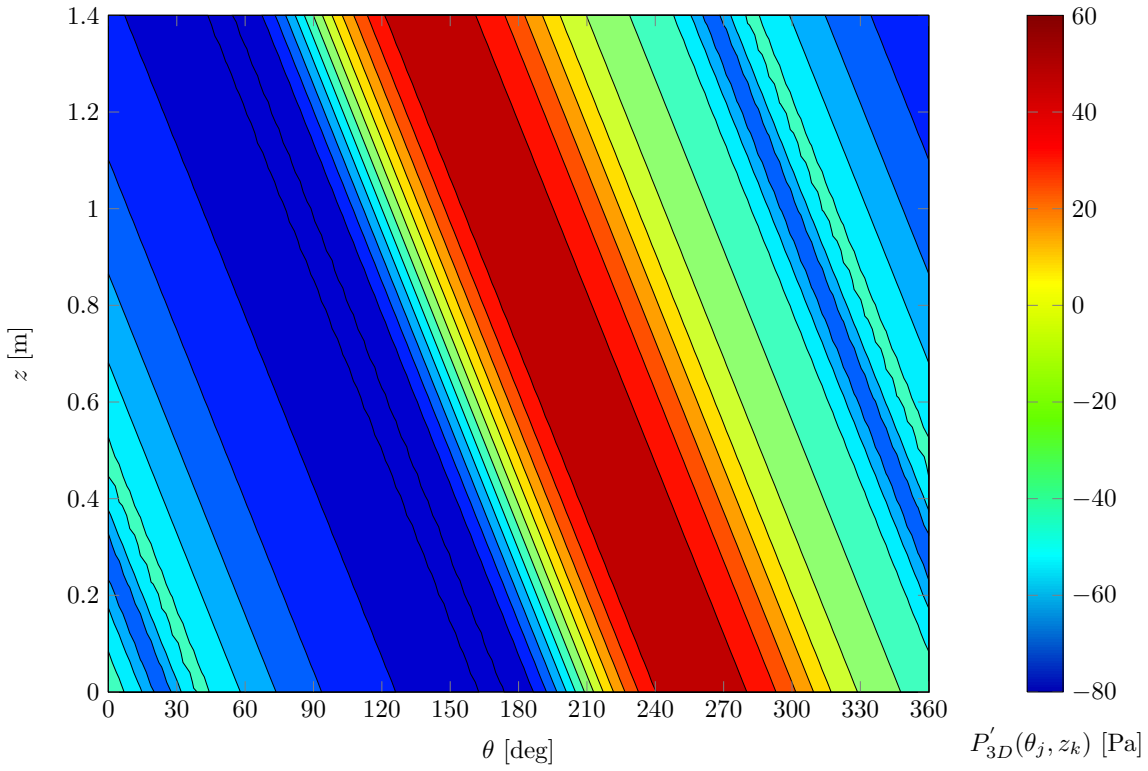

Figure 7.7: Simplified 3-D pressure distribution for a point over the airfoil. Contour plot.

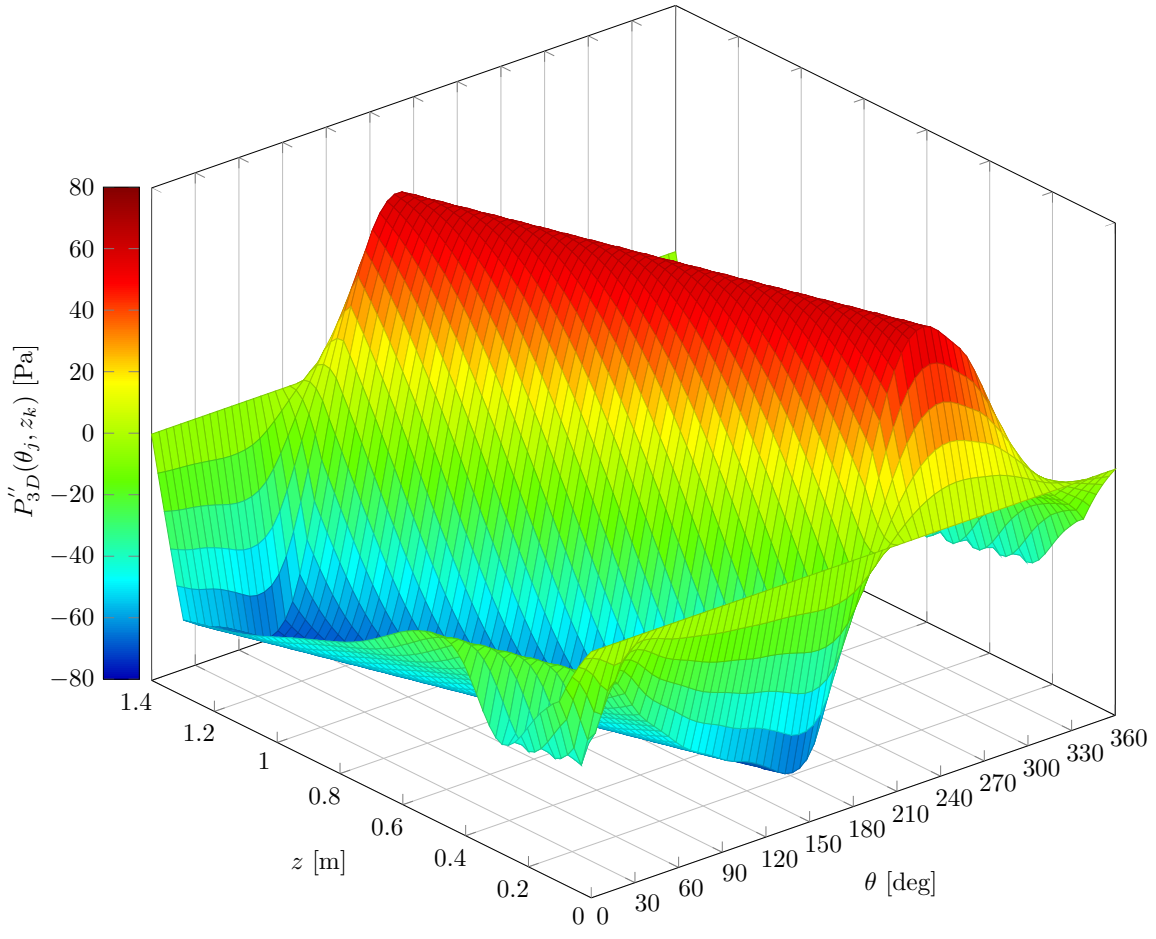

Figure 7.8: Corrected simplified 3-D pressure distribution for a point over the airfoil.

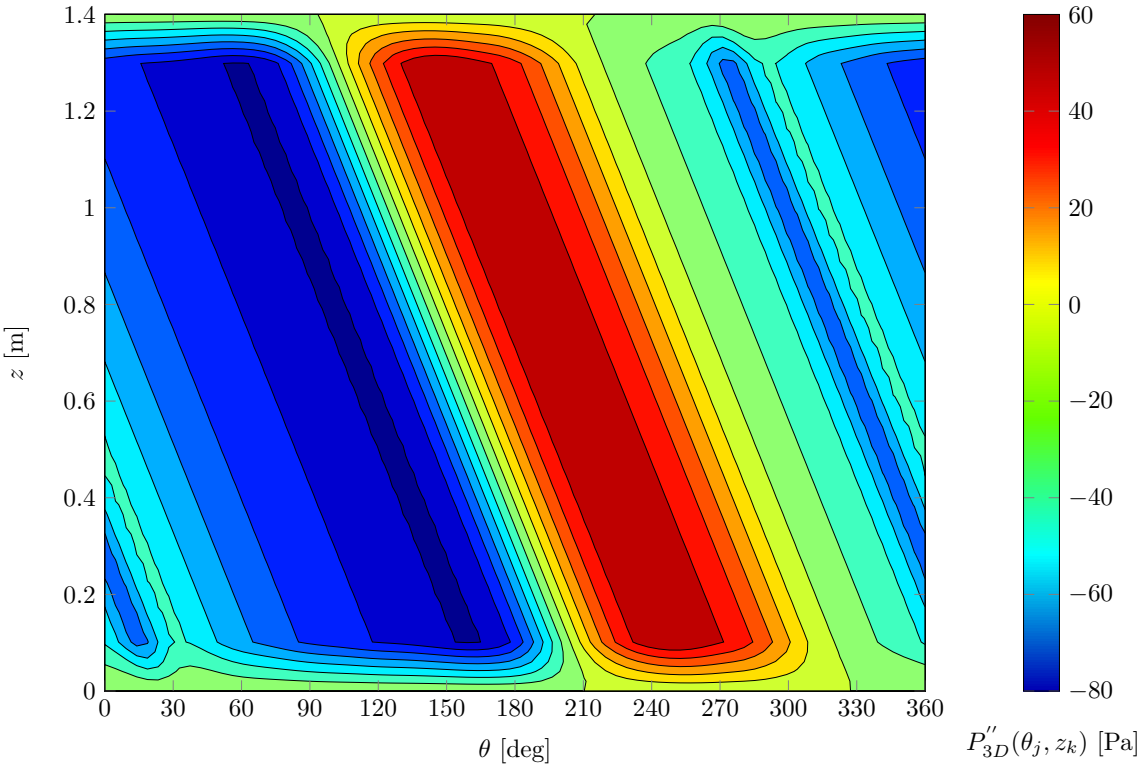

Figure 7.9: Corrected 3-D pressure distribution for a point over the airfoil. Contour plot.

As mentioned in Chapter 5, results of the pressure distribution for the detailed three-dimensional model are not available. However, it is possible to perform a comparison of the estimated distribution with the results of the simplified three-dimensional model. In this way, the extracted values for the same point over the airfoil along the blade can be found in Figure 7.10. Once again, the results were filtered to reduce high frequency variations. It can be seen that there is a similarity in the global shape of the distribution. However, in the areas of lower pressure, there is a presence of localized minimums and a more oscillatory behavior can be observed.

In order to have a better visualization of the results and the contrast with the predicted values, in Figure 7.11 both the contour plot of the simplified distribution in (a) and the three-dimensional model in (b) are plotted with the same color scale as reference.

Analyzing both figures it can be seen that, as mentioned before, there is a similarity in the general distribution but for the zone of the higher pressures, the maximum value is about 40% less than the predicted one. Concerning the areas where the lower pressures are present, the results from the three-dimensional simulation are less regular, with oscillations and localized minimums in different zones. Taking into account the fact that the selected point where the pressure is being analyzed is located in the exterior face of the blade (intrados of the airfoil), the low pressure areas correspond to the times when it is moving through the downwind half of its trajectory. As mentioned in Chapter 2, the turbulent effects are important due to the detachment of the boundary layer beginning in the last

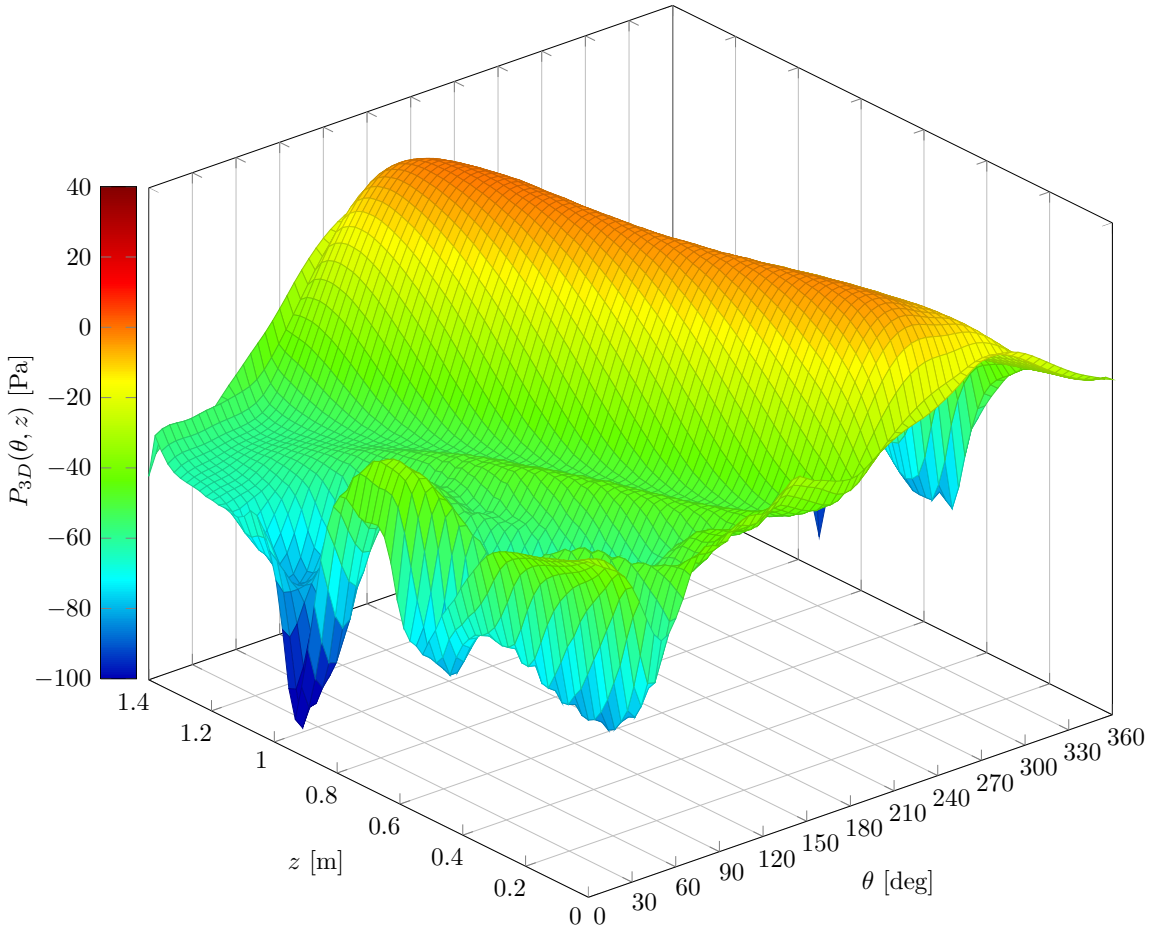

Figure 7.10: Pressure for a point over the airfoil. Simplified 3-D CFD model.

part of the upwind section, explaining the presence of the oscillations in the pressure field. The effect of the tip vortex might also be responsible of shaping the distribution in the vicinity of the blades extremities.

With respect to the function used to correct the simplified distribution, it can be seen that the pressure variation toward the tips is slightly more uniform and less blunt that the one assumed. However, considering that the main objective was to assess the structural loads and not the aerodynamic performance, the selected function complies with the intended objective.

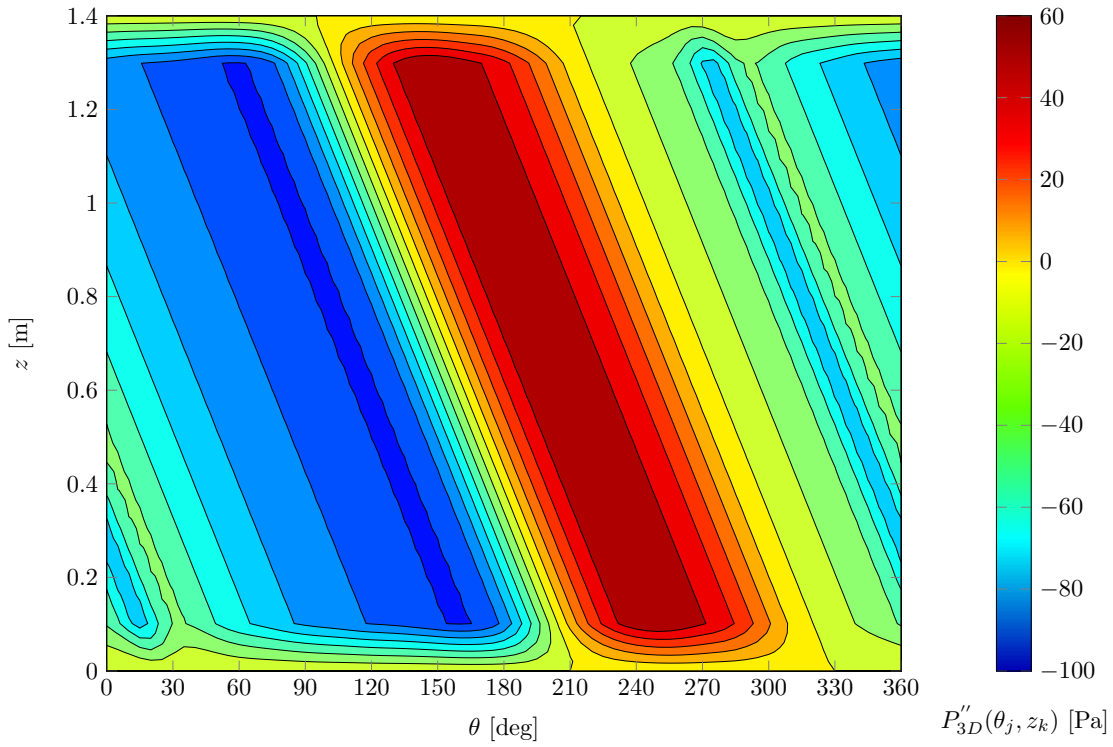

(a) Estimation from 2-D CFD model

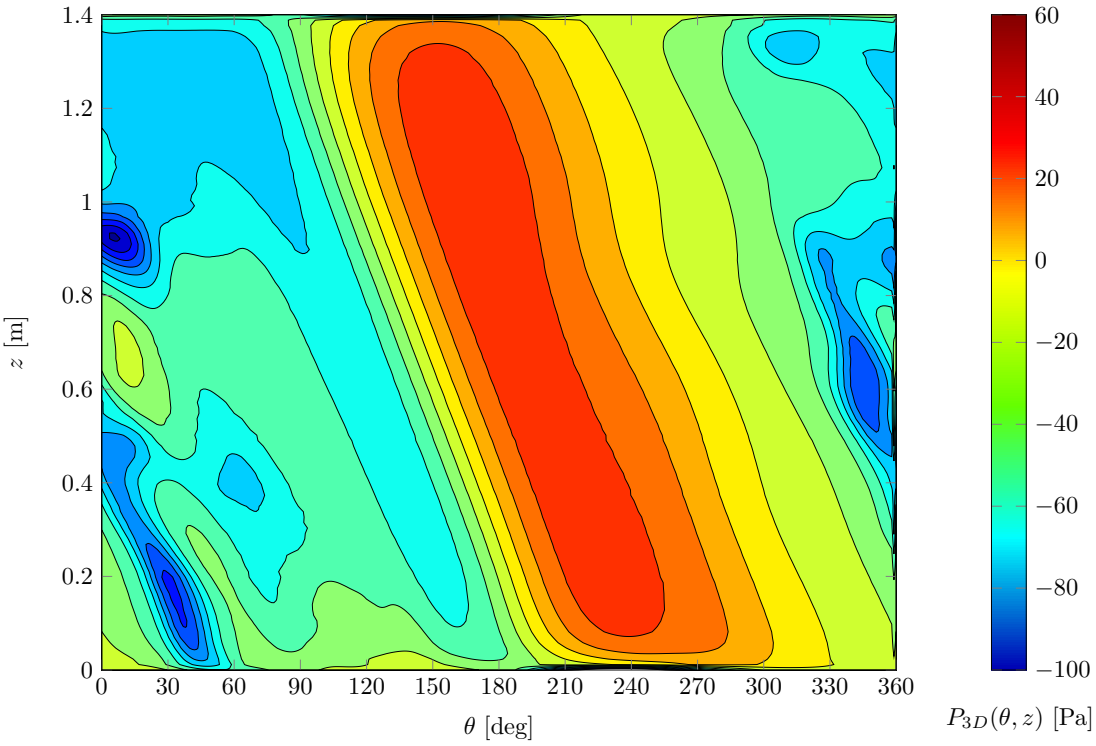

(b) Simplified 3-D CFD model.

Figure 7.11: Comparison of the 3-D pressure for a point over the airfoil. Contour plots.

Chapter 8

Conclusions and Recommendations

This report describes different stages in the preliminary design process of an optimized VAWT. Nowadays, small and medium–sized VAWTs designed to operate efficiently under the wind conditions of the Nantes region are not available on the market. The Aérojoules project is an attempt to fill this gap through the development of three turbines of 300W, 1500W and 3000W, oriented to these particular conditions and including the optimization in geometry and material of an existing Darrieus–type wind turbine. In this framework, the current study focuses on the initial stages of a optimized 300W VAWT design The main conclusions are presented in Section 8.1, whereas Section 8.2 details the recommendations for future work and research.

8.1 Conclusions

Turbine Design

The continuation and improvement of the turbine design was based on a study of the current state of the art in small and medium–sized VAWTs (Chapter 1), followed by familiarization with the theoretical and practical aspects of the turbine operation (Chapter 2), and analysis of the previous works performed in the framework of the project (Chapter 3). From the aerodynamic point of view, the main focus of the optimization process is placed on the airfoil selection and the characteristics of the blade support and interface. Regarding the structural aspect, the material selection and also the interface design and placement are studied. A global design cycle is defined according to the needs and characteristics of the project, implementing a decoupled fluid–structure analysis within an optimization loop.

With respect to the general configuration of the turbine, it was considered that the blade support structure is located at their extremities. In this way, the blades do not have an interruption on their continuity and it is also possible to work on the interface design to reduce the negative effects of the tip vortices. As these two factors are directly related to a reduction in the overall efficiency of the turbine, this design option provided an attractive solution for the work on the optimization process.

Three different configurations were presented for the blade – support interface. Each of

them has its advantages and disadvantages from the structural and constructive point of view, and their aerodynamic behavior is yet to be established in the future stages of the project.

Aerodynamic design and analysis As it has been mentioned in the previous paragraphs, a decoupled fluid–structure analysis is carried out to evaluate the performance of the proposed design alternatives. Concerning the aerodynamic study, two different stages of analysis are implemented in order to assess the aerodynamic efficiency of the turbine. The first stage consists of simplified two-dimensional CFD analysis of a turbine section (Chapter 4), whereas the second stage implies three-dimensional CFD analysis (Chapter 5), which, at the same time, can be subdivided according to the grade of detail employed to model the turbine geometry, as explained in the following paragraphs.

Regarding the airfoil selection, a group of twelve NACA four-digit airfoils were preselected based on a study of the state of the art in VAWTs and considering manufacturability and operational aspects. Simplified two-dimensional CFD simulations were used to narrow down the list of candidate airfoils to those that appeared more promising. Regarding this, some complications have been observed in relation to the results in the low λ range of the turbine operation, that could be preliminarily associated to the combination of the grid characteristics and the selected turbulence model. On the other hand, the results at higher values of λ appear to be consistent with the expected behavior. Based on these results and contemplating structural aspects of the blades, two design alternatives, the NACA 0015 and the NACA 2415, were selected to continue with the studies by means of three-dimensional CFD simulations.

Simplified three-dimensional CFD simulations of the candidate design with an airfoil NACA 0015 were performed. The main characteristic of this model is that its complexity is reduced excluding the blade support structure. Despite this fact, the results capture the effects of the flow three-dimensionality. This includes the presence of vortices being shed from the blade tips and, more importantly, it can be observed in the global reduction of the turbine efficiency curve.

The analysis of a detailed three-dimensional CFD model, including the blade support structure, not only allows to assess the variation on the flow patterns and the effect on the turbine efficiency, but more importantly, it enables to carry out the study on the performance of the selected blade – support interface. Following this reasoning, a detailed model of the NACA 0015–based turbine was implemented. Several attempts were made to obtain a converged solution with this model but, however, none of them produced satisfactory results. A combination of several factors such as the complex geometry, the grid characteristics and the employed turbulence models were thought to be responsible for this fact. As a consequence, the model was modified in an attempt to develop a satisfactory solution. Two different turbine geometries were used, in order to evaluate the

influence of the blade – support interface in the problem, with no change in the results. An attempt to modify the mesh characteristics, particularly with a reduction of the mesh size, proved to be limited by the available computational resources. The same limitations did not allow implementing an improved turbulence model, such as LES, to the modeling of the turbine. As the tasks related to this problem were performed in the last stages of the involvement with the project, it was not possible to continue with the development of a functional detailed CFD model of the turbine. It should be noted, however, that based on the experience acquired while performing these tasks, further works will be continued at ICAM outside the scope of this study.

Structural design The optimization of the turbine structure is mainly based on the selection of the material characteristics and its configuration, in accordance with a composite materials–based design. The general aspects related to the structural design were presented (Chapter 6), with a description of the loads arising during the turbine life and an analysis of the criteria for selection of the material layup and distribution. Due to the nature of the decoupled analysis performed, as well as the end of the involvement with the project, it was not possible to proceed with the structural modeling and analysis of the turbine. However, the performed study sets the foundations for future works in the area, expanding the simplified analyses carried out in previous stages into a more precise definition of the material layup and analysis.

Preliminary assessment of pressure loads It has been previously mentioned that the design process of the turbine is based on decoupled fluid–structure analyses. This implies that, in order to perform the three-dimensional structural simulations of the turbine, it is required to carry out beforehand the three-dimensional CFD simulations that will provide the necessary inputs concerning the loads on the turbine. Due to the considerable amount of time required to obtain reasonable CFD results with modest computational resources, an alternative that avoids the use of three-dimensional CFD simulations at the early stages of the design process was proposed (Chapter 7). This simplified method is aimed at obtaining the three-dimensional time–dependent pressure distribution for the blades, based on less complex two-dimensional CFD simulations. As a consequence, it is possible to introduce a new design work flow that includes a preliminary structural verification at the early stages of the design.

A simple algorithm and correction functions were developed and applied to the analysis of a particular point over the airfoil. The obtained pressure distribution was compared with results available from three-dimensional CFD simulations, turning out to be conservative. This means that, if the simplified distribution is used to perform a first optimization loop, the overestimation of the loads over the blades could lead, consequently, to an overestimation of the required structural strength of the blades. Due to the similarity between the CFD simulations of the diverse design alternatives, it is then expected that

the overestimation in the loads will have a similar effect on all of them, not affecting the selection of plausible alternatives. Moreover, the advantages of having an insight into the load distribution at the early stages of the design encourage the continuation of the work in this area in order to accelerate the convergence of the structural design towards an optimized alternative.

8.2 Recommendations and Future Work

In the framework of the project and considering the nature of the involvement with it, several fundamental aspects of the design work flow were not covered in this study. However, the performed tasks allow providing several recommendations for future research and activities, presented as follows.

Aerodynamic analysis and CFD modeling It has been previously mentioned that some complications arose during the estimation of the turbine performance using CFD models. Particularly, it was not possible to obtain satisfactory results in relation to the detailed three-dimensional models during the involvement with the project, and it is, therefore, necessary to continue with the works in the area. Besides the alternatives considered in the previous section, another variant not implemented in the models is related to the simplification of the domain under study, reducing the amount of regions and, consequently, of interfaces. This may prove to be useful when studying the influence of the software behavior in the characteristics of the solution. Taking also into consideration the preliminary grid–sensitivity study performed for the two-dimensional simulations, it is recommended to proceed with a systematic analysis and validation of the CFD models, including a thorough study of the employed methods and simulation parameters, in order to assess the grade and range of validity of future result. Some guidelines concerning this aspect can be found in the work of, for example, Murphy (2008).

Taking also into account the time constraints of the project, CFD might not be the best tool to assess the turbine performance at the preliminary stages of the design. The complexity of the models combined with the available computational power and the lack of experimental data to validate the results could lead to simulations that provide misleading results. Alternatively, in order to obtain satisfactory results at the early stages of the design, it may be beneficial to implement a momentum–based method, such as the Double Multiple Streamtube mentioned in Section 2.3. With this approach, once the bases of the model are implemented, the calculation process for different turbine configurations could be made within a short period of time. It should be noted, however, that the effect of the flow pattern in the blade's extremities will still require a detailed CFD simulation to be adequately quantified.

Structural analysis Considering the works performed in the previous stages of the project, several simplifications were done concerning the structural analysis of the turbine. The main one was related to the modeling of the composite as an isotropic material. If an optimized layer distribution, as the one presented in Chapter 6, is carried out, this approach might not be adequate due to the inherently orthotropic behavior of the material. It is then recommended that studies based on the classic laminate theory (CLT) are implemented, in order to assess the structural behavior of different components in a more rigorous way. Further information related to this theory and its application can be found in the works of Jones (1999), Kollar and Springer (2003) or Daniel and Ishai (2006).

Wind tunnel testing It is of fundamental importance to have experimental data concerning the turbine behavior and performance. Having data obtained from controlled tests in wind tunnel can be used to validate and to provide valuable feedback to the CFD simulations.

Material and manufacturing process The final mechanical characteristics of the composite materials will vary depending on the manufacturing process and the material layup. Moreover, the choice of the curing cycle may induce residual deformations and stresses of the different components. These issues should be taken into account during the structural design phase to have a clear idea of the final material strength and the effect on the desired geometry.

Acknowledgments

This thesis was developed in the frame of the European Master Course in Integrated Advanced Ship Design named EMSHIP for European Education in Advanced Ship Design, Ref.: 159652-1-2009-1-BE-ERA MUNDUS-EMMC.

To Professor Le Sourne and the personnel at ICAM for their assistance with this work.

I would like to thank Professor Maciej Taczała and the academic team at the West Pomeranian University of Technology for their contribution, support and assistance with this thesis.

To Marcos K, Nacho and Fernando, for their involuntary motivation to using the LaTeX 2_ε Documentation System to typeset this report.

To my family, that, regardless of the distance, supported me along my journey.

Special thanks go to Elena, who not only contributed with a thorough revision of this report but also supported me unconditionally in my brightest and darkest hours.

References

Allet, A., Hallé, S. and Paraschivoiu, I., 1999. Numerical Simulation of Dynamic Stall Around an Airfoil in Darrieus Motion. *Journal of Solar Energy Engineering*, 121 (1), 69–76.

Bergey, K.H., 1979. The Lanchester-Betz limit (energy conversion efficiency factor for windmills). *Journal of Energy*, 3 (6), 382–384.

Brahimp, M., Allet, A. and Paraschivoiu, I., 1995. Aerodynamic Analysis Models for Vertical-Axis Wind Turbines. *International Journal of Rotating Machinery*, 2 (1), 15–21.

Brunellière, K. and Bibard, A., 2011. *Project Aérojoules: Rapport Phase A1*. Tech. Rep. RD.1544.01.01, ICAM Nantes.

CFDORN, 2005–2012. *CFD Online Resource Network*. Website. `http://www.cfd-online.com/Wiki/Main_Page` [Accessed 20 July 2011].

Claessens, M., 2006. *The Design and Testing of Airfoils for Application in Small Vertical Axis Wind Turbines*. Master's thesis, Delft University of Technology.

Clancy, L., 1975. *Aerodynamics*. Pitman Aeronautical Engineering Series. Wiley.

Daniel, I. and Ishai, O., 2006. *Engineering mechanics of composite materials*. No. 13 in Engineering mechanics of composite materials. Oxford University Press.

Dixon, K.R., 2008. *The Near Wake Structure of a Vertical Axis Wind Turbine Including the Development of a 3D Unsteady Free-Wake Panel Method for VAWTs*. Master's thesis, Delft University of Technology.

Dragomirescu, A., 2011. Performance assessment of a small wind turbine with crossflow runner by numerical simulations. *Renewable Energy*, 36 (3), 957 – 965.

ES, 2008. *EcoSources*. Website. `http://www.ecosources.info/dossiers/Eolienne_verticale_Darrieus` [Accessed 15 July 2011].

Ferreira, C.S.a., Bijl, H., van Bussel, G. and van Kuik, G., 2007a. Simulating Dynamic Stall in a 2D VAWT: Modeling strategy, verification and validation with Particle Image Velocimetry data. *Journal of Physics: Conference Series*, 75 (1), 012023.

Ferreira, C.S.a., Van Bussel, G. and Van Kuik, G., 2007b. *2D CFD simulation of dynamic stall on a vertical axis wind turbine: verification and validation with PIV measurements*. January. American Institute of Aeronautics and Astronautics.

Ferziger, J.H. and Perić, M., 2002. *Computational Methods for Fluid Dynamics*. 3rd ed. Springer.

Fujisawa, N. and Shibuya, S., 2001. Observations of dynamic stall on Darrieus wind turbine blades. *Journal of Wind Engineering and Industrial Aerodynamics*, 89 (2), 201 – 214.

Gormont, R.E., 1973. *A mathematical model of unsteady aerodynamics and radial flow for application to helicopter rotors*. Eustis Directorate, US Army Air Mobility Research and Development Laboratory.

Habtamu, B. and Yingxue, Y., 2011. Effect of Camber Airfoil on Self Starting of Vertical Axis Wind Turbine. *Journal of Environmental Science and Technology*, 4 (3), 302–312.

Hepperle, M., 1996–2008. *How to read polar diagrams?* Website. `http://www.mh-aerotools.de/airfoils/hdipolar.htm` [Accessed 25 October 2011].

Howell, R., Qin, N., Edwards, J. and Durrani, N., 2010. Wind tunnel and numerical study of a small vertical axis wind turbine. *Renewable Energy*, 35 (2), 412 – 422.

IE, 2009–2010. *Info Éolien*. Website. `http://www.info-eolien.com/eoliennes-vertical.html` [Accessed 12 July 2011].

Iida, A., Mizuno, A. and Fukudome, K., 2004. Numerical Simulation of Aerodynamic Noise Radiated from Vertical Axis Wind Turbines. *Equals*, 1–4.

Iida, A., Kato, K. and Mizuno, A., 2007. *Numerical Simulation of Unsteady Flow and Aerodynamic Performance of Vertical Axis Wind Turbines with LES*, 1295–1298. December.

Jacobs, E. and Sherman, A., 1937. *Airfoil section characteristics as affected by variations of the Reynolds number*. Tech. Rep. 586, N.A.C.A.

Jain, P., 2011. *Wind Energy Engineering*. 2nd ed. McGraw-Hill.

Jones, R., 1999. *Mechanics of composite materials*. Materials Science and Engineering Series. Taylor & Francis.

Kirke, B. and Lazauskas, L., 1991. Enhancing the Performance of Vertical Axis Wind Turbine Using a Simple Variable Pitch System. *Wind Engineering*, 15 (4), 187–195.

Klimas, P., 1984. *Tailored Airfoils for Vertical Axis Wind Turbines*. Tech. Rep. SAND84–1062, Sandia National Laboratories.

Klimas, P. and Berg, D., 1983. *Aerodynamic design of a midsized vertical-axis wind turbine using natural laminar-flow blade elements*. Tech. Rep. SAND83–1200C, Sandia National Laboratories.

Kollar, L.P. and Springer, G.S., 2003. *Mechanics of Composite Structures*. 1st ed. Cambridge University Press.

Kuik, G.A.v., 2007. The Lanchester–Betz–Joukowsky Limit. *Wind Energy*, 10, 289–291.

Launder, B. and Spalding, D., 1974. The numerical computation of turbulent flows. *Computer Methods in Applied Mechanics and Engineering*, 3 (2), 269 – 289.

Lobitz, D.W. and Ashwill, T.D., 1985. *Aeroelastic Effects in the Structural Dynamic Analysis of Vertical Axis Wind Turbines*. Tech. Rep. SAND85–0957, Sandia National Laboratories.

Loth, J.L. and McCoy, H., 1983. Optimization of Darrieus turbines with an upwind and downwind momentum model. *Energy*, 7 (4), 313–318.

Manwell, J.F., McGowan, J.G. and Rogers, A.L., 2009. *Wind energy explained - Theory, Design and Application*. 2nd ed. United Kingdom: Wiley.

McCormick, B.W., 1979. *Aerodynamics, aeronautics, and flight mechanics*. Wiley.

Mcgowan, J.G. and Connors, S.R., 2000. Windpower: A Turn of the Century Review. *Annual Review of Energy Environment*, 25, 147–197.

Milne-Thomson, L.M., 1966. *Theoretical aerodynamics*. 1st ed. New York: Dover Publications.

Moutaki, A., 2010. *Projet Aérojoules: État de l'art sur les oliennes a axe vertical*. Master's thesis, ICAM Nantes.

Murphy, L., 2008. *Journal of Fluids Engineering Editorial Policy*. Online document. American Society of Mechanical Engineers. `http://journaltool.asme.org/Content/JFENumAccuracy.pdf` [Accessed 13 July 2011].

Newman, B., 1983. Actuator-disc theory for vertical-axis wind turbines. *Journal of Wind Engineering and Industrial Aerodynamics*, 15 (1-3), 347–355.

Noll, R. and Ham, N., 1982. Effects of dynamic stall on SWECS. *Journal of Solar Energy Engineering*, 104 (May), 96.

Paraschivoiu, I., 1982. Aerodynamic loads and performance of the Darrieus rotor. *Journal of Energy*, 6, 406–412.

Paraschivoiu, I., 2002. *Wind turbine design: with emphasis on Darrieus concept*. 1st ed. Canada: Polytechnic International Press.

Paraschivoiu, I. and Delclaux, F., 1983. Double Multiple Streamtube Model with Recent Improvernents. *Journal Of Energy*, 7 (3), 250–255.

Ponta, F.L. and Jacovkis, P.M., 2001. A vortex model for Darrieus turbine using finite element techniques. *Renewable Energy*, 24 (1), 1–18.

Popelka, D., 1982. *Aeroelastic Stability Analysis of a Darrieus Wind Turbine*. Tech. Rep. SAND82–0672, Sandia National Laboratories.

REUK, 2006–2012. *Renewable Energy UK*. Website. `http://www.reuk.co.uk/Darrieus-Wind-Turbines.htm` [Accessed 14 July 2011].

Saeed, F., Paraschivoiu, I., Trifu, O., Hess, M. and Gabrys, C., 2008. Inverse Airfoil Design Method for Low-Speed Straight-Bladed Darrieus-Type VAWT Applications. *In: 7th World Wind Energy Conference 2008: Community Power: Energy Autonomy for Local Economies*, 1–11.

Sathaye, S.S., 2004. *Lift Distributions on Low Aspect Ratio Wings at Low Reynolds Numbers*. Master's thesis, Worcester Polytechnic Institute.

Schlichting, H. and Truckenbrodt, E., 1979. *Aerodynamics of the airplane*. Advanced Book program. McGraw-Hill.

Sheldahl, R. and Klimas, P., 1980. *Aerodynamic Characteristics of Seven Symmetrical Airfoil Sections Through 180-Degree Angle of Attack fo Use in Aerodynamic Analysis of Vertical Axis Wind Turbines*. Tech. Rep. SAND80–2114, Sandia National Laboratories.

Shih, T.H., Liou, W.W., Shabbir, A., Yang, Z. and Zhu, J., 1994. A new k-epsilon eddy viscosity model for high Reynolds number turbulent flows: Model development and validation. *Computers & Fluids*, 24 (3), 227–238.

South, P., Mitchell, R. and Jacobs, E., 1983. *Strategies for the Evaluation of Advanced Wind Energy Concepts*. Tech. Rep. SERI/SP-635-1142, Solar Energy Research Institute.

Speral, D.A., 2009. *Wind Turbine Technology. Fundamental Concepts of Wind Turbine Engineering*. 2nd ed. New York: ASME.

Strickland, J., 1975. *The darrieus turbine: A performance prediction model using multiple streamtubes*. Tech. Rep. SAND75–0431, Sandia National Laboratories.

Strickland, J.H., Webster, B.T. and Nguyen, T., 1980. Vortex model of the Darrieus turbine: An analytical and experimental study. *NASA STI/Recon Technical Report N*, 802, 25887.

Tangler, J.L. and Somers, D.M., 1995. NREL Airfoil Families for HAWTs. *Wind Energy*, 95, 1–12.

TPE, 2008. *Tpe éolienne*. Website. `http://tpeeolienne.e-monsite.com` [Accessed 4 October 2011].

UIUC, A.A.G., 1995–2011. *UIUC Airfoil Data Site*. Website. `http://www.ae.illinois.edu/m-selig/ads.html` [Accessed 22 June 2011].

Watson, J.C. and Serrano, J.C., 2010. Composite Materials for Wind Blades. *Wind Systems*, 46 – 51. `http://windsystemsmag.com/media/pdfs/Magazines/0910_WindSystems.pdf` [Accessed 20 December 2011].

Wilcox, D., 2006. *Turbulence modeling for CFD*. No. v. 1 in Turbulence Modeling for CFD. DCW Industries.

Appendix A

Wind Data for the Nantes Region

This Appendix contains the results of a study of the wind power availability in the Nantes region. In Table A.1, the information of the observed winds at a station in Bouguenais during a period of ten years (1997–2007) can be seen. The frequency of occurrence can be found for different wind intensities and directions.

In Figure A.1, the same results are plotted as a probability distribution function according to the wind speed intensity.

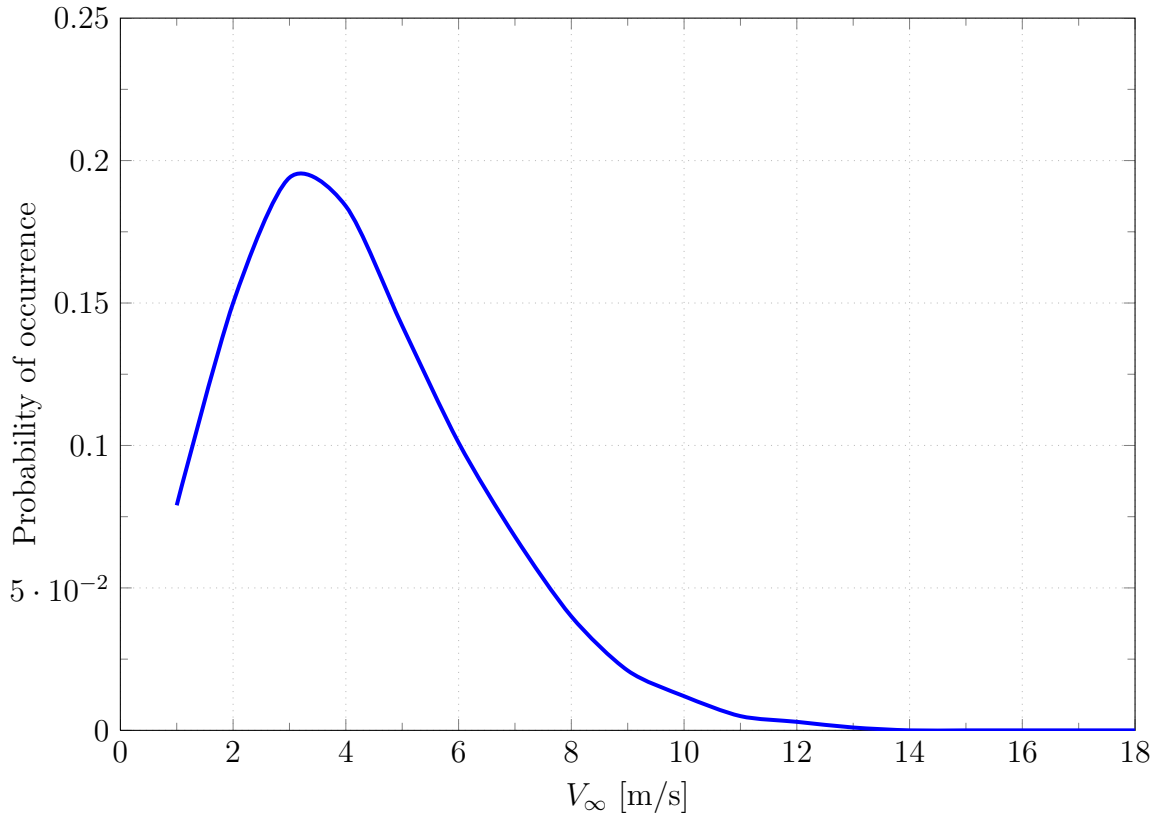

Figure A.1: Probability distribution function for the Nantes region.

Table A.1: Occurrences of wind speed and direction recorded in Bouguenais in the Nantes region.

U	**Direction [deg]**																	
$[\frac{m}{s}]$	**0**	**20**	**40**	**60**	**80**	**100**	**120**	**140**	**160**	**180**	**200**	**220**	**240**	**260**	**280**	**300**	**320**	**340**
1	136	105	83	48	62	95	125	83	80	71	69	52	50	54	73	98	148	145
2	259	228	183	107	95	154	168	161	170	154	107	105	104	105	114	179	227	257
3	272	281	248	181	155	196	225	193	210	191	173	154	145	140	153	205	235	277
4	185	219	226	201	178	218	204	210	184	191	199	177	158	140	160	176	163	164
5	99	106	135	174	191	150	151	172	134	146	154	150	134	151	147	137	109	86
6	32	38	70	128	137	107	68	96	91	101	102	134	131	127	127	97	65	49
7	9	17	36	84	98	55	35	46	64	68	76	96	110	103	93	55	31	11
8	5	5	13	45	49	17	16	23	32	35	47	65	70	79	65	27	14	7
9	2	1	4	22	25	6	4	9	17	22	29	31	46	45	29	11	5	2
10	0	1	1	6	8	1	4	6	6	11	18	21	28	29	19	8	1	2
11	0	0	0	2	1	1	0	2	7	3	15	8	12	15	7	4	0	1
12	0	0	0	1	0	0	0	0	3	3	6	4	9	8	7	1	1	0
13	0	0	0	0	0	0	0	0	1	1	2	2	1	3	4	0	0	0
14	0	0	0	0	0	0	0	0	0	1	2	1	1	0	2	0	0	0
15	0	0	0	0	0	0	0	0	0	0	1	0	1	0	0	0	0	0
16	0	0	0	0	0	0	0	0	0	1	1	0	0	0	0	0	1	0
17	0	0	0	0	0	0	0	0	1	0	0	0	0	1	0	0	0	0
18	0	0	0	0	0	0	0	0	0	1	0	0	0	0	0	0	0	0

Measurements performed at: Nantes-Bouguenais

Position: 47°09N 1°37E.

Period: 1997–2007

Height of the anemometer: 10m

Appendix B

Study of Grid Sensitivity

The results of a preliminary study of the grid sensitivity for the two-dimensional CFD simulations are presented here. As mentioned in Section 4.2, this results are not used to define the grid sizes.

It should be noted that the work in this area should be continued and rigorously expanded. Special attention should be placed on the procedure to determine the accuracy of the solution, which could be done following the guidelines established by, for example, Murphy (2008).

Four different sized grids corresponding to the domain presented in Figure 4.5 are analyzed. The corresponding base sizes are presented in Table B.1 and the corresponding resultant characteristics regarding the number of elements can be found in Table B.2. The model number three correspond to the one analyzed in Chapter 4.

Table B.1: Grid base sizes for the different zones of the studied 2-D models.

Zone	**Base size [m]**			
	Model 1	**Model 2**	**Model 3**	**Model 4**
I	0.018	0.012	0.008	0.006
II	0.05	0.025	0.015	0.012
III	0.2	0.15	0.1	0.08
IV	0.4	0.35	0.3	0.3

Table B.2: Mesh characteristics of the studied 2-D models.

	Model 1	**Model 2**	**Model 3**	**Model 4**
Cells	40264	50669	72649	125794
Faces	115602	146290	211587	369253
Vertices	77497	99008	144489	248862

In order to assess the variation of the solution with the grid size, the generated torque, a global variable, will be analyzed. Two different values of tip speed ratio, λ, are considered to assess the effect of the grid size at different Reynolds numbers of the simulation. The results of the torque variation for the four models can be observed in Figure B.1 for $\lambda = 3$ and in Figure B.3 for $\lambda = 1.5$. For better clarity, close ups of both plots are presented in

Figure B.2 and Figure B.4 for $\lambda = 3$ and $\lambda = 1.5$, respectively. In Table B.3, the results for the extracted power and the efficiency of the turbine are presented.

Table B.3: Power and efficiency. 2-D Models. NACA 0015.

Model	$\boldsymbol{\lambda = 1.5}$			$\boldsymbol{\lambda = 3}$		
	$\boldsymbol{P_a}$[W]	$\boldsymbol{C_P}$	$\boldsymbol{e_{rel}}$[%]	$\boldsymbol{P_a}$[W]	$\boldsymbol{C_P}$	$\boldsymbol{e_{rel}}$[%]
1	13.5650	0.1309	–	61.02	0.5889	–
2	13.9030	0.1342	2.49	60.23	0.5813	-1.29
3	14.3848	0.1388	3.47	60.87	0.5875	1.06
4	11.7465	0.1134	-18.34	60.84	0.5872	-0.06

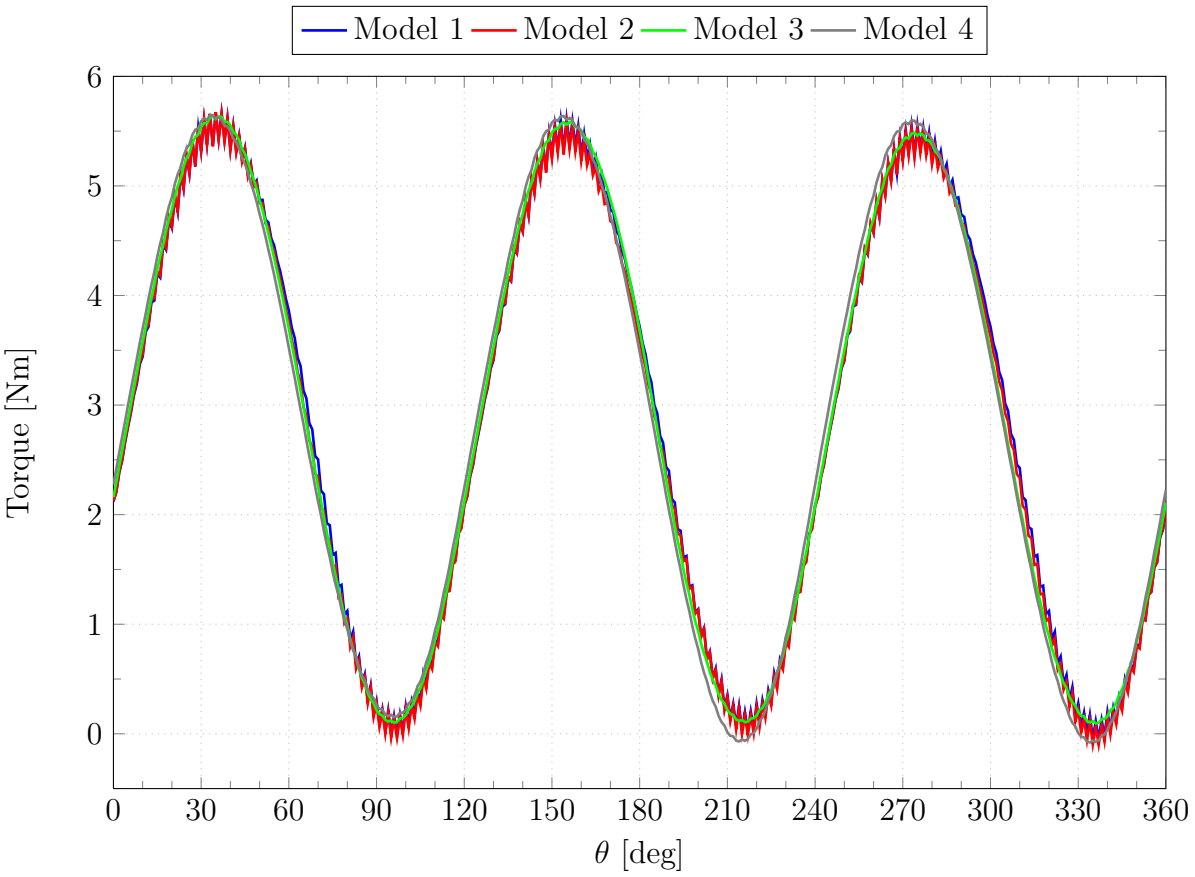

Figure B.1: Torque vs azimuthal angle. 2-D Models. NACA 0015. $\lambda = 3$

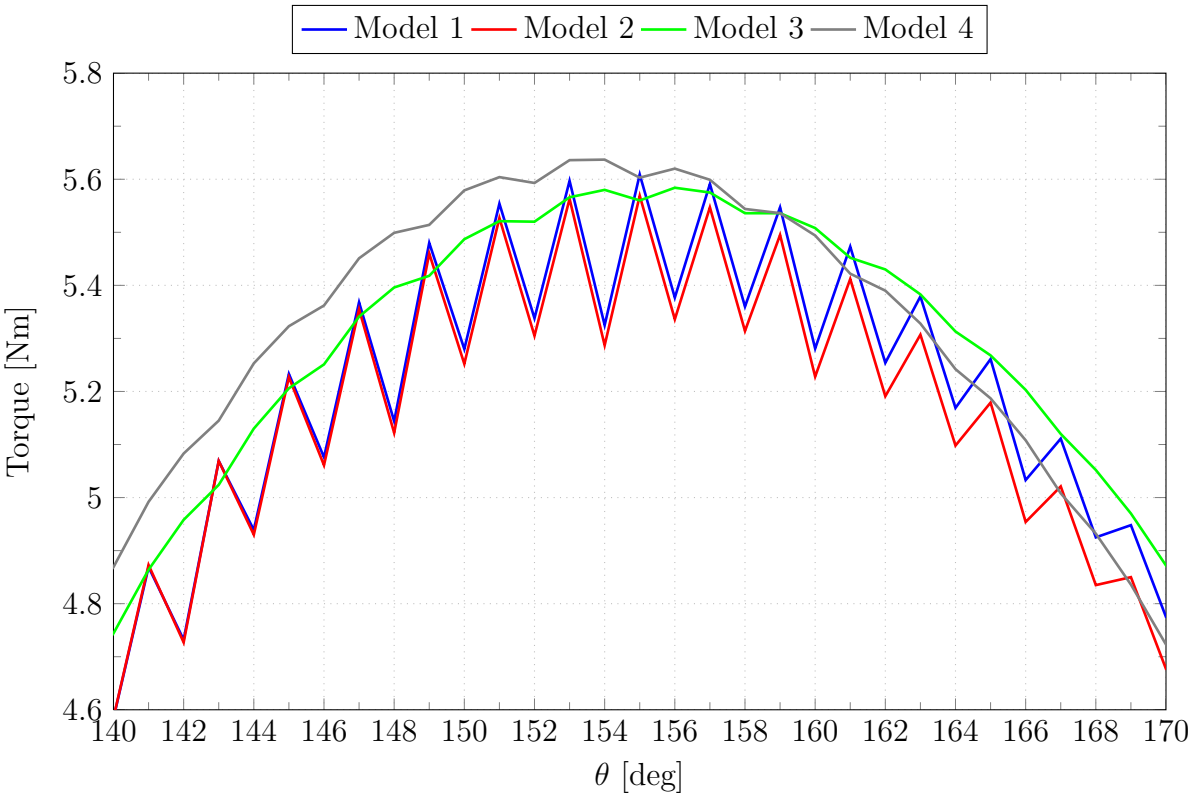

Figure B.2: Torque vs azimuthal angle. 2-D Models. NACA 0015. $\lambda = 3$. Close up.

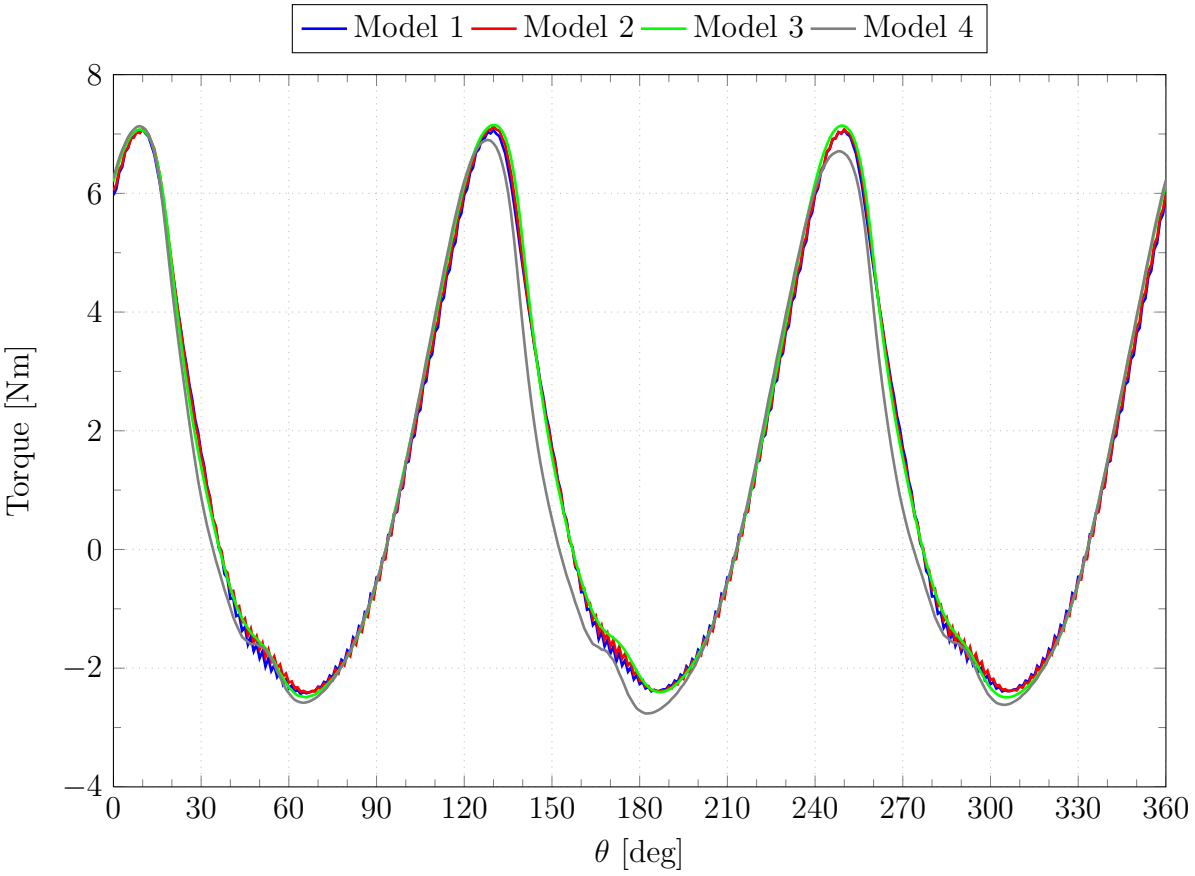

Figure B.3: Torque vs azimuthal angle. 2-D Models. NACA 0015. $\lambda = 1.5$

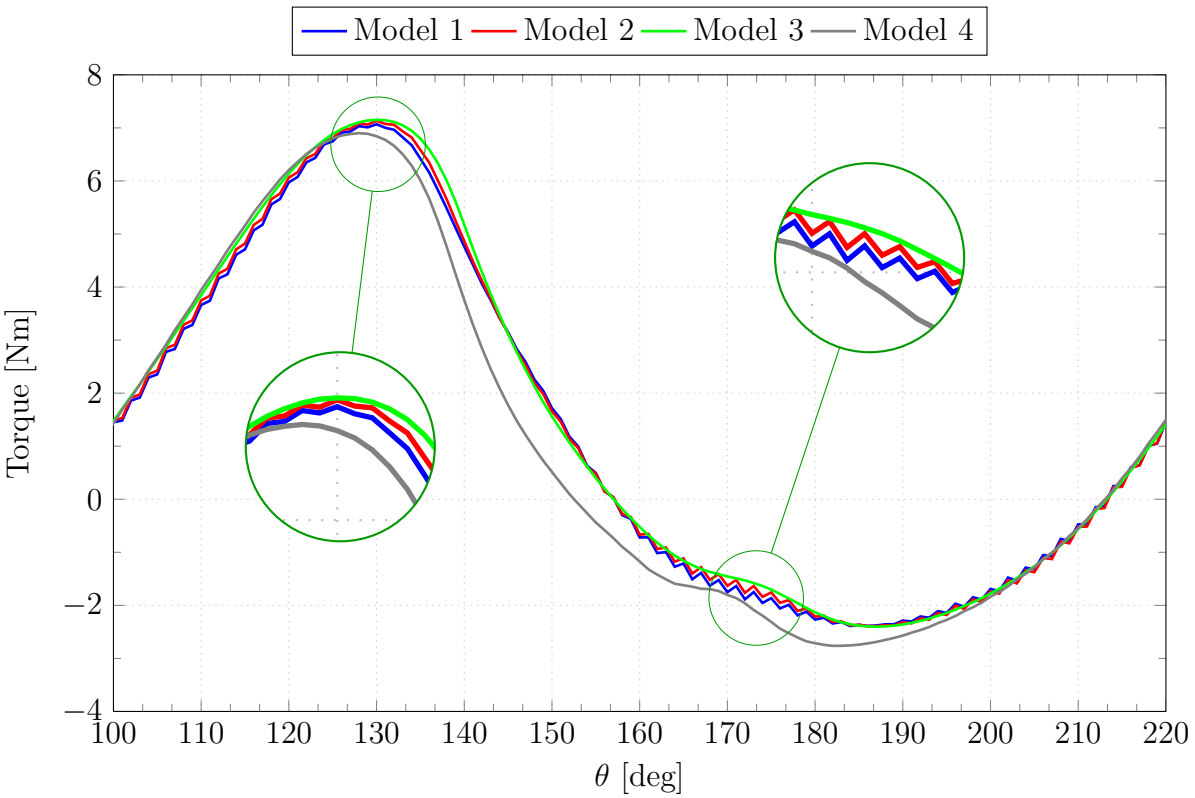

Figure B.4: Torque vs azimuthal angle. 2-D Models. NACA 0015. $\lambda = 1.5$. Close up.

It can be seen in the figures that the model with coarser meshes present a highly oscillatory behavior in the time-dependent results. For the smaller mesh size considered, the results start to differ from the models with coarser mesh. This is more evident for low Reynolds numbers, as can be seen in the relative error between models. It can be concluded then, that the employed model is not grid–independent and therefore further studies should be performed. In the framework of this project, this was not possible and the results of Chapter 4 are used anyway for comparative purposes between the different designs.

Appendix C

Detailed Results. Two–dimensional CFD Simulations

The detailed results of the produced torques corresponding to the analyses performed in Chapter 4 are presented here.

In Figures C.1, C.2 and C.3, the results for the symmetric airfoil are presented for the thicknesses of 12%, 15% and 18%, respectively.

In Figures C.4, C.5 and C.6, the results for the airfoil with a curvature of 2% and thicknesses of 12%, 15% and 18% are presented.

Finally, in Figures C.7, C.8 and C.9, the results for the airfoil with a curvature of 4% are presented for thicknesses of 12%, 15% and 18%, respectively.

Finally, in Figures C.10, C.11 and C.12, the results for the airfoil with a curvature of 6% and thicknesses of 12%, 15% and 18% are presented.

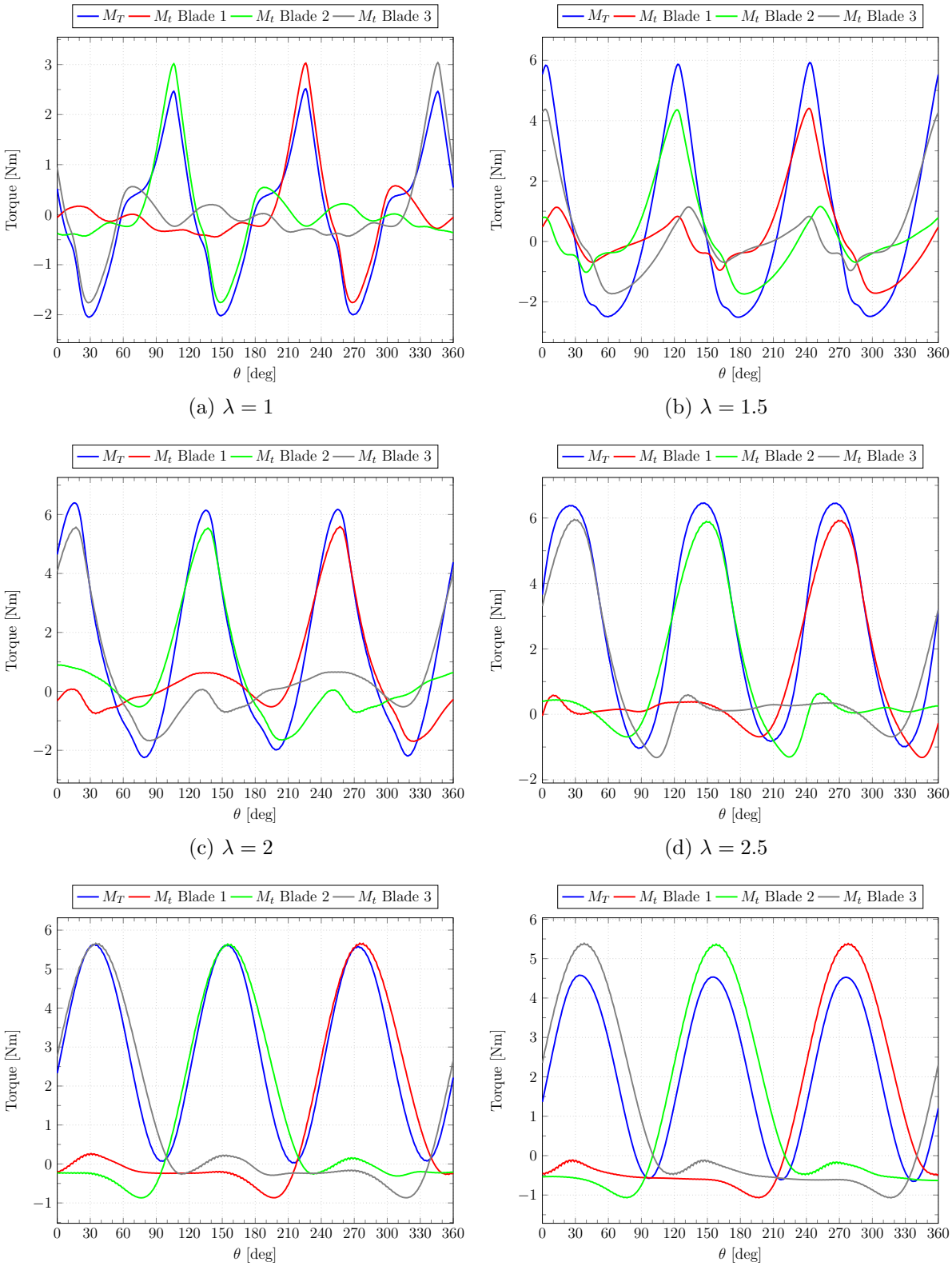

(a) $\lambda = 1$ (b) $\lambda = 1.5$

(c) $\lambda = 2$ (d) $\lambda = 2.5$

(e) $\lambda = 3$ (f) $\lambda = 3.5$

Figure C.1: Torque vs azimuthal angle. NACA 0012.

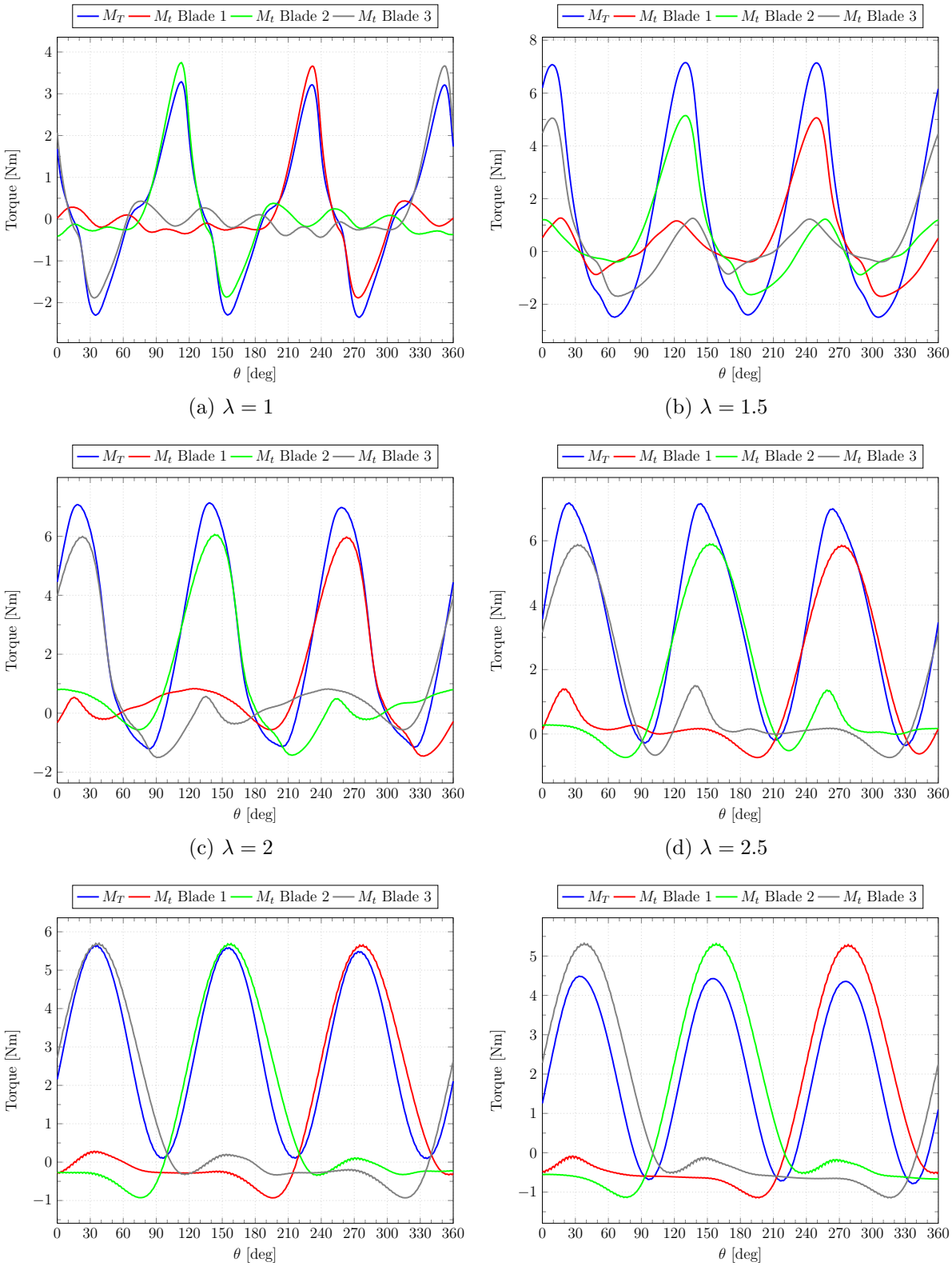

(a) $\lambda = 1$ (b) $\lambda = 1.5$

(c) $\lambda = 2$ (d) $\lambda = 2.5$

(e) $\lambda = 3$ (f) $\lambda = 3.5$

Figure C.2: Torque vs azimuthal angle. NACA 0015.

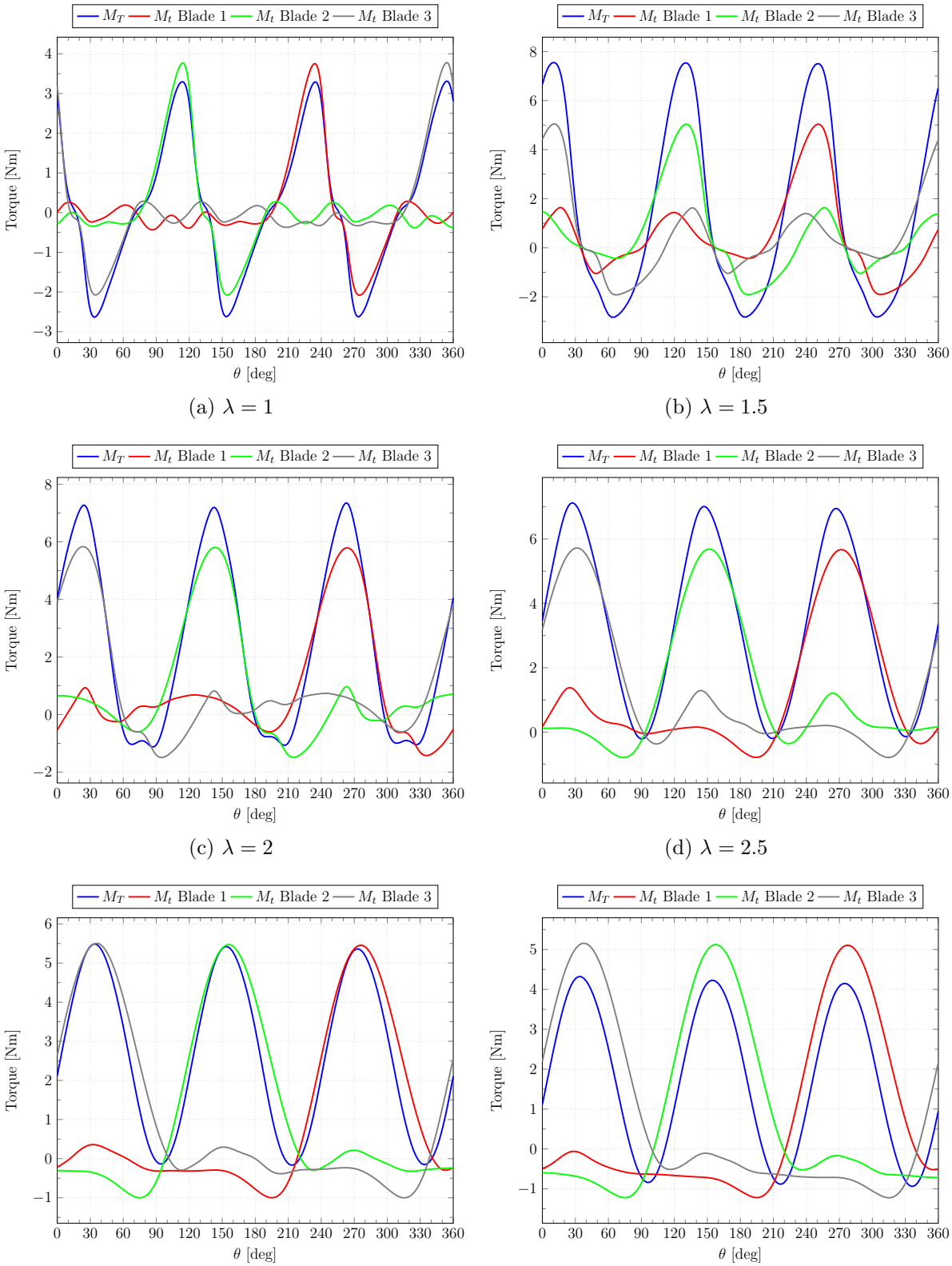

(a) $\lambda = 1$ (b) $\lambda = 1.5$

(c) $\lambda = 2$ (d) $\lambda = 2.5$

(e) $\lambda = 3$ (f) $\lambda = 3.5$

Figure C.3: Torque vs azimuthal angle. NACA 0018.

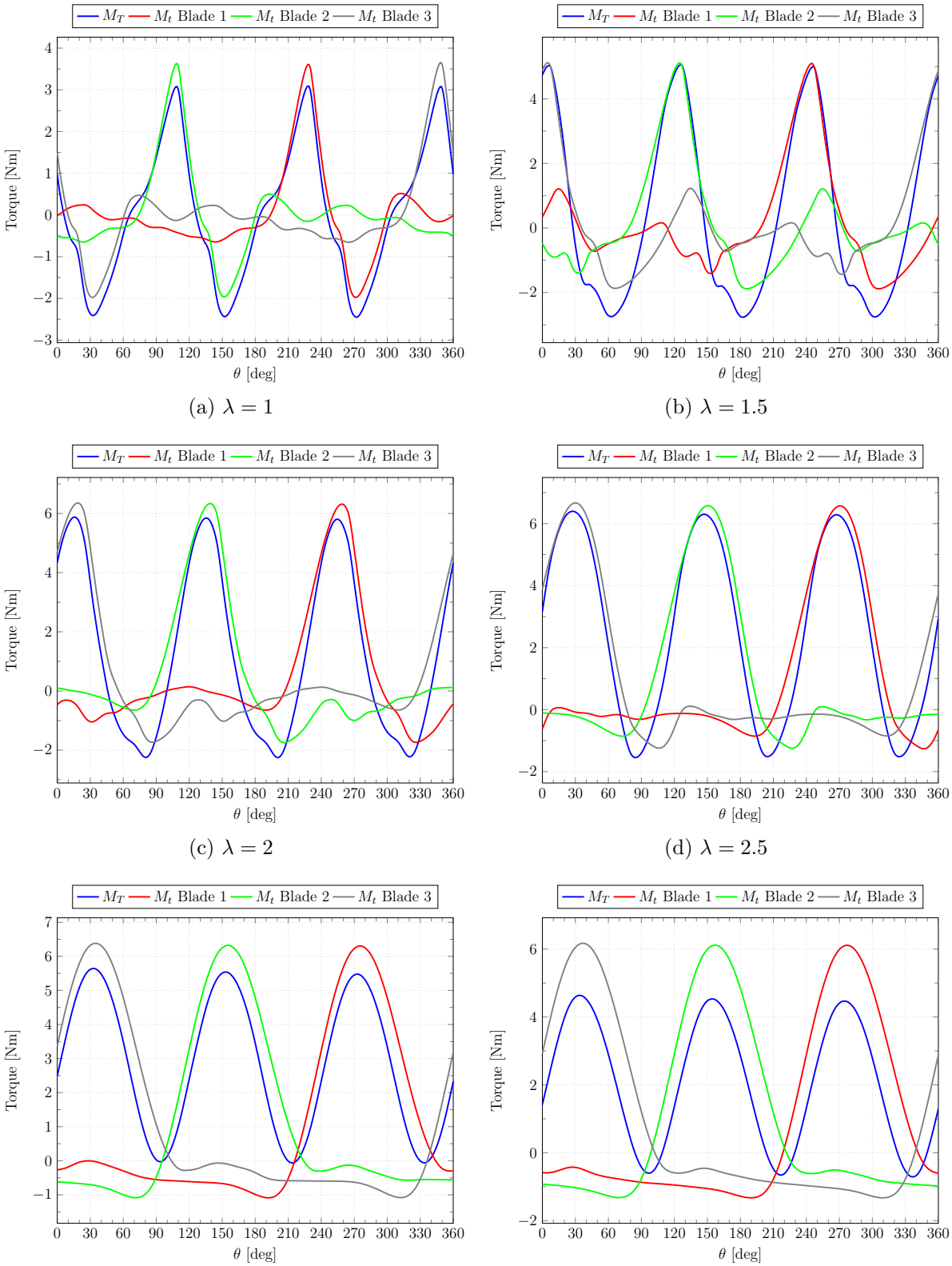

(a) $\lambda = 1$ (b) $\lambda = 1.5$

(c) $\lambda = 2$ (d) $\lambda = 2.5$

(e) $\lambda = 3$ (f) $\lambda = 3.5$

Figure C.4: Torque vs azimuthal angle. NACA 2412.

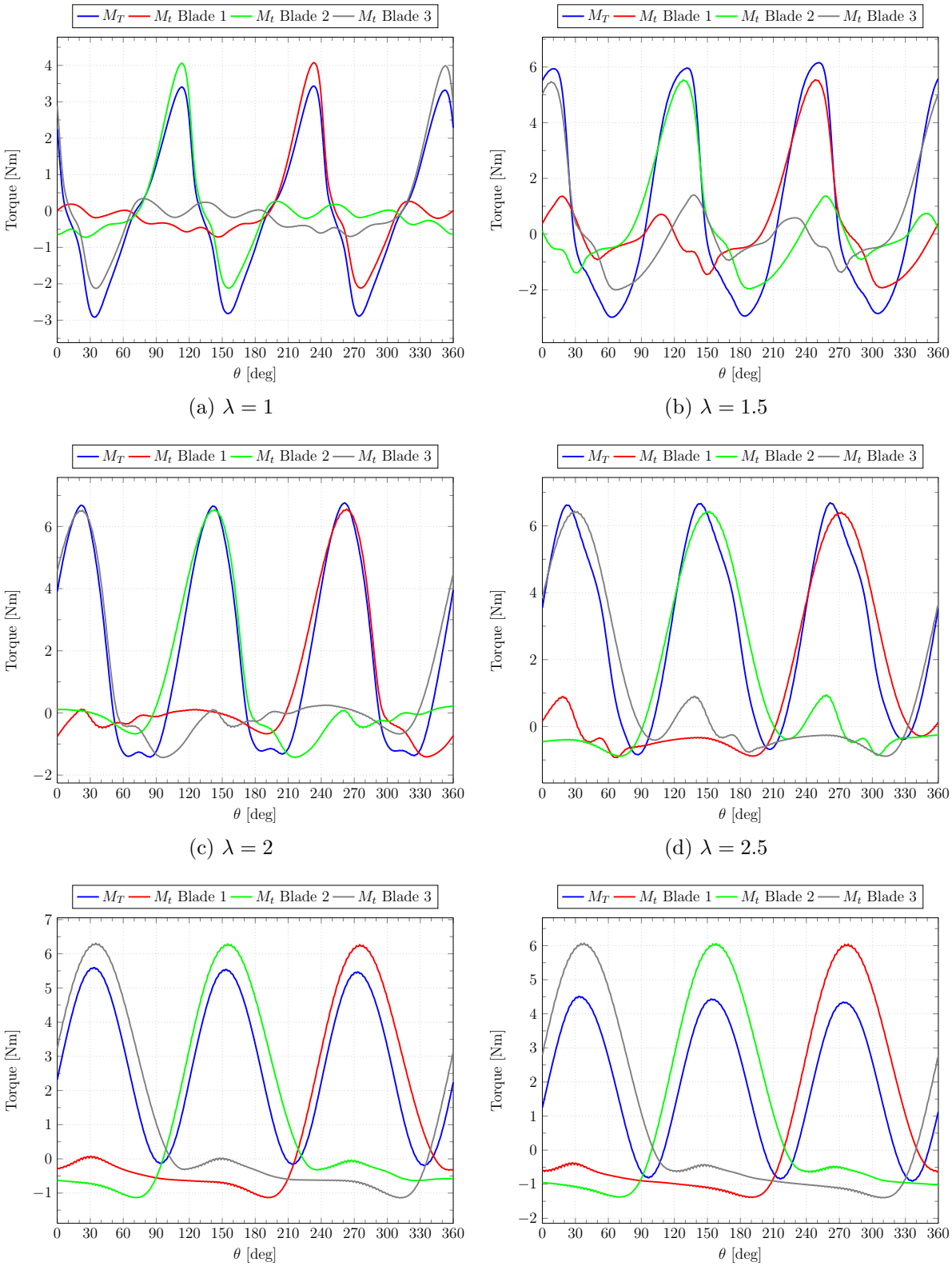

(a) $\lambda = 1$ (b) $\lambda = 1.5$

(c) $\lambda = 2$ (d) $\lambda = 2.5$

(e) $\lambda = 3$ (f) $\lambda = 3.5$

Figure C.5: Torque vs azimuthal angle. NACA 2415.

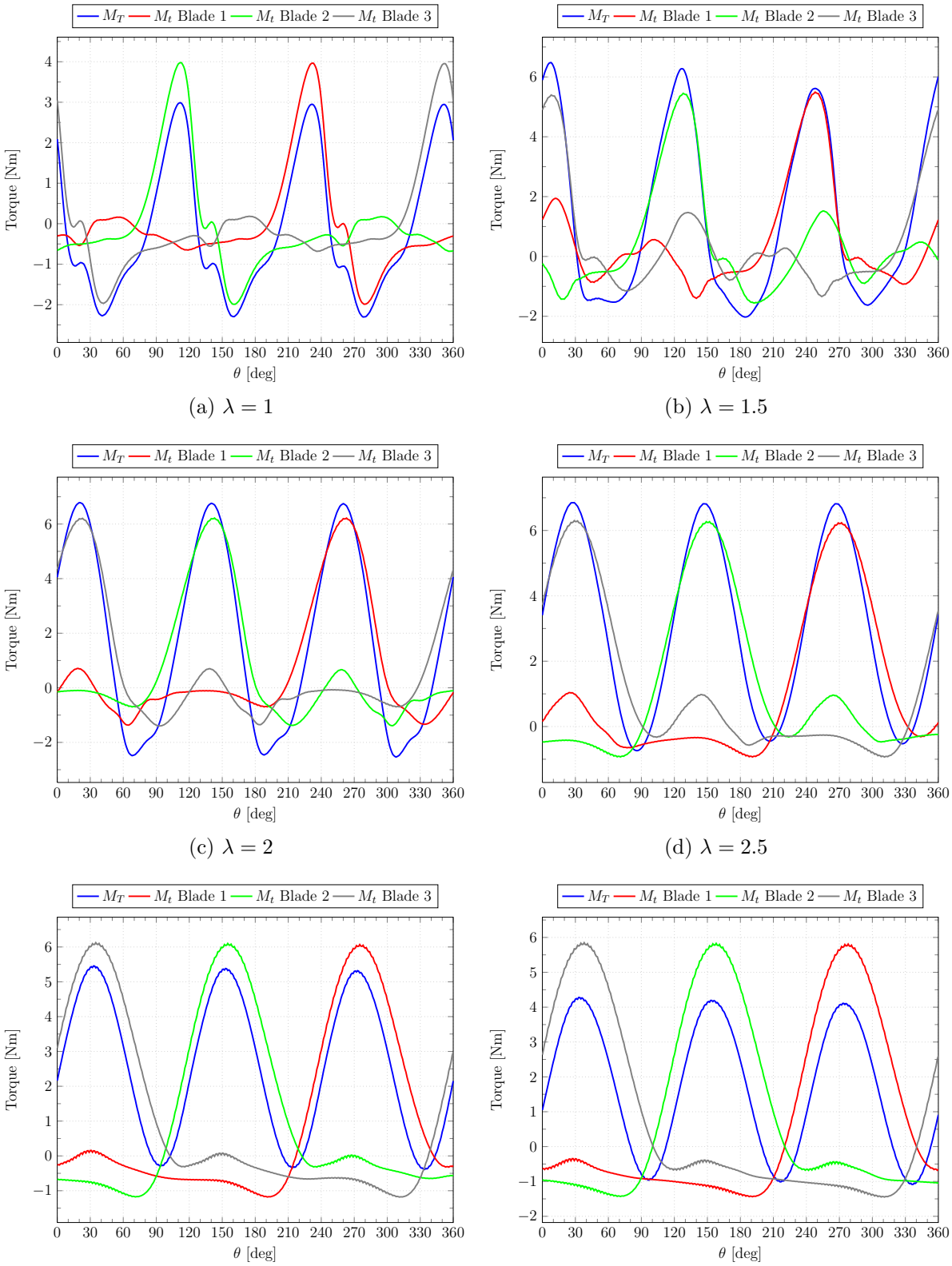

(a) $\lambda = 1$

(b) $\lambda = 1.5$

(c) $\lambda = 2$

(d) $\lambda = 2.5$

(e) $\lambda = 3$

(f) $\lambda = 3.5$

Figure C.6: Torque vs azimuthal angle. NACA 2418.

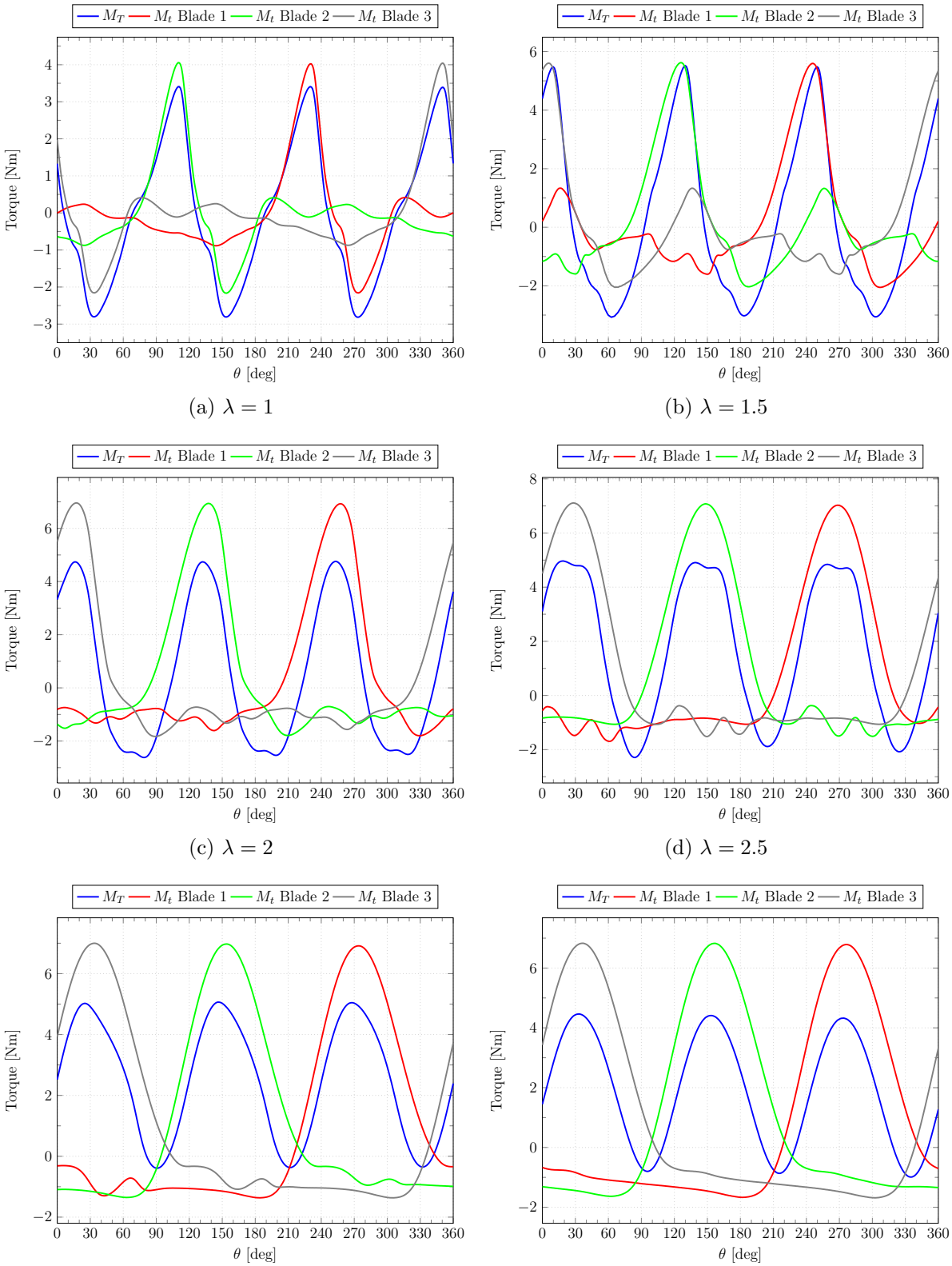

(a) $\lambda = 1$ (b) $\lambda = 1.5$

(c) $\lambda = 2$ (d) $\lambda = 2.5$

(e) $\lambda = 3$ (f) $\lambda = 3.5$

Figure C.7: Torque vs azimuthal angle. NACA 4412.

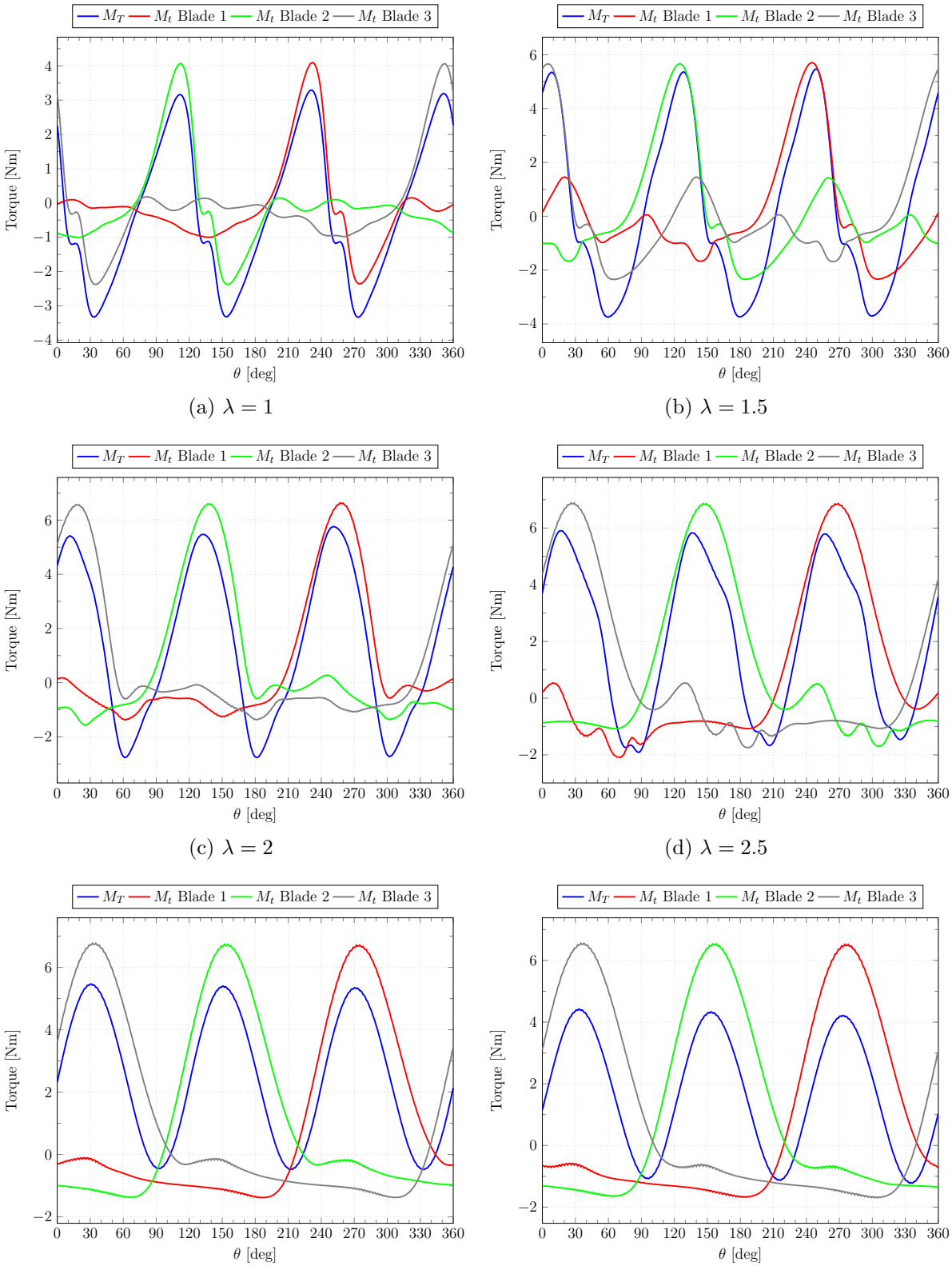

(a) $\lambda = 1$

(b) $\lambda = 1.5$

(c) $\lambda = 2$

(d) $\lambda = 2.5$

(e) $\lambda = 3$

(f) $\lambda = 3.5$

Figure C.8: Torque vs azimuthal angle. NACA 4415.

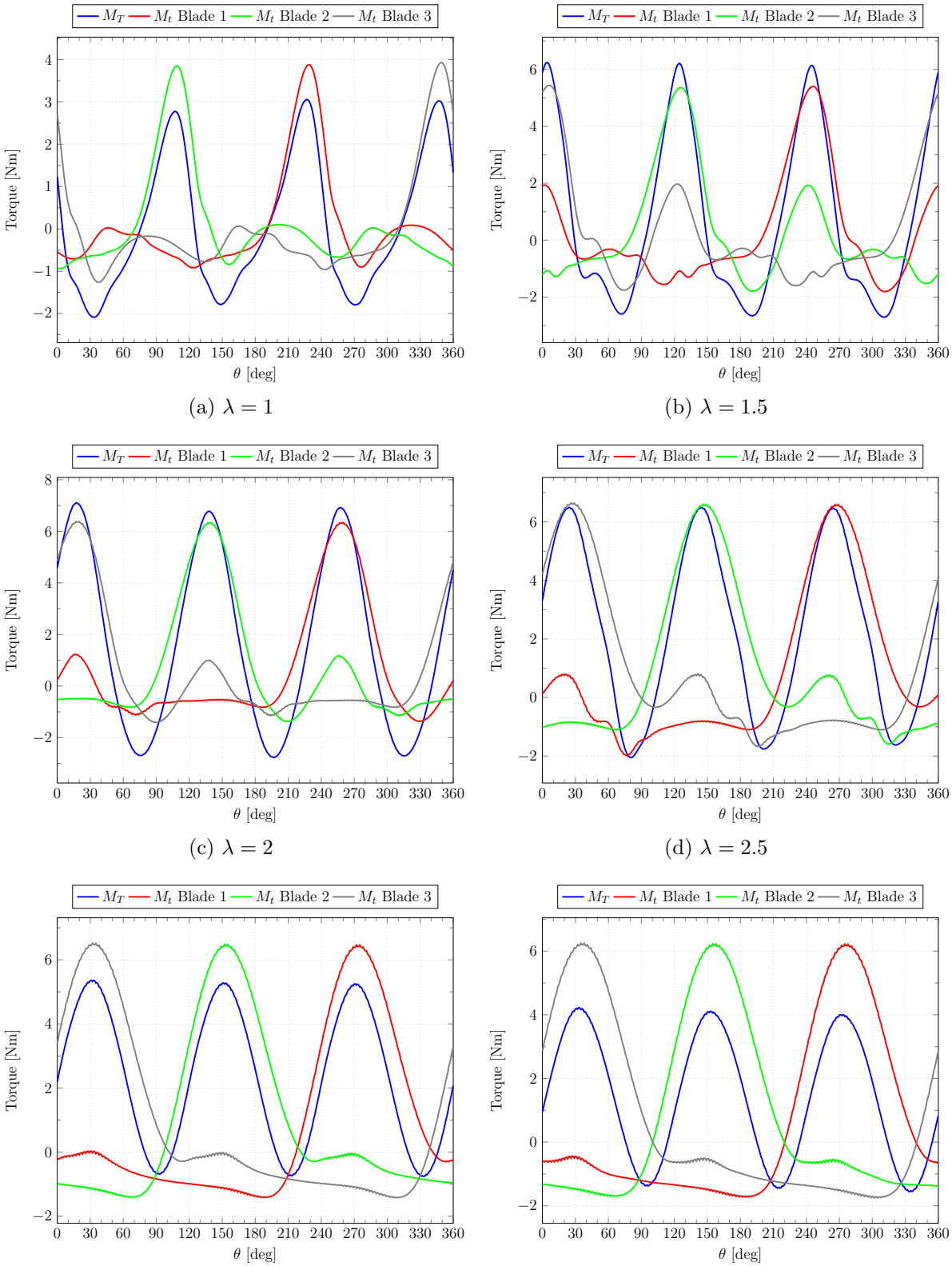

(a) $\lambda = 1$ (b) $\lambda = 1.5$

(c) $\lambda = 2$ (d) $\lambda = 2.5$

(e) $\lambda = 3$ (f) $\lambda = 3.5$

Figure C.9: Torque vs azimuthal angle. NACA 4418.

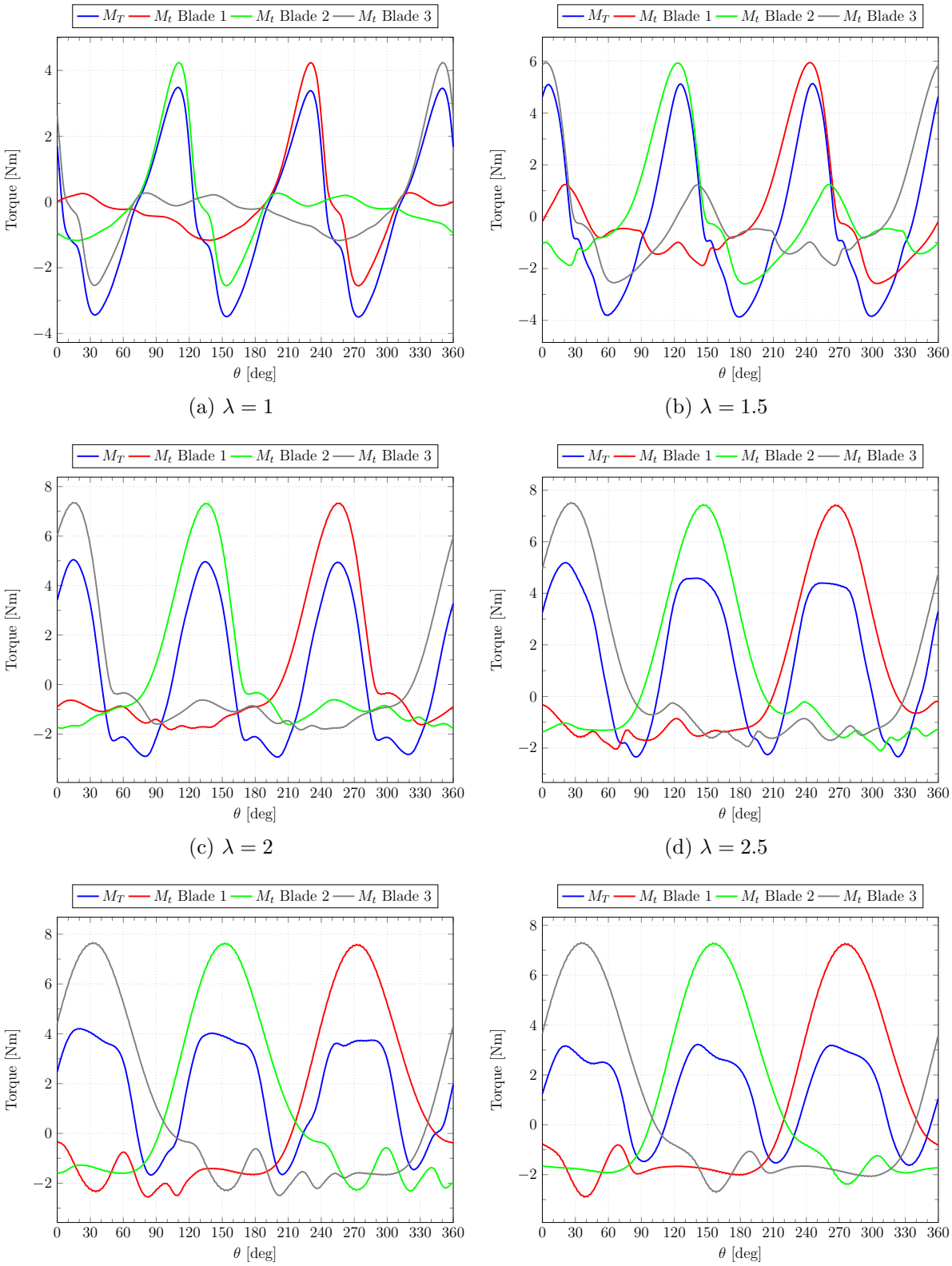

(a) $\lambda = 1$ (b) $\lambda = 1.5$

(c) $\lambda = 2$ (d) $\lambda = 2.5$

(e) $\lambda = 3$ (f) $\lambda = 3.5$

Figure C.10: Torque vs azimuthal angle. NACA 6412.

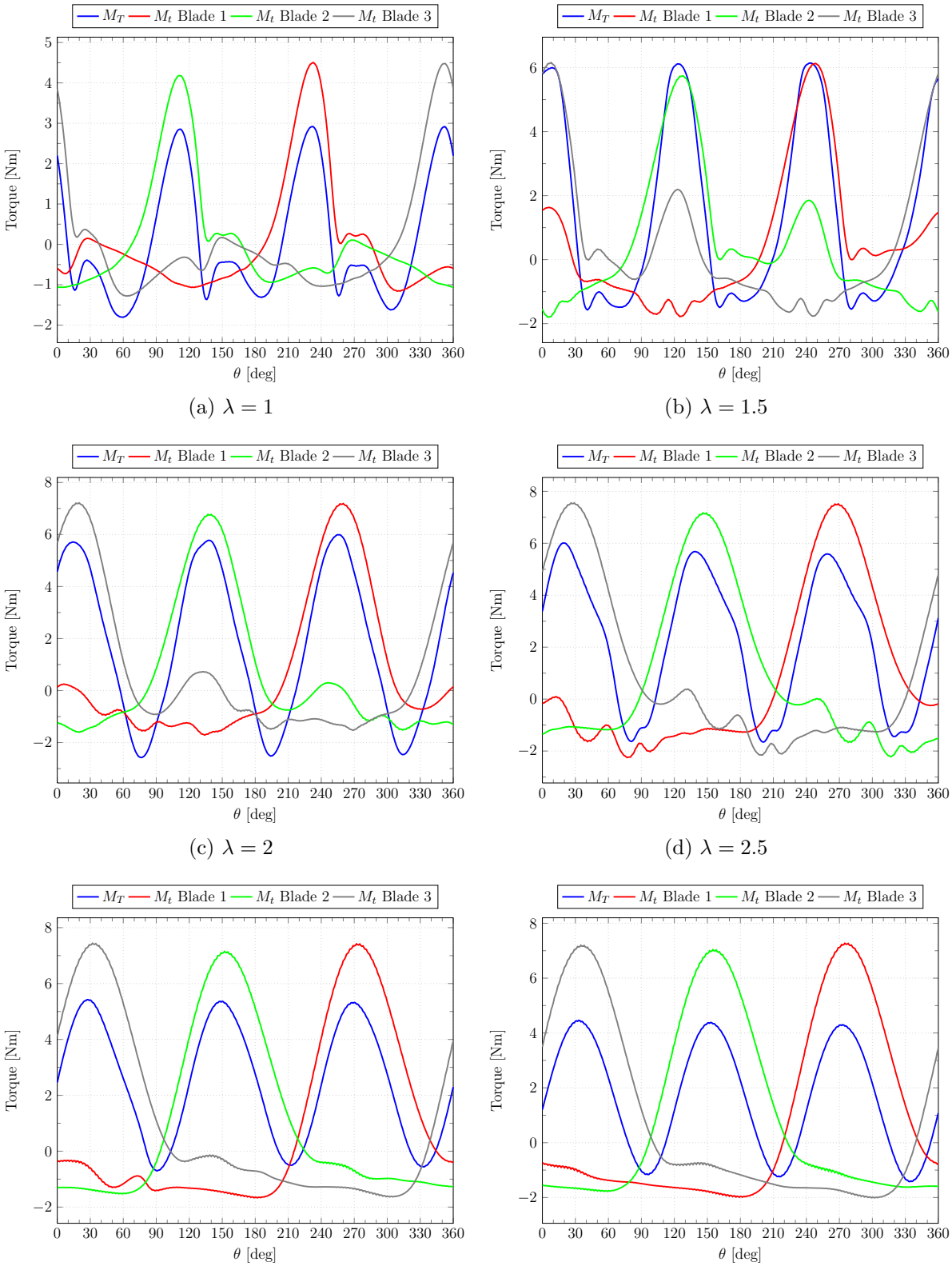

(a) $\lambda = 1$ (b) $\lambda = 1.5$

(c) $\lambda = 2$ (d) $\lambda = 2.5$

(e) $\lambda = 3$ (f) $\lambda = 3.5$

Figure C.11: Torque vs azimuthal angle. NACA 6415.

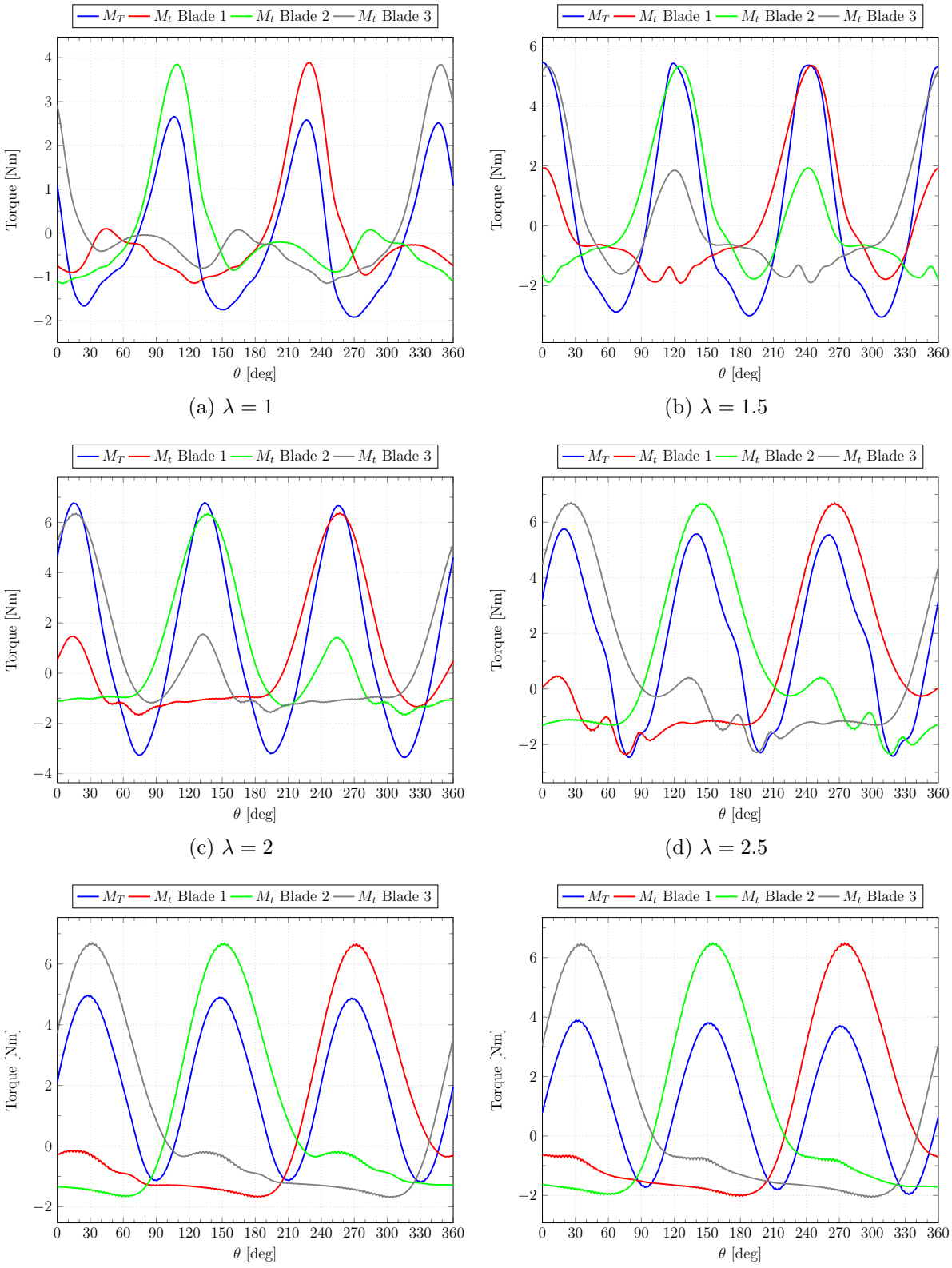

(a) $\lambda = 1$ (b) $\lambda = 1.5$

(c) $\lambda = 2$ (d) $\lambda = 2.5$

(e) $\lambda = 3$ (f) $\lambda = 3.5$

Figure C.12: Torque vs azimuthal angle. NACA 6418.

Appendix D

Detailed Results. Three–dimensional CFD Simulations

The detailed results of the produced torques corresponding to the analyses performed in Chapter 5 are presented here.

In Figure D.1 the results for the simplified model of the turbine with a NACA 0015 airfoil are presented for the different tip speed ratios, λ.

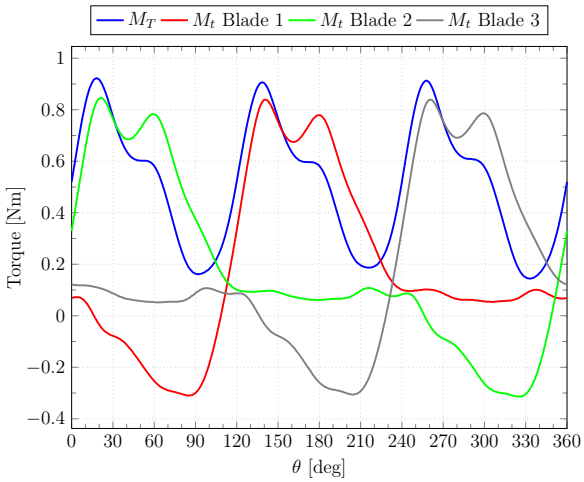

(a) $\lambda = 1$

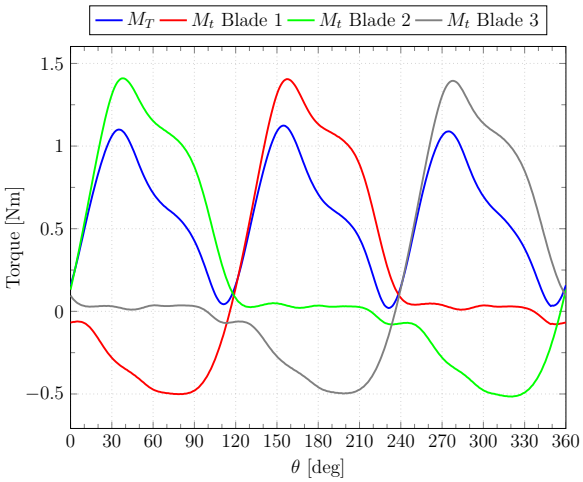

(b) $\lambda = 1.5$

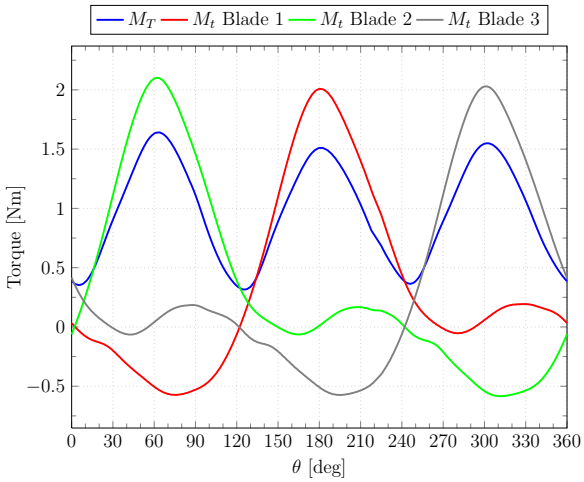

(c) $\lambda = 2$

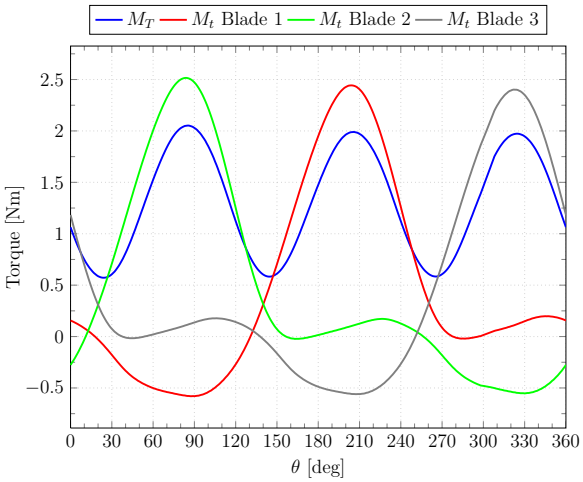

(d) $\lambda = 2.5$

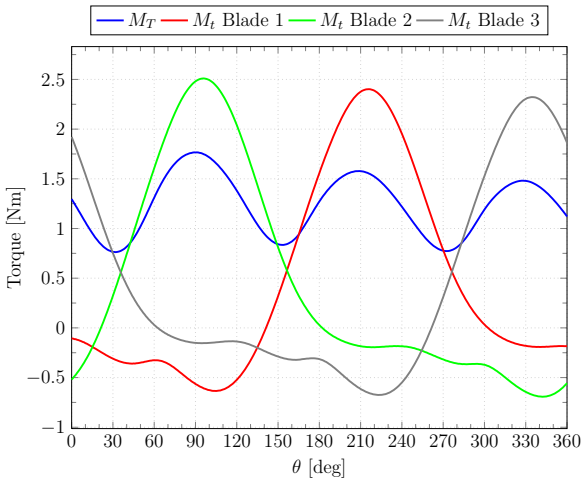

(e) $\lambda = 3$

Figure D.1: Torque vs azimuthal angle. 3-D Model. NACA 0015.

Appendix E

Codes Employed

E.1 STAR CCM+ Macro

The following macro written in Java language was used to extract the values of the different variables of the simulation along the calculations in the software STAR CCM+. This is a modified version of the original code used by Brunellière and Bibard (2011) in previous works performed at ICAM.

```
package macro;
import java.util.*;
import star.common.*;
import star.base.neo.*;
import star.vis.*;
import java.io.File;
public class StarCCMExportationScript extends StarMacro
{
  static final String OUTPUTBASEPATH = "/dataPressions/";
  static final String EXT = ".csv";
  static int i = 0;
  static int ENDMkr = 0;
  public void execute()
  {
  final String[] PlotNames = {"P1 fc Cid", "X1 fc Cid", "Y1 fc Cid",
     "Z1 fc Cid","P2 fc Cid", "X2 fc Cid", "Y2 fc Cid", "Z2 fc Cid","
     P3 fc Cid", "X3 fc Cid", "Y3 fc Cid", "Z3 fc Cid","PA fc Cid", "
     XA fc Cid", "YA fc Cid", "ZA fc Cid", "Pressure Blade 1", "
      Pressure Blade 2", "Pressure Blade 3" , "Forces Blade 1", "
      Forces Blade 2", "Forces Blade 3", "Torque","Residuals"};

  File ExportFile;
   StarPlot[] MyPlots = new StarPlot[PlotNames.length];
  final Simulation MySim = getActiveSimulation();
  final Solution MySol = MySim.getSolution();
```

```
21  MySim.println("MACRO> ##################################");
    MySim.println("MACRO> ####  Macro v2 STARTED  ####");
23  MySim.println("MACRO> ##################################");      final
       File MySimFile = new File(MySim.getSessionPath());
    final String SimName = MySimFile.getName();
25  final String SimTitle = SimName.substring(0,SimName.lastIndexOf(".")
       ));
    final String SimPath = OUTPUTBASEPATH + SimTitle + MySimFile.
       separator;
27
    if (MySol.isInitialized() == false) MySol.initializeSolution();
29   for (int i = 0; i < PlotNames.length; i++)
     {
31   MyPlots[i] = MySim.getPlotManager().getObject(PlotNames[i]);
     }
33   ExportPlots(MySim,MySol,SimPath,SimTitle,MyPlots,PlotNames);
     int TimeLevel = MySim.getSimulationIterator().getCurrentTimeLevel
        ();
35   PhysicalTimeStoppingCriterion MyCrit1 = ((
        PhysicalTimeStoppingCriterion) MySim.
        getSolverStoppingCriterionManager().getSolverStoppingCriterion(
        "Maximum Physical Time"));
     StepStoppingCriterion MyCrit2 = ((StepStoppingCriterion) MySim.
        getSolverStoppingCriterionManager().getSolverStoppingCriterion(
        "Maximum Steps"));
37   do
     {
39   MySim.getSimulationIterator().run(1,true);
     if (TimeLevel == MySim.getSimulationIterator().getCurrentTimeLevel
        ())
41    {
        MySim.println("MACRO> ##################################");
43      MySim.println("MACRO> ######## Macro ABORTED! ########");
        MySim.println("MACRO> ## Time step hasn't changed ##");
45      MySim.println("MACRO> ##################################");
        return;
47    }
      else
49      TimeLevel = MySim.getSimulationIterator().getCurrentTimeLevel()
           ;
        ExportPlots(MySim,MySol,SimPath,SimTitle,MyPlots,PlotNames);
51   }
```

```
    while (IsCriteriaSatisfied(MySim,MyCrit1,MyCrit2) == false);
53
    ENDMkr=1;
55  ExportPlots(MySim,MySol,SimPath,SimTitle,MyPlots,PlotNames);
    MySim.println("MACRO> ########################################");
57  MySim.println("MACRO> ### Macro FINISHED succesfully! ###");
    MySim.println("MACRO> ########################################");
59  }

61  private void ExportPlots(Simulation MySim, Solution MySol, String
      SimPath, String SimTitle, StarPlot[] MyPlots, String[] PlotNames)
    {
63  String TimeStr = String.format("%.5f", MySol.getPhysicalTime());
    for (int i = 0; i < MyPlots.length; i++)
65  {
    ExportPlot(MySim,MySol,SimPath,SimTitle,TimeStr, MyPlots[i],
       PlotNames[i]);
67  }
    }
69
    private void ExportPlot(Simulation MySim, Solution MySol, String
       SimPath, String SimTitle, String TimeStr, StarPlot MyPlot,
       String PlotName)
71  {
    String Fname;
73  if ( (PlotName == "P1 fc Cid") || (PlotName == "P2 fc Cid") || (
       PlotName == "P3 fc Cid") || (PlotName == "PA fc Cid") || (
       PlotName == "Pressure Blade 1") || (PlotName == "Pressure Blade
        2") || (PlotName == "Pressure Blade 3")  ) Fname = SimPath +
       PlotName + "     " + TimeStr + " sec" + EXT;
    else Fname = SimPath + PlotName + EXT;
75
    if ( (ENDMkr == 0) && ((PlotName == "P1 fc Cid") || (PlotName == "
       P2 fc Cid") || (PlotName == "P3 fc Cid") || (PlotName == "PA fc
        Cid") || (PlotName == "Pressure Blade 1") || (PlotName == "
       Pressure Blade 2") || (PlotName == "Pressure Blade 3")) )
77  {
    MyPlot.export(resolvePath(Fname));
79  MySim.println("MACRO> Exported plot " + PlotName + EXT);
    MySim.println("MACRO> .. " + Fname);
81  MySim.println("MACRO> .. i=" + i);
    }
```

```
83      if (ENDMkr == 1)
        {
85       MyPlot.export(resolvePath(Fname));
         MySim.println("MACRO> Exported plot " + PlotName + EXT);
87       MySim.println("MACRO> .. " + Fname);
         MySim.println("MACRO> .. i=" + i);
89      }

91    }

93    private boolean IsCriteriaSatisfied(Simulation MySim,
         PhysicalTimeStoppingCriterion MyCrit1, StepStoppingCriterion
         MyCrit2)
      {
95     if (MyCrit1.getIsUsed() && MyCrit2.getIsUsed())
       return MyCrit1.getIsSatisfied() || MyCrit2.getIsSatisfied();
97     else if (MyCrit1.getIsUsed())
       return MyCrit1.getIsSatisfied();
99     else if (MyCrit1.getIsUsed())
       return MyCrit2.getIsSatisfied();
101    else return false;
      }
103 }
```

E.2 MATLAB Code for the Load Approximation

The following code is the implementation in MATLAB of the proposed method to obtain the approximate pressure load distribution and the corresponding plots presented in Chapter 7. The data corresponding to the pressure values and the point coordinates are imported from an external file.

```
1  close all
   clear
3  load('Data2D0015TSR2.mat') % Import 2D pressure data
   Point=49; % Selected point over the airfoil
5  P1=DataP2D(Point,:); % Pressure at the point
   deg=linspace(0,359,360);
7  Z=linspace(0,1.4,120);
   P1s=smooth(P1,9);  % Filter averaged
```

```
for i=1:10  % Used 380 points for continuity in the extremes,
   removing the extra 20
    P1s(1,:)=[];
    P1(:,1)=[];
    P1(:,length(P1))=[];
    P1s(length(P1s),:)=[];
end

% To create the 3D approximation
Hel=+1; % Helix direction
Pest=zeros(120,360); % 3D Pressure estimate
for i=0:119
    for j=1:360
        if ((j+Hel*i)<=360) && ((j+Hel*i)>0)
            Pest(i+1,j)=P1s(j+Hel*i);
        else
            if ((j+Hel*i)>360)
                Pest(i+1,j)=P1s(j+Hel*i-360);
            else
                Pest(i+1,j)=P1s(j+Hel*i+360);
            end
        end
    end
end

% Simplify the 3D surface (reduced size)
deg(1,361)=360;
Pest(:,361)=Pest(:,1);
deg1=linspace(0,360,73);
z1=linspace(0,1.4,70);
[Deg1,Z1]=meshgrid(deg1,z1);
PS2=griddata(deg,Z,Pest,Deg1,Z1);

% Adding shape function
f=zeros(length(z1),1);
for i=1:length(z1)
    if (z1(i)>0.1) && (z1(i)<1.3)
        f(i)=1;
    end
    if (z1(i)<0.1)
       f(i)=10*z1(i);
    end
```

```
    if (z1(i)>1.3)
51      f(i)=-10*(z1(i)-1.4);
    end
53  PS2f(i,:)=PS2(i,:).*f(i);
end
55
% Plots
57 figure  % 3D Pres. estimate without shape function
surf(deg1,z1,PS2)
59 shading interp
figure % 3D Pres. estimate with shape function
61 surf(deg1,z1,PS2f)
shading interp
63
cl = [-80:10:60];
65 caxis([-80 60])
figure %3D Pres. estimate without shape function. Contour
67 contourf(deg1,z1,PS2,cl)
figure %3D Pres. estimate with shape function. Contour
69 contourf(deg1,z1,PS2f,cl)

71 % 3D simulation data analysis
H=1.4;
73 Z=linspace(0,H,120);
load('Data3D0015TSR2.mat') % Import 2D pressure data
75 b=H/120; %Helix parameter
% Matching of point in 3D and 2D
77 x2d=CoordAirfoilPress(Point,1);
y2d=CoordAirfoilPress(Point,2);%
79 ang=atan(y2d/x2d);
angdeg=90+radtodeg(ang); % correct quadrant
81 radial=x2d/cos(ang);
Rp=radial; %Radius at which the helix is drawn over the airfoil
83 Theta0=angdeg; %Position at which the helix starts.

85 for i=1:121  % Helix
    Xh(i)=Rp*cos(degtorad((i-1)+Theta0));
87  Yh(i)=Rp*sin(degtorad((i-1)+Theta0));
    Zh(i)=b*(i-1);
89 end

91 figure % Plot points corresponding to the 3D blade data and helix
```

```
plot3(Xh,Yh,Zh,'b')
grid on
hold on
xlabel('x')
plot3(Coord3D(1:59,1),Coord3D(1:59,2),Coord3D(1:59,3),'x')
axis equal

% Point matching in for the 3D model
RangeZ=0.1; % Tolerance to search for matching points
Ph=zeros(length(Zh(1,:)),length(DataPress3D(1,:)));
Phs=Ph;
CCvect=zeros(length(Zh(1,:)),1);
Xp=Coord3D(:,1);
Yp=Coord3D(:,2);
Zp=Coord3D(:,3);
CC=1; % Initial distance for convergence criteria
for i=1:length(Zh(1,:))  % Match the pressure over the airfoil with
    the selected point along the blade
    for j=1:length(Zp(:,1))
        if (Zh(i)-Zp(j))<RangeZ
            Dist=((Xh(i)-Xp(j))^2+(Yh(i)-Yp(j))^2+(Zh(i)-Zp(j))^2)
                ^0.5;
            if Dist<CC
                Pto=j; % Saves point ID
                CC=Dist;
            end
        end
    end
    Ph(i,:)=DataPress3D(Pto,:);  % Assign the pressure of the
        corresponding point
    Phs(i,:)=smooth(Ph(i,:),9);  % Filter averaged
    CCvect(i)=CC;
    CC=1;
end
for i=1:10
    Ph(:,1)=[];
    Ph(:,length(Ph(1,:)))=[];
    Phs(:,1)=[];
    Phs(:,length(Ph(1,:)))=[];
end
Ph(:,361)=Ph(:,1);
Phs(:,361)=Phs(:,1);
```

```
% Plots
cl = [-100:10:60];
figure
contourf(deg1,z1,PS2f,cl) %3D Pres. estimate with shape function.
    Contour
caxis([-100 60])
figure
contourf(deg,Zh,Phs,cl) %3D Pres. from CFD. Contour
caxis([-100 60])
figure
contourf(deg,Zh,Ph,cl) % 3D Pres. from CFD. Contour. Not filtered
caxis([-100 60])
figure
surf(deg,Zh,Ph) %3D Pres. from CFD
shading interp
zlim([-100,60])
```